

For Reference

NOT TO BE TAKEN FROM THIS ROOM

For Reference

NOT TO BE TAKEN FROM THIS ROOM

Ex LIBRIS
UNIVERSITATIS
ALBERTAEASIS



THE UNIVERSITY OF ALBERTA

FATIGUE STRENGTH OF DEFORMED
REINFORCING BARS

by



ISHWAR C. JHAMB

A THESIS

SUBMITTED TO THE FACULTY OF GRADUATE STUDIES
IN PARTIAL FULFILMENT OF THE REQUIREMENTS FOR THE DEGREE OF
MASTER OF SCIENCE

DEPARTMENT OF CIVIL ENGINEERING

EDMONTON, ALBERTA
SPRING, 1969

Thesis
1969
60

UNIVERSITY OF ALBERTA
FACULTY OF GRADUATE STUDIES

The undersigned certify that they have read, and recommend
to the Faculty of Graduate Studies for acceptance, a thesis entitled
FATIGUE STRENGTH OF DEFORMED REINFORCING BARS submitted by ISHWAR CHAND
JHAMB in partial fulfilment of the requirements for the degree of Master
of Science.

ABSTRACT

The effect of diameter, yield strength, and stress range on the fatigue strength of intermediate and high strength reinforcing bars was studied experimentally. The test program included tests of hot-rolled deformed bars of ASTM A 15 (Intermediate), A 432 and A 431 steel and bar sizes Nos. 5, 8 and 10. A total of 72 reinforced concrete beam specimens and 72 rotating beam specimens were tested under repeated loads. Metallographic observations were also carried out.

The results of tests suggest that there is no significant increase in fatigue strength as the tensile strength of the reinforcement is increased. A slight reduction in fatigue strength was observed as the diameter of the bar was increased. The effect of variations in the stress range of the stress cycle could be explained using a Modified Goodman Diagram with a straight line envelope.

ACKNOWLEDGEMENTS

The author wishes to express his deep gratitude to Professor J.G. MacGregor for his continuous advice and valuable guidance without which this dissertation could not have been completed. Special thanks are due to the following for their contributions toward the completion of the investigation reported herein:

Professor F.H. Vitovec, Department of Mining and Metallurgy for his valuable advice in the metallographic investigations.

Mr. Norm Nuttall for fabricating and testing of the reinforced concrete beams in the earlier phase of the test program.

Mr. H. Panse and the Staff of the Department of Civil Engineering for assisting during the testing of the beam specimens.

Mr. M.R. Scott, technician, metallographic laboratory, for useful suggestions and preparation of metallographs of bars specimens.

This investigation was made possible through the financial assistance provided by the Portland Cement Association. The author gratefully acknowledges the financial and other assistance received from the sponsor during the course of investigation.

TABLE OF CONTENTS

	Page
Title Page	i
Approval Sheet	ii
Abstract	iii
Acknowledgements	iv
Table of Contents	v
List of Tables	viii
List of Figures	ix
List of Symbols	xiii
 CHAPTER I INTRODUCTION	 1
 CHAPTER II SURVEY OF LITERATURE DEALING WITH THE FATIGUE STRENGTH OF STEEL AND THE FATIGUE STRENGTH OF REINFORCING BARS	
2.1 Introduction and Nomenclature	3
2.2 Factors Affecting the Fatigue Strength of Machined Steel Specimens	4
2.2.1 Effect of Yield and Tensile Strength	4
2.2.2 Effect of Size	7
2.2.3 Effect of Notches	10
2.2.4 Effect of Minimum Stress and Stress Range	15
2.2.5 Effect of Changes in Stress Amplitude	17
2.2.6 Effect of Frequency of Testing	20
2.2.7 Effect of Metallurgical and Chemical Composition	20
2.2.8 Effect of Mill Scale and Decarburization	21
2.3 Fatigue Tests on High Strength Deformed Bars as Concrete Reinforcement	23
2.3.1 Modes of Failure Observed in Fatigue Testing of Reinforced Concrete Beams	24
2.3.2 Effect of Concrete Encasement	25
2.3.3 Effect of Minimum Stress and Stress Range	28

	Page
2.3.4 Effect of Yield and Ultimate Strength	35
2.3.5 Effect of Deformations	35
2.3.5.1 Effect of Lug Base Radius and Lug Height	36
2.3.5.2 Effect of Lug Inclination	38
2.3.5.3 Effect of Intersection Between Longitudinal and Transverse Lugs	39
2.3.6 Effect of Bar Diameter	41
CHAPTER III TEST SPECIMENS, MATERIALS AND TESTING EQUIPMENT	
3.1 Description of Test Program	43
3.2 Properties of Reinforcement	44
3.3 Fatigue Tests on Beams	53
3.3.1 Details of Test Beams	53
3.3.2 Properties of Concrete	57
3.3.3 Form Work	58
3.3.4 Testing Equipment	59
3.3.5 Test Procedure	62
3.4 Rotating Beam Fatigue Tests	64
3.4.1 Details of Rotating Beam Specimens	64
3.4.2 Testing Equipment and Procedure	66
3.5 Hardness Tests and Metallographic Investigation	67
CHAPTER IV TEST RESULTS	
4.1 Reinforced Concrete Beam Specimens	69
4.1.1 Description of Failures	69
4.1.2 Presentation of Test Results	71
4.2 Presentation of Test Data for Rotating Beam Specimens	71
4.3 Hardness Test Results and Metallographic Observations	72

	Page
CHAPTER V DISCUSSION OF TEST RESULTS	
5.1 Effect of Minimum Stress	95
5.2 Effect of Yield and Tensile Strength	96
5.3 Effect of Bar Diameter	106
5.4 Effect of Deformation Pattern	109
5.5 Effect of Stress Concentrations and Decarburization	111
CHAPTER VI CONCLUSIONS AND RECOMMENDATIONS	117
LIST OF REFERENCES	119
APPENDIX A PRESENTATION OF TEST DATA	125

LIST OF TABLES

	Page
TABLE 3.1 Properties of Reinforcing Bars	45
TABLE 3.2 Properties of Reinforcing Bars	46
TABLE 3.3 Outline of Testing Program	47
TABLE 4.1 Characteristics at Fatigue Limit in Reinforced Concrete Beam Tests	75
TABLE 4.2 Characteristics at Fatigue Limit in Rotating Beam Fatigue Tests	76
TABLE 5.1 Effect of Bar Diameter on Fatigue Strength of Reinforcing Bars	107
TABLE 5.2 Calculation of Theoretical Stress Concentration Factors for Reinforcing Bars	112
TABLE 5.3 Analysis of Fatigue Strength of Reinforcing Bars	113
TABLE A.1 Reinforced Concrete Beam Data	126
TABLE A.2 Results of Fatigue Tests on Reinforced Concrete Beams	130
TABLE A.3 Results of Fatigue Tests on Reinforced Concrete Beams	142
TABLE A.4 Results of Rotating Beam Fatigue Tests	147

LIST OF FIGURES

	Page
FIGURE 2.1 Typical S-N Curve for Ferrous Metal	5
FIGURE 2.2 The Effect of Tensile Strength on Metal Fatigue Strength	6
FIGURE 2.3 The Effect of Specimen Size on Fatigue Strength of Specimen Under Direct Stress and Bending	8
FIGURE 2.4 The Effect of Size on Fatigue Strength	8
FIGURE 2.5 Stress Concentration Factors for Projecting Notches	11
FIGURE 2.6 The Effect of Notch Radius on Notch Sensitivity	13
FIGURE 2.7 The Effect of a Notch on the Flexural Stresses in a Rotating Beam	14
FIGURE 2.8 Modified Goodman Diagram	16
FIGURE 2.9 Relationship Between the Alternating Stress and the Mean Stress	16
FIGURE 2.10 Non-Dimensional Smith Diagram for Steels	18
FIGURE 2.11 The Effect of Concrete Encasement on Fatigue Strength of No. 5 Reinforcing Bars	27
FIGURE 2.12 Modified Goodman Diagram for ASTM A 15 Bars at 2 Million Cycles (Pfister and Hognestad)	30
FIGURE 2.13 Modified Goodman Diagram for ASTM A 432 Bars at 2 Million Cycles (Pfister and Hognestad)	31
FIGURE 2.14 Modified Goodman Diagram for ASTM A 431 Bars at 2 Million Cycles (Pfister and Hognestad)	32

	Page
FIGURE 2.15 Modified Goodman Diagram for Un-embedded High-Bond-Steel (Wascheidt)	33
FIGURE 2.16 Modified Goodman Diagram for Un-embedded Multirib-TOR-STAHL (Wascheidt)	34
FIGURE 2.17 The Effect of Inclination of Lug to the Bar Axis on Fatigue Strength	40
FIGURE 3.1 Deformation Patterns on Reinforcing Bars	48
FIGURE 3.2 Mid Lug Profiles of Bars	49
FIGURE 3.3 Stress-Strain Curves for Test Bars	52
FIGURE 3.4 Details of Beam Specimens	55
FIGURE 3.5 Reinforcement for Group I Beam in Form Prior to Placing Concrete	56
FIGURE 3.6 Overall View of Testing Arrangement	61
FIGURE 3.7 Details of Roller Support	61
FIGURE 3.8 Details of Rotating Beam Fatigue Specimens	65
FIGURE 4.1 Typical Crack Pattern in Beam Specimen After Failure	77
FIGURE 4.2 Typical Fracture Surfaces	78
FIGURE 4.3 Fatigue Cracks and Fatigue Failure of Bars	79
FIGURE 4.4 S-N Curves for No. 8 Bars-Minimum Stress = 0.1 f_y	80
FIGURE 4.5 S-N Curves for No. 8 Bars-Minimum Stress = 0.4 f_y	81
FIGURE 4.6 S-N Curves for No. 5 Bars-Minimum Stress = 0.1 f_y	82
FIGURE 4.7 S-N Curves for No. 10 Bars-Minimum Stress = 0.1 f_y	83
FIGURE 4.8 S-N Curves for Plain Rotating Beam Specimens	84

		Page
FIGURE 4.9	S-N Curves for Filleted Rotating Beam Specimens	85
FIGURE 4.10	Profile at Base of Fillet in Rotating Beam Specimens	86
FIGURE 4.11	Vickers Pyramid Hardness Values for No. 8 Bars	87
FIGURE 4.12	Macro-Structure of No. 8 Reinforcing Bars	88
FIGURE 4.13	Macro-Structure of No. 8 Reinforcing Bars	89
FIGURE 4.14	Micro-Structure of No. 8 Reinforcing Bars	90
FIGURE 4.15	Micro-Structure of No. 8 Reinforcing Bars at Base of Deformation Lug	91
FIGURE 4.16	Non-Metallic Inclusions in Longitudinal Sections-No. 8 Reinforcing Bars	92
FIGURE 4.17	Micro-Structure of No. 5 Reinforcing Bars at Base of Deformation Lug	93
FIGURE 4.18	Micro-Structure of No. 10 Reinforcing Bars at Base of Deformation Lug	94
FIGURE 5.1	Modified Goodman Diagram for No. 8 ASTM A 15 Bars	97
FIGURE 5.2	Modified Goodman Diagram for No. 8 ASTM A 432 Bars	98
FIGURE 5.3	Modified Goodman Diagram for No. 8 ASTM A 431 Bars	99
FIGURE 5.4	Effect of Yield and Tensile Strength on Fatigue Strength - Alberta Tests	103
FIGURE 5.5	Effect of Yield and Tensile Strength on Fatigue Strength of Reinforcing Bars	104

	Page
FIGURE 5.6 Effect of Bar Diameter on Fatigue Strength of Reinforcing Bars	108
FIGURE 5.7 Effect of Lug Base Radius on Fatigue Strength of Reinforcing Bars	110
FIGURE 5.8 Effect of Decarburization on Fatigue Strength	115

LIST OF SYMBOLS

f_y	- yield strength in tension
f_u	- ultimate tensile strength
$F_{2,000,000}$	fatigue strength for 2,000,000 cycles
h	- height of deformation lug
K_f	- experimental stress concentration factor
K_t	- theoretical stress concentration factor
n	- number of stress cycles
N	- number of stress cycles at endurance limit
q	- notch sensitivity factor
r	- minimum notch radius or radius at base of deformation lug
R	- algebraic ratio of minimum stress to maximum stress in cycle
$s_{r(-1)}$	- stress range at complete reversal
s_a	- stress amplitude
s_0	- stress range at minimum stress equal to zero ($R = 0$)
s_m	- mean stress
s_{\max}	- maximum stress
s_{\min}	- minimum stress
s_r	- stress range
w	- half width of deformation lug
θ	- face angle of deformation lug
σ	- stress

CHAPTER I

INTRODUCTION

In the last two decades, high strength deformed bars have largely replaced ordinary round mild steel bars as concrete reinforcement due to their better strength, bond and crack control characteristics and improved overall economy. These reinforcing bars are available with a variety of deformation patterns and yield strengths ranging from 50 to 90 ksi.

Extensive laboratory tests and field experience have led to the conclusion that within certain crack and deflection limitations the permissible stresses of high strength deformed bars can safely be increased over those for ordinary mild steel bars for static loading. In the case of highway bridges, crane runway girders, turbine foundations, railway ties and other structures which are loaded by repeated or predominantly dynamic loads, however, the allowable stresses have been increased more cautiously because of the fear that these structures may fail due to fatigue failure of the high strength deformed reinforcing bars.

In the past few years investigators have reported on the fatigue behavior of high strength deformed reinforcing bars from Europe, U.S.A., Canada and Japan. These investigations included a variety of deformed hot rolled and cold worked reinforcing bars. Such variables as tensile strength, deformation shape, and stress range have been considered.

This investigation was designed to study the effect of bar

size, bar yield strength, and stress range on the fatigue strength of one kind of commercially available deformed reinforcing bar.

The testing program consisted of flexural fatigue tests on 72 reinforced concrete beams containing ASTM A 15 - Intermediate, A 432, and A 431 reinforcement of bar sizes Nos. 5, 8 and 10. The minimum stresses in the cycles were set at 10 and 40 percent of the yield stress in the tests of No. 8 bars and 10 percent of yield stress in tests of No. 5 and No. 10 bars. In order to isolate the variables under investigation, the beam size and the concrete strength were kept approximately constant for each diameter of bars. The beam dimensions were varied in proportion to the bar diameter so that the steel percentage was kept approximately equal for all beams. The beams were tested under repeated loads applied at 500 cpm at mid span with tensile reinforcement stresses varying between predetermined minimum and maximum stress levels.

To find the fatigue properties of the metal in the bars, the fatigue strength at completely reversed bending stresses was found from rotating beam tests. For these tests a total of 36 plain and 36 filleted specimens were tested. The specimens were machined from No. 8 bars of the three grades of steel. This investigation was extended to find the variation in the metal properties in the cross-section of the bar by hardness tests and metallographic observations.

Chapter II of this report reviews the recent engineering literature on the fatigue strength of steel and the literature on the fatigue strength of reinforcing bars. The investigation, specimens, and testing procedure are discussed in Chapter III. The test data are presented in Chapter IV and Appendix A and are discussed in Chapter V. Chapter VI presents the main conclusions from this investigation.

CHAPTER II

SURVEY OF LITERATURE DEALING WITH THE FATIGUE STRENGTH OF STEEL AND THE FATIGUE STRENGTH OF REINFORCING BARS

2.1 Introduction and Nomenclature

Structural elements and machine parts subjected to large numbers of repeated loads will frequently fail due to "fatigue". A fatigue failure starts as a small crack which spreads across the member until the remaining metal fails in a brittle manner. Such cracks are generally initiated at points of high stress although the stresses required to cause a fatigue failure are generally much lower than the stresses corresponding to a static fracture of the same material.

The maximum stress which can be repeated a prescribed number of times without causing failure of a machine element or fatigue specimen is known as the fatigue strength, F , for the particular type of stress cycle and number of cycles under consideration. Although engineering parts are frequently subjected to a complex sequence of stress cycles in service, fatigue testing is generally carried out under uniform sinusoidal stress cycles or other very simple loading cycles.

Fatigue tests can be classified by the type of stress that is applied to the specimen. This action may be direct or axial stress, bending or torsion or combined stress. The literature review in this chapter will be limited to direct and bending stresses in steels similar to those used in reinforcing bars in reinforced concrete structures.

The most common test used to find the fatigue strength is the

rotating beam test in which completely reversed cycles of stress of constant amplitude are applied to the specimen, until failure occurs or until a prescribed number of cycles are endured. Standard shaped machined specimens are used in this type of test. When necessary, however, fatigue tests can be carried out on structural elements or machine parts. Such tests frequently involve other types of stress cycles.

The results of fatigue tests are plotted in the form of an S-N diagram (FIGURE 2.1). This is a curve relating the applied alternating stress or stress range and the logarithm of the fatigue life. As can be seen from the FIGURE 2.1, the fatigue life of the specimen decreases as the applied stress increases. In most ferrous metals, this curve becomes horizontal between 1 and 10 million cycles. The stress corresponding to the horizontal branch of the curve is known as the "Endurance Limit" or "Fatigue Limit" of the material. The stress corresponding to a given number of cycles is known as the "fatigue strength" for that number of cycles.

This discussion will be limited to factors affecting the endurance limit and/or the fatigue strength at 2 to 5 million cycles because this is the type of fatigue problem generally encountered in civil engineering structures.

2.2 Factors Affecting the Fatigue Strength of Machined Steel Specimens

2.2.1 Effect of Yield and Tensile Strength

Within the range of steel strength encountered in concrete reinforcing bars, it is generally accepted that the fatigue limit of conventional fatigue test specimens without stress concentration increases roughly in proportion to the tensile strength as shown in FIGURE 2.2.

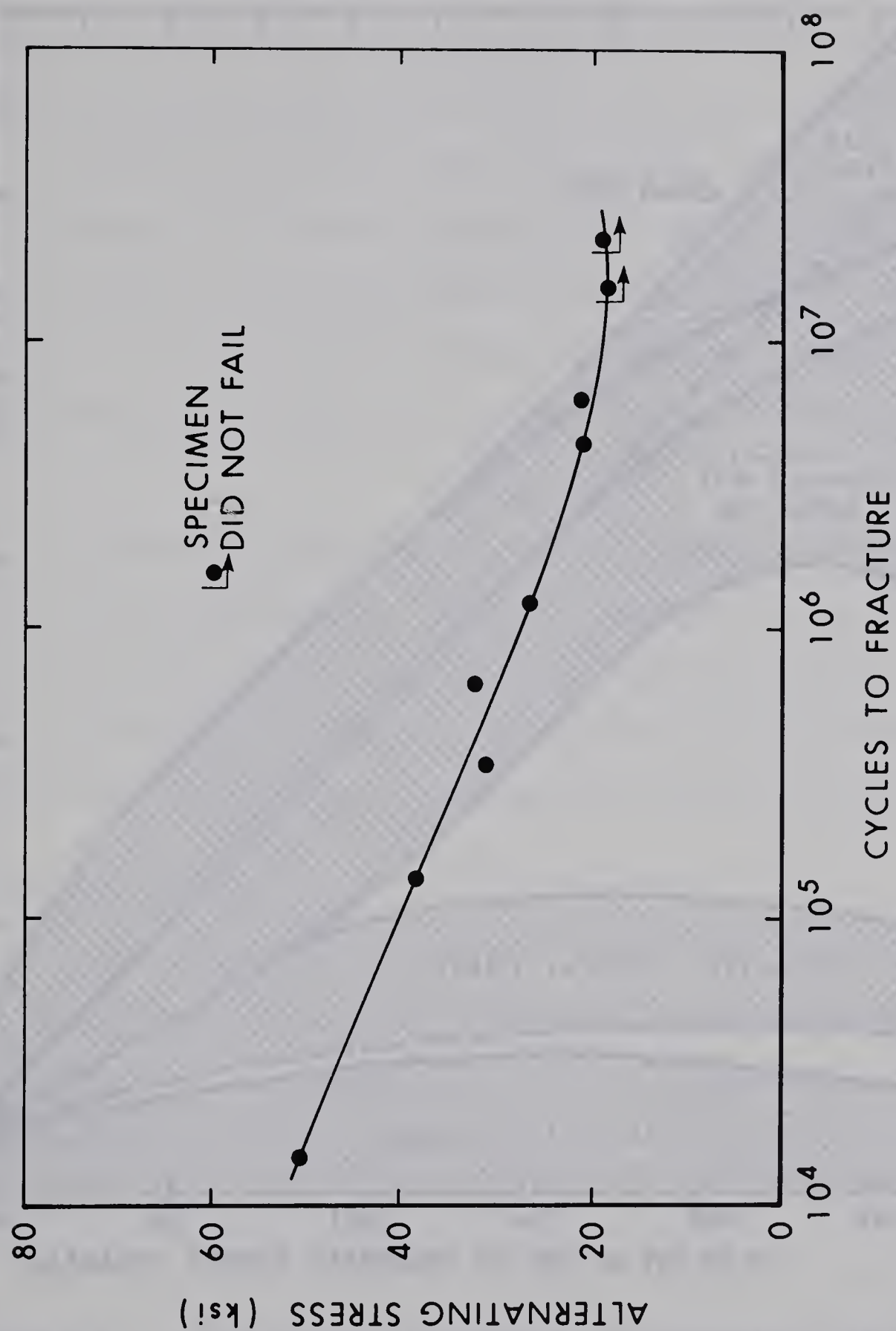


FIGURE 2.1 S-N CURVE FOR A FERROUS METAL

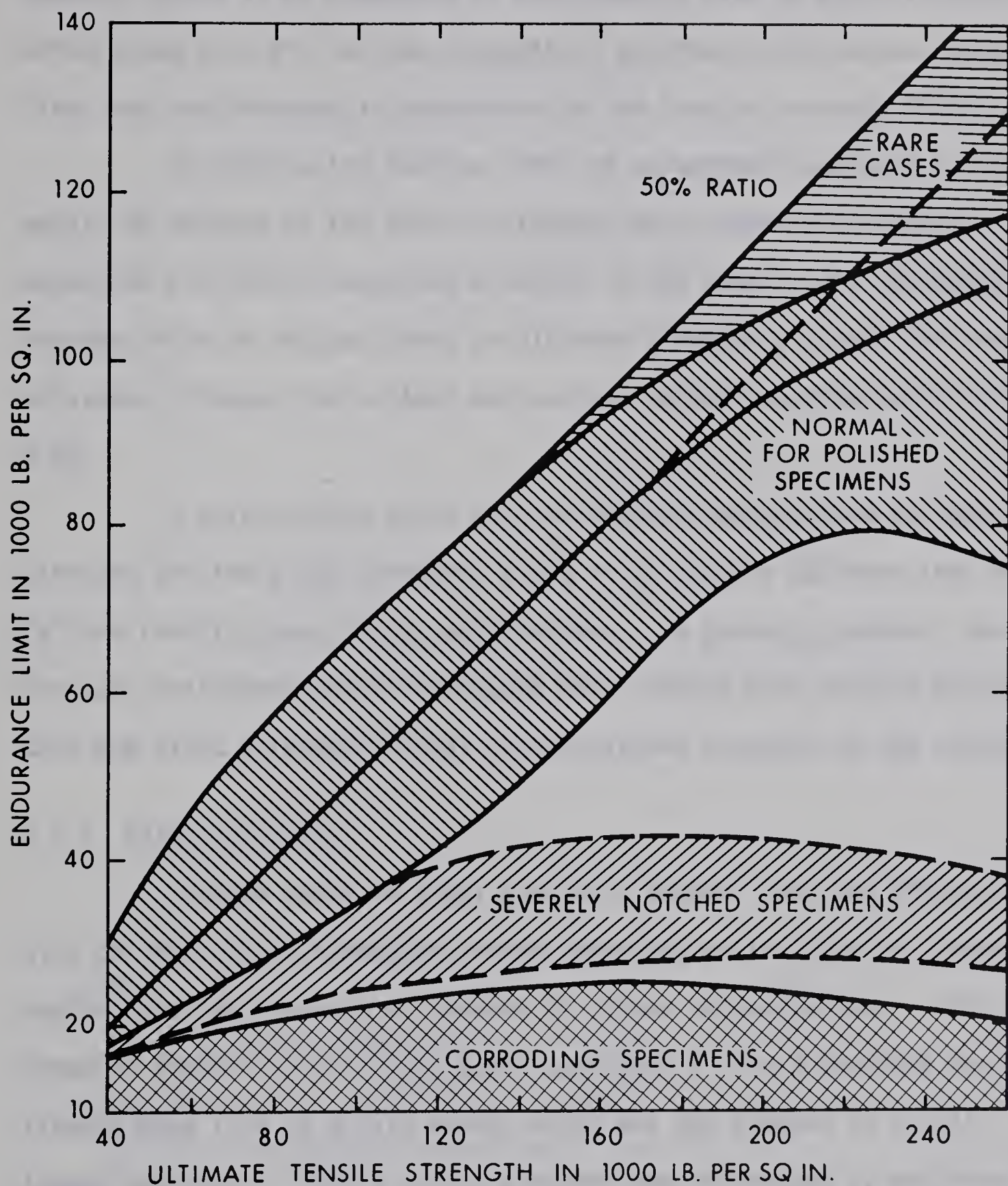


FIGURE 2.2

RELATIONSHIP BETWEEN THE ENDURANCE LIMIT AND ULTIMATE TENSILE STRENGTH OF VARIOUS STEELS

However, there is an abundance of experimental data on metal fatigue which shows that the fatigue strength of specimens with stress concentrations may not increase in proportion to the tensile strength (FIGURE 2.2).

In steels, the fatigue limit of un-notched specimens is approximately 50 percent of the tensile strength up to tensile strengths of about 200 ksi (29). Data from a survey of 288 steels (27) indicated an average ratio of fatigue limit to ultimate strength of 0.456 for reversal of stress although the minimum and maximum ratios reported were 0.23 and 0.65.

A relationship might also be expected between the fatigue strength and the yield strength, since it is usually believed that fatigue failure results from plastic deformations. In general, however, the fatigue limit seems to be correlated more closely with tensile strength than the yield strength in most investigations reported in the literature.

2.2.2 Effect of Size

Fatigue tests on steel specimens suggest that the effect of size on the fatigue strengths varies depending on the type of stress applied and the presence or absence of stress concentrations. This is shown in FIGURE 2.3 (21). In plain specimens a stress gradient due to flexure gave rise to a size effect which was not present in axially loaded specimens. When a stress gradient was introduced by notching the specimens, a size effect was also observed. It should be noted, however, that very little size effect was noted for diameters greater than one-half inch. Most reinforcing bars fall in the latter range and thus should not be affected severely by size.

The effect of size on fatigue strength has been explained in

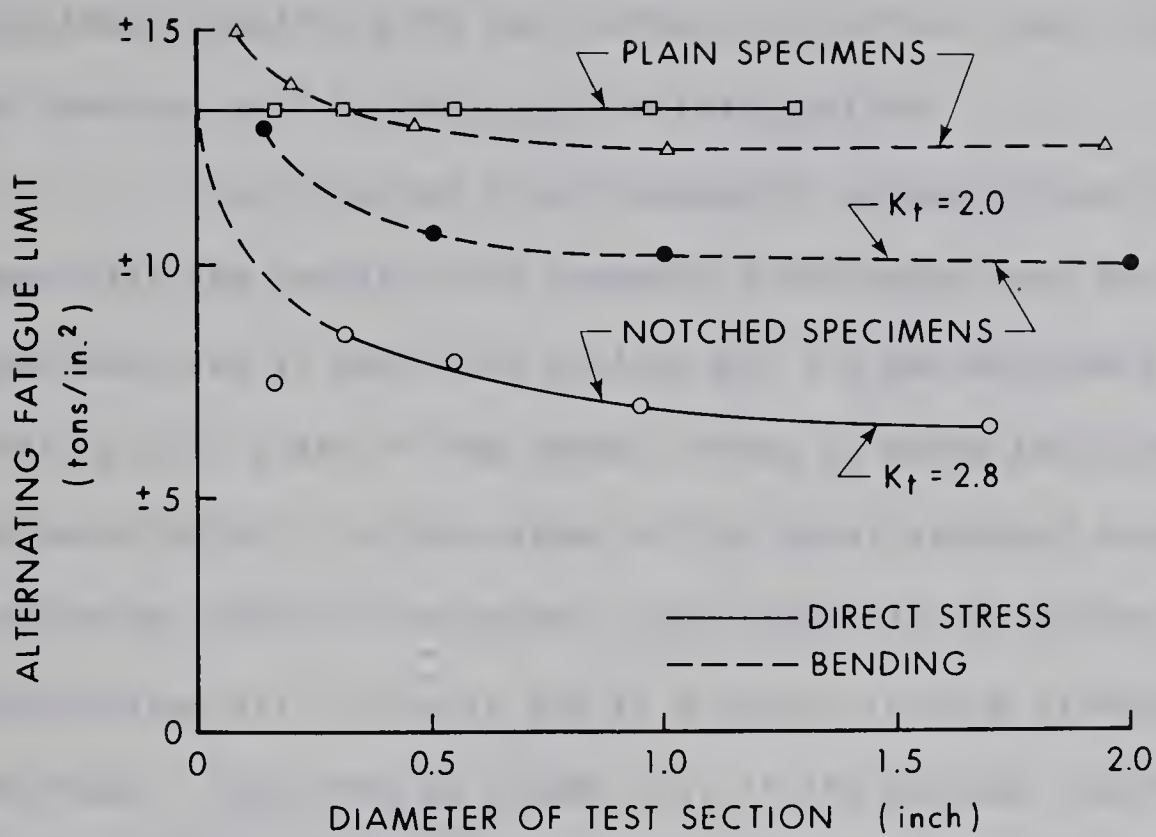


FIGURE 2.3 THE EFFECT OF SPECIMAN SIZE ON FATIGUE STRENGTH OF SPECIMENS, UNDER DIRECT STRESS AND BENDING(AFTER FORREST)

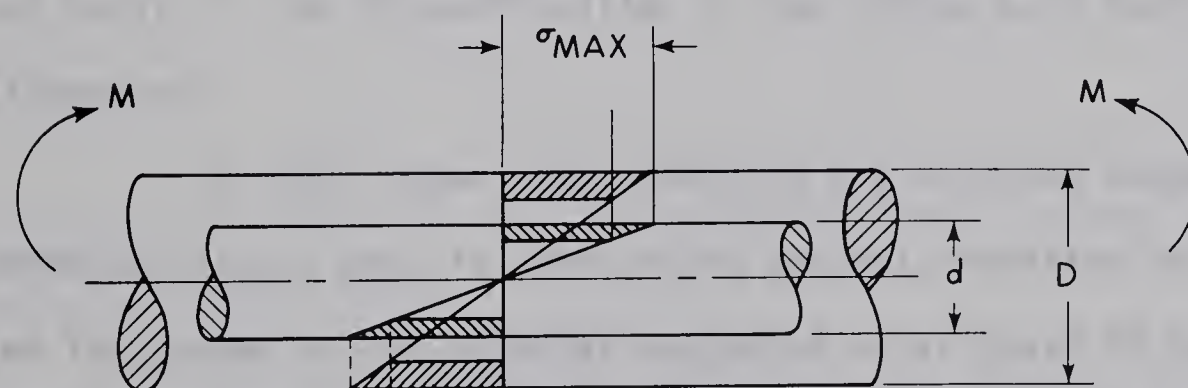


FIGURE 2.4 THE EFFECT OF SIZE ON FATIGUE STRENGTH.

the macroscopic view in terms of the "inherent flaw" hypothesis and by hypotheses dealing with the increase in surface area. These two types of theories will be discussed in this section.

The "inherent flaw hypothesis" suggests that if the inhomogeneities are sparsely but randomly distributed over the volume of the specimen, and if each such nucleus has its own endurance limit, no failure will start if the normal stress is below the appropriate endurance limits. As the volume of the metal stressed above the localized endurance limits is increased, the probability of having flaws in this region also will increase and as a result fatigue strength will tend to decrease. Referring to FIGURE 2.4, if the maximum flexural stresses are equal in the two bars, the bigger specimen has a larger volume subjected to stress greater than the endurance limit. Therefore on the basis of the inherent flaw hypothesis it should exhibit poorer fatigue strength.

Currently there is no agreement about the types of flaws which might be critical. Such things as inclusions, grains unfavorably oriented and point or line discontinuities in the lattice have been mentioned in the literature.

In 1961, Kuguel (19) examined the size and shape effect in existing fatigue data in terms of an analysis relating the fatigue strength and the volume of the material subjected to at least 95 percent of the maximum stress. He found a linear relationship between the logarithm of the appropriate volume and the fatigue life. This approach was found equally valid for smooth and notched specimens.

Russian tests (26) suggest two explanations for the reduction of fatigue strength due to an increase in the absolute dimensions of a

specimen. First, an increase in absolute dimensions increases the surface area, which is subjected to maximum stress in a bending or torsion test. This increases the probability of defects due to machining, blow holes, non-metallic inclusions and micro-cracks occurring in the surface layer. Secondly, the machining of the test specimens leads to considerable artificial strain hardening of surface layers and formation of compressive stresses near the surface. This effect is particularly marked on small test pieces, where the surface layer may represent a significant part of the volume and this could tend to increase the endurance limit of such specimens.

2.2.3 Effect of Notches

The fatigue strength of notched specimens depends in part on the size of the specimen, the stress concentration and the notch sensitivity of the metal. A considerable amount of work has been done on the effects of stress concentrations on fatigue (6,11) and the theoretical stress concentration factor (K_t) for some common shapes used in service have been analysed by the theory of elasticity and by photo-elasticity. Recently, Derecho and Munse (38) presented the curves reproduced in FIGURE 2.5 for protruding "external notches" having the shape shown in FIGURE 2.5(a).

The notch-sensitivity of a material relates the actual effect of a notch on the fatigue strength to the effect predicted using the theoretical stress concentration factor. The notch sensitivity 'q' is defined by Eq. (2.1).

$$q = \frac{K_f - 1}{K_t - 1} \quad (2.1)$$

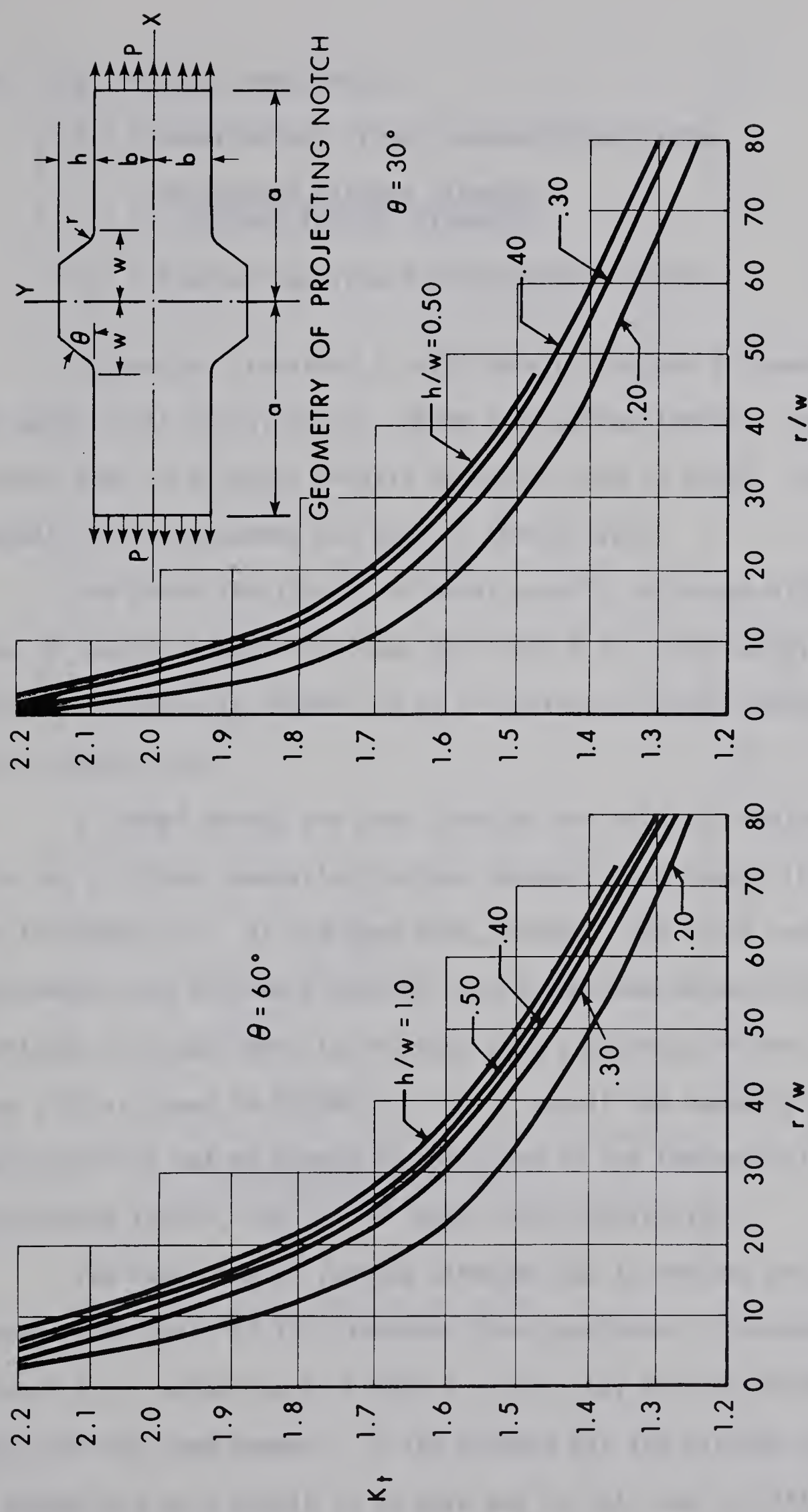


FIGURE 2.5
STRESS CONCENTRATION FACTORS FOR
PROJECTING NOTCHES. (DERECHO AND MUNSE)

where q = notch sensitivity
 K_f = experimental stress concentration factor
= $\frac{\text{un-notched fatigue strength}}{\text{notched fatigue strength}}$
 K_t = theoretical stress concentration factor.

Extensive literature is available on factors influencing the notch sensitivity (6,10,11,21). Among the various factors, the most important seem to be metal tensile strength, type of notch, size of component, stress gradient and type of stress cycle.

The notch sensitivity of steel usually increases with an increase in static strength as shown by FIGURE 2.2. Notch sensitivity factors are plotted in FIGURE 2.6 as a function of notch radius and steel strength (10).

If other things are kept constant the notch of smaller base radius has a higher theoretical stress concentration factor (K_t) as shown in FIGURE 2.5. At the same time, however, the notch sensitivity of specimens with different notches having the same theoretical stress concentration factor tends to decrease with a decrease in the notch radius (10) as shown in FIGURE 2.6. As a result the damaging effect of a sharp notch is not as severe as indicated by the theoretical stress concentration factor, due to the lower notch sensitivity.

The reduction of fatigue strength due to notches may be explained on the basis of the "inherent flaw hypothesis" discussed in section 2.1.2. Referring to FIGURE 2.7, bars (a) and (b) have been loaded with the same moment. In the notched bar the maximum stress is much higher and as a result it is more apt to fail due to fatigue. A

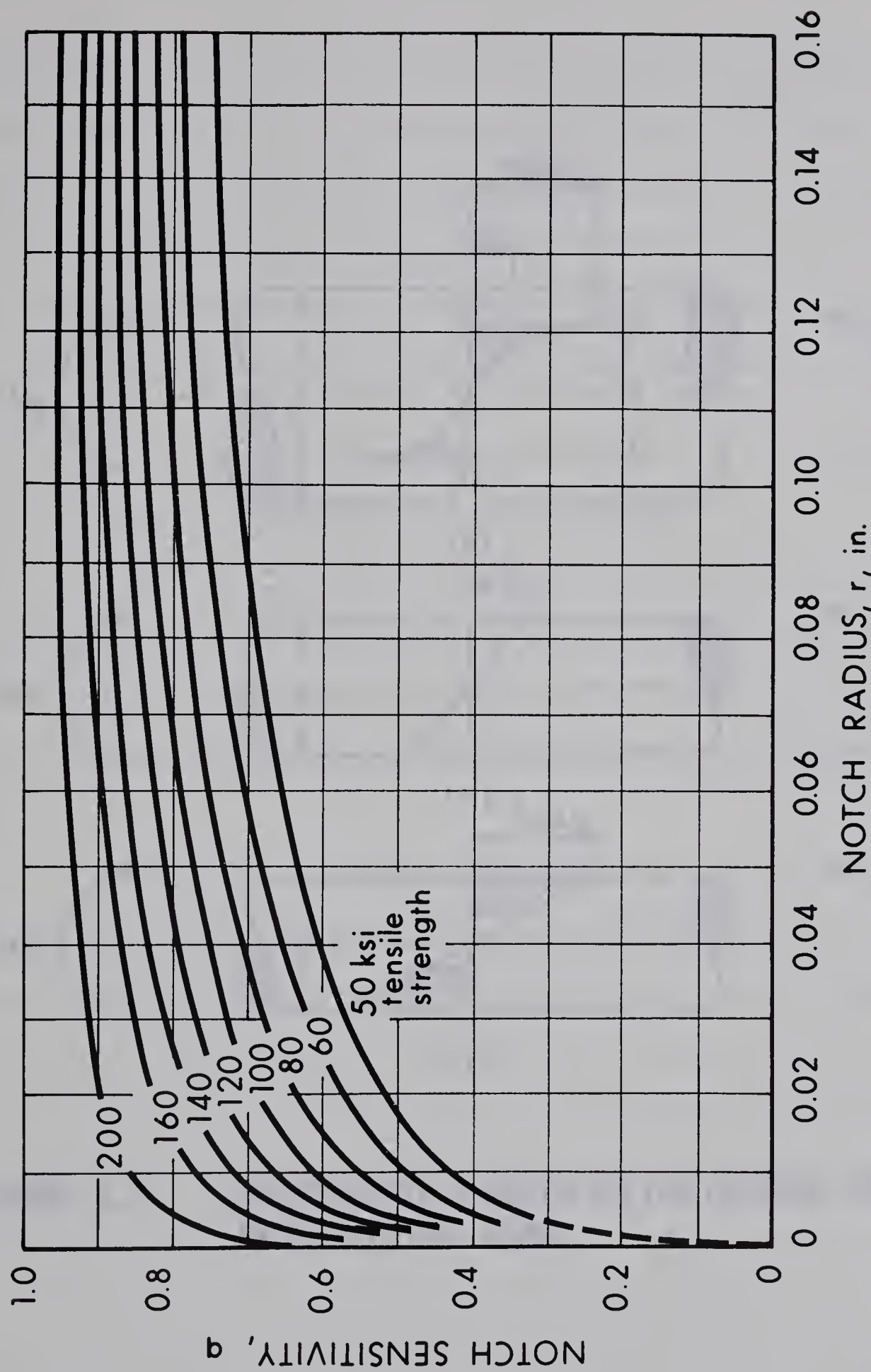


FIGURE 2.6
THE EFFECT OF NOTCH RADIUS ON NOTCH
SENSITIVITY (AFTER KUHN AND HARDRATH)

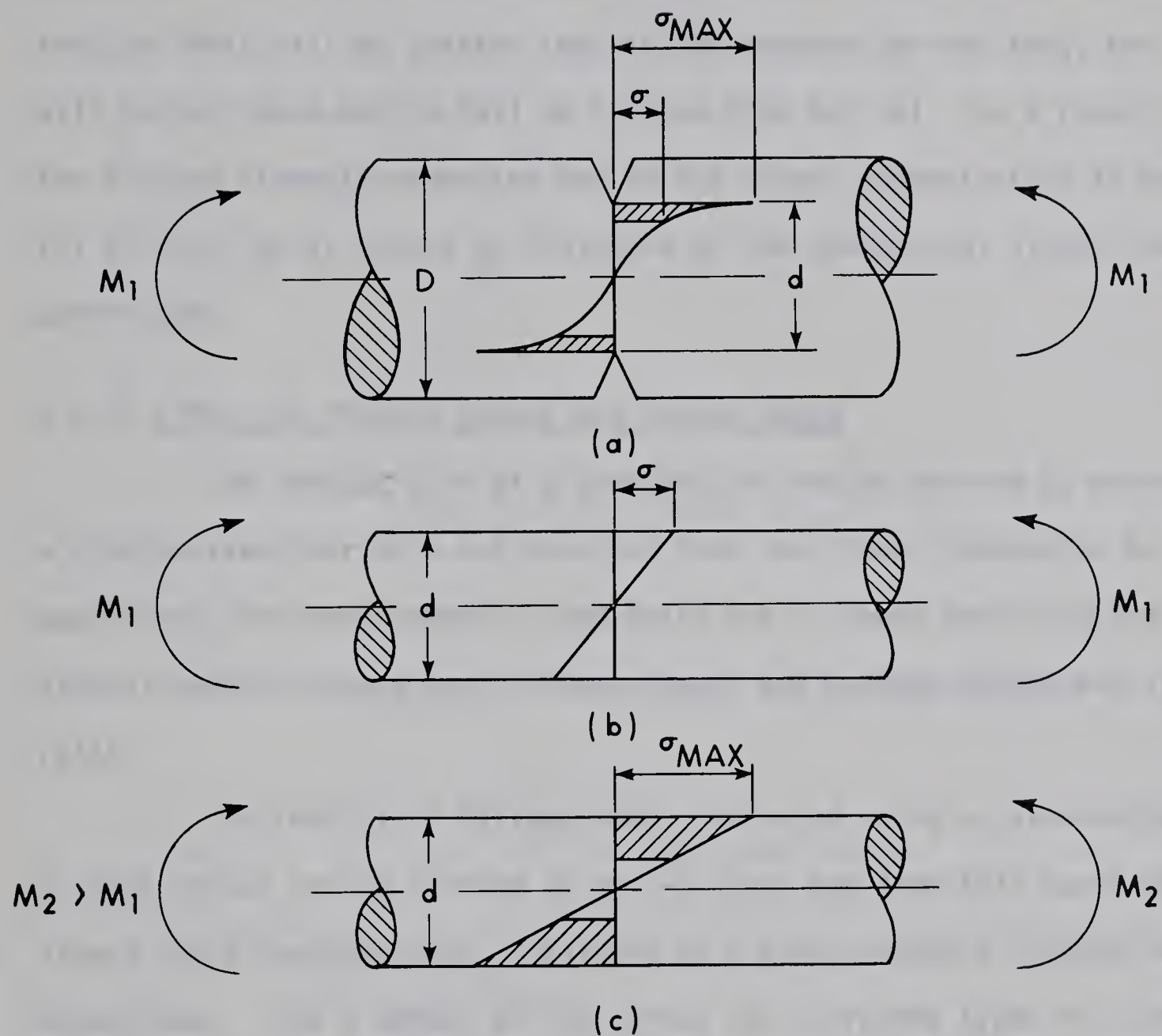


FIGURE 2.7

THE EFFECT OF A NOTCH ON THE FLEXUAL STRESSES
IN A ROTATING BEAM

comparison of bars (a) and (c), which are stressed to the same maximum stress shows that in the un-notched bar the volume stressed over the fatigue limit will be greater than in the notched bar and thus, bar (c) will be much more apt to fail in fatigue than bar (a). As a result, the fatigue strength reduction due to the stress concentration in bar (a) will not be as severe as indicated by the theoretical stress concentrations.

2.2.4 Effect of Minimum Stress and Stress Range

The fatigue life of a specimen can not be defined by means of a single stress variable but requires that two stress components be specified. The most commonly used pairs are: stress amplitude and mean stress; maximum stress and minimum stress; and maximum stress and stress ratio.

The results of fatigue tests conducted using a given minimum or mean stress can be plotted in an S-N curve and from this curve the stress cycle corresponding to failure at a given number of cycles can be determined. From a series of S-N curves for different types of stress cycles a relationship between the stress parameters in the cycle can be obtained for any given number of cycles. The data from different stress cycles can be summarized in diagrams similar to FIGURE 2.8 or 2.9. The most widely used empirical relations are given by Eq. (2.2) and Eq. (2.3) and are graphically illustrated in FIGURES 2.8 and 2.9.

$$\text{Modified Goodman Law: } S_a = S_{a(-1)} (1 - S_m/f_u) \quad (2.2)$$

$$\text{Gerber's Law: } S_a = S_{a(-1)} [1 - (S_m/f_u)^2] \quad (2.3)$$

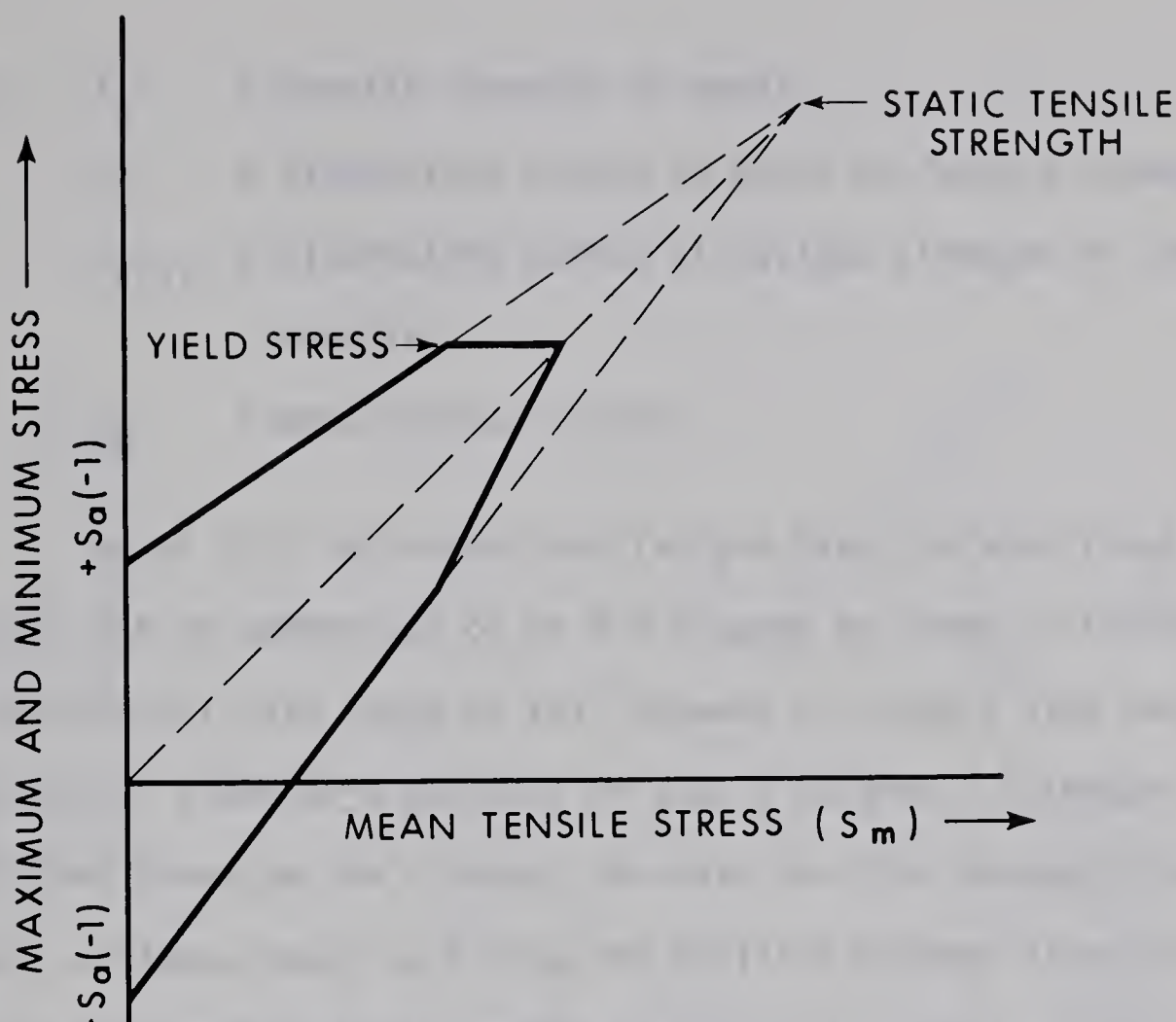


FIGURE 2.8 MODIFIED GOODMAN DIAGRAM

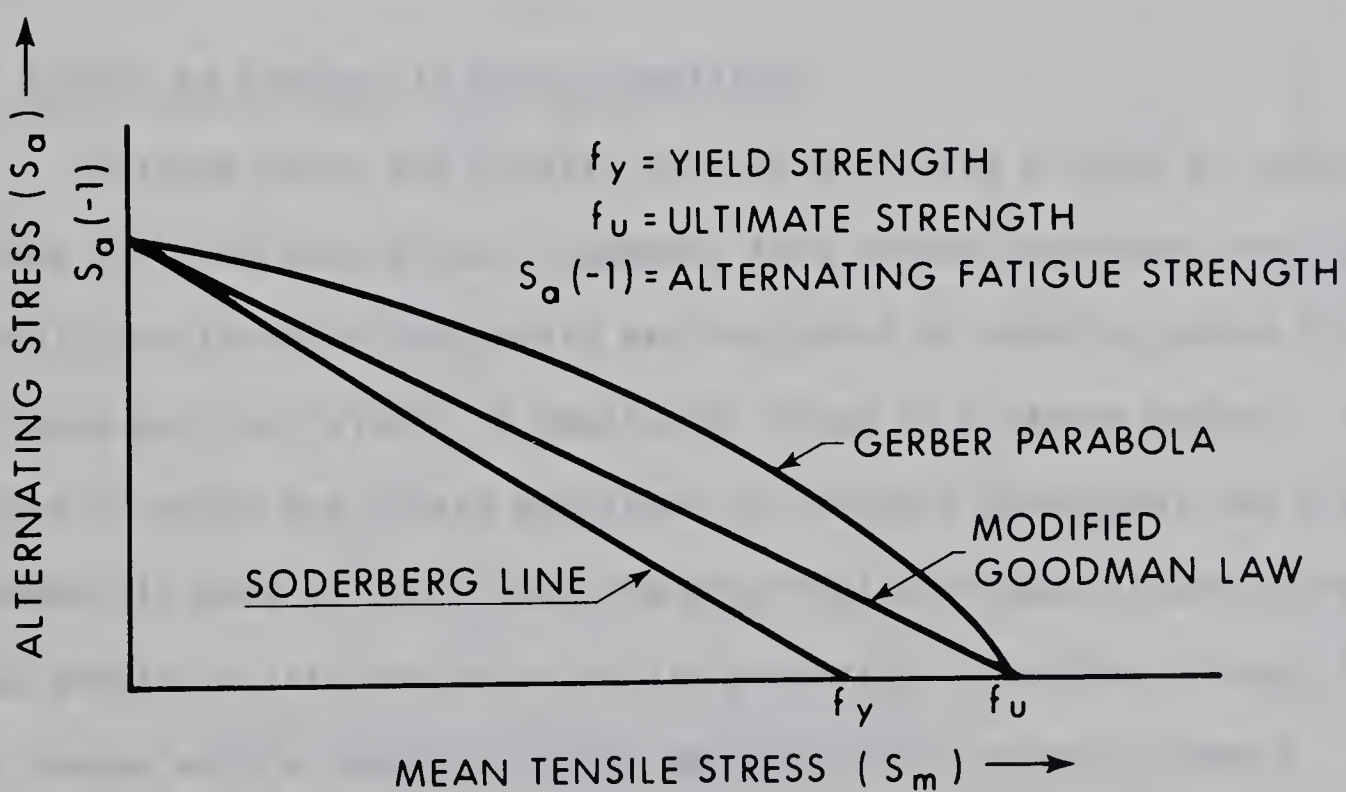


FIGURE 2.9 RELATIONSHIP BETWEEN THE ALTERNATING STRESS AND THE MEAN TENSILE STRESS

where f_u = tensile strength of metal
 S_a = alternating stress in cycle at fatigue strength
 $S_{a(-1)}$ = alternating stress at fatigue strength in complete reversal
 S_m = mean stress in cycle

Smith (21) has shown that fatigue data for wide range of materials can be summarized on an R-M diagram as shown in FIGURE 2.10. The experimental data tends to fall between a straight line and the equivalent of a Gerber's parabola on such a diagram. Although no well established trend can be claimed, the data for high strength steels and notched specimens tends to follow the Modified Goodman line while the data for cold worked steels tended to follow the Gerber parabola.

2.2.5 Effect of Changes in Stress Amplitude

Fatigue tests are usually carried out using a cycle of constant amplitude for each test piece. However, this seldom represents the loading conditions to which components are subjected in service, where fluctuating loads may vary widely in amplitude, often in a random manner. This situation in which the stress amplitude is constant throughout the life of a member is more critical than the more realistic case in which the maximum stress is attained in a certain percentage of cycles. Thus, a member loaded with a constant stress amplitude will normally have a shorter life for a given maximum stress.

The simplest method of predicting the fatigue life under varying stresses from the data of conventional fatigue tests is to apply Miner's Law (5) or linear damage law. In applying this theory it is assumed that

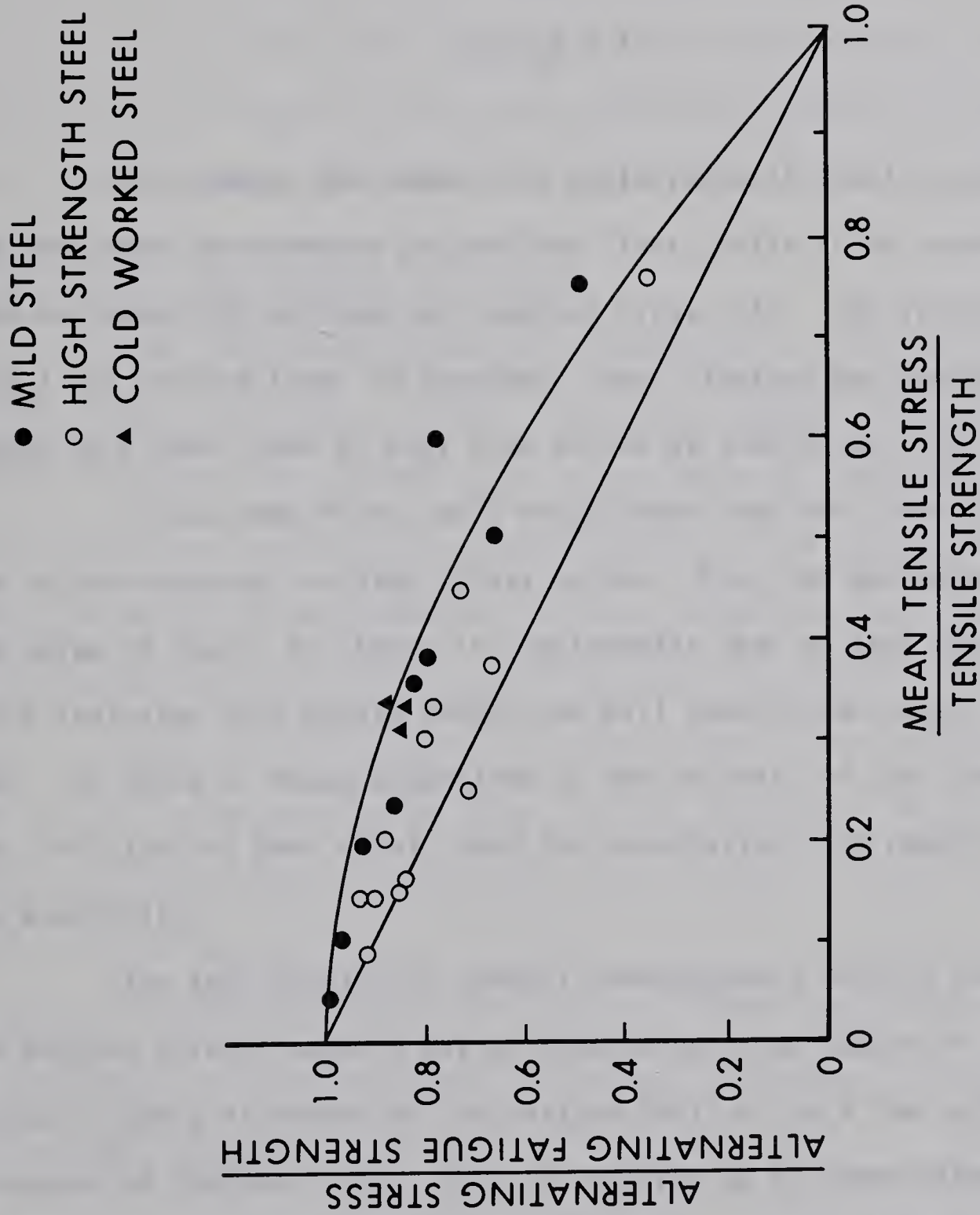


FIGURE 2.10
NON-DIMENSIONAL SMITH DIAGRAM FOR STEELS
(AFTER FORREST)

the application of n_1 cycles at stress range S_r for which the average number of cycles to failure is N_1 , causes an amount of fatigue damage n_1/N_1 and failure will occur when:

$$\sum(n/N) = 1 \quad (2.4)$$

For steels, the cumulative cycle ratio is usually greater than one when low stresses are applied first, while it is usually less than one when high stresses are applied first (21). The value of $\sum(n/N)$ for various types of specimens, mean stresses and sequences of stress have been found to vary from as low as 0.65 to as high as 2.26 (21).

It has been fairly well established that the linear damage law is not accurate for high stress ratios. Even for zero mean stress the value of $\sum(n/N)$ for tests is consistently near or less than one, which indicates that unsafe prediction will result from Miner's criterion (25). In spite of these objections to the validity of the linear damage law, this law has been widely used for correlating test results, due to its simplicity.

The test results of several investigators (20,21) conclude that the fatigue life of members may be reduced by large number of stress cycles slightly in excess of the fatigue limit or by a few cycles greatly in excess of fatigue limit. This is referred to as "over-stressing". The fatigue life on the other hand, may be raised by a large number of cycles slightly less than the fatigue limit and this is referred to as "under-stressing".

An even greater increase in the fatigue limit can be obtained,

if the stress range is increased in small increments at intervals of several million cycles. This process is known as "coaxing". Originally it was thought that the beneficial effect of under-stressing was due to strain-hardening, but recent tests (29) have shown that the fatigue strength can be increased in those materials, whose strength can be increased by strain-aging. The fatigue literature suggests that carbon steels benefit appreciably from under-stressing (21).

2.2.6 Effect of Frequency of Testing

Most fatigue testing machines operate at a frequency between 200 to 10,000 cycles/min. In this range, the fatigue strength of most metals is affected very little by testing frequency. The existing test data indicate that there is a slight decrease in the fatigue strength at low frequencies and low number of cycles. In general, however, the endurance limit was not affected by the testing frequency (13,27).

There are two factors, which may explain this behavior. First, the fatigue resistance may be related to the amount of plastic deformation which can occur during each cycle of stress. At high frequencies there is less time available during each cycle for deformation to occur, so that the resultant damage may be less. Second, the corrosion effect of atmosphere is known to reduce the fatigue strength of some materials and a bigger reduction would occur at low frequencies.

2.2.7 Effect of Metallurgical and Chemical Composition

Although studies of the mechanical properties of metal tested in fatigue failed to explain metal failure, recent investigations into the micro-structure and chemical composition of metals have led to the

following general conclusions (20,21,29):

1. The fatigue limit and fatigue notch sensitivity vary inversely as grain size.
2. The ratio of the fatigue strength of the tensile strength of steels is relatively insensitive to chemical composition.
3. Metals used in engineering are likely to be anisotropic, therefore scatter of test results is an inherent property of these metals.

2.2.8 Effect of Mill Scale and Decarburization

Munse (27) reports that the fatigue strength of as-rolled plates and plain rolled members of structural steel have fatigue strengths proportional to the ultimate strength of the metal. For zero to tension load, $R = 0$, he proposes the following relationship between the tensile strength and the fatigue strength at 2 million cycles for this type of member:

$$F_{2,000,000} = 20 + \frac{\text{Ultimate Tensile Strength}}{4} \text{ ksi} . \quad (2.5)$$

For other conditions of loading he suggests the fatigue resistance may be estimated using the equation:

$$F = \frac{2.2 F_r}{1.2 - R} \quad (2.6)$$

where F = fatigue strength for particular value of R

F_r = fatigue strength for $R = -1$

R = algebraic ratio of minimum to maximum stress in cycle.

For completely reversed stress cycles, $R = -1$, Eq. 2.5 can be rewritten as:

$$F_{r2,000,000} = 11 + \frac{\text{Ultimate Tensile Stress}}{7.2} \text{ ksi} . \quad (2.7)$$

This should be compared with the average ratio of 0.48 to 0.50 reported in section 2.2.1 for un-notched machined surfaces.

The reduced fatigue strength of as-rolled plates is believed to be caused by three factors:

1. The roughness of the surface (2).
2. The irregular and brittle mill-scale coating. If cracks developed in this layer during fatigue loading they could act as stress-raisers for the metal at the surface of the plate.
3. The decarburization of the surface layer due to exposure to air during cooling (1,2,3,7,12).

Of these three, the latter appears to be very significant.

Decarburization removes some of the carbon from the surface of a bar or plate leaving a surface layer of relatively soft, weak ferrite. Fatigue cracks tend to start earlier in this layer than they would in the base metal due to the lower strength of the layer. At the same time, however, the surface tends to become less notch sensitive because of its lower strength and greater ductility. The overall effect is generally a reduction in the fatigue strength of structural steels or steels having a composition similar to reinforcing bars.

2.3 Fatigue Tests on High Strength Deformed Bars as Concrete Reinforcement

Unlike metal fatigue failure in machinery and aircraft components, few fatigue failures of the reinforcement in reinforced concrete beams have been recorded. The probability of fatigue failure of concrete structures due to the fracture of tensile reinforcement has increased with the use of high strength deformed bars as concrete reinforcement, however. For this reason, extensive tests have been carried out. These tests on the fatigue behavior of reinforcing bars may be classified into following categories:

- (a) Tensile fatigue tests on un-embedded reinforcing bars in air.
- (b) Tensile fatigue tests on reinforcing bars embedded in concrete.
- (c) Bending tests on reinforced concrete beams with the bar to be tested acting as tensile reinforcement.

The methods (a) and (b), though convenient and less expensive, do not represent the actual stress conditions. Therefore the test results are not directly applicable for design. These testing procedures may be useful in comparing the influence of various factors on the fatigue resistance but, because the laws of geometrical similitude do not always apply in fatigue, the results obtained from these tests must be used with caution.

The testing procedure listed in (c) is intended to produce a fatigue failure of a reinforced concrete beam due to fatigue fracture of the tensile reinforcement in the beam. This procedure is a good representation of steel stresses in structural members, and therefore has been widely adopted. The results from beam tests can be used for finding safe permissible stresses, after applying appropriate factors of safety.

In fatigue tests on reinforced concrete beams loaded in flexure, the concrete cracks in the tensile zone and almost the full tensile force is transferred to the reinforcement. In this cracked zone, it is expected that the fatigue behavior of the tensile reinforcement will be similar to general metal fatigue, already described in section 2.2. The following sections examine the influence of various parameters on the fatigue resistance of reinforcing bars in concrete beams loaded in flexure.

2.3.1 Modes of Failure Observed in Fatigue Testing of Reinforced Concrete Beams

The fatigue behavior of reinforced concrete beams is complex due to the various modes of failures which are possible. In general, a concrete beam subjected to repeated loads may fail in the following modes:

- (a) Fatigue fracture of the tensile reinforcement.
- (b) Bond failure between the reinforcement and the concrete (8,22).
- (c) Crushing of the concrete in the compression zone.
- (d) Diagonal tension failure of the concrete (13,14).

The mode of failure of reinforced concrete beams under static or repeated loads is strongly dependent on the properties of beam and loading conditions. For most beams designed according to the current codes, the fatigue strength of the reinforcement will limit the fatigue strength of the beams and thus most of the research work in this field has been oriented towards a study of the fatigue strength of tensile reinforcement. The present investigation is also limited to a study of this failure mode.

2.3.2 The Effect of Concrete Encasement

Although it would be easier to test individual reinforcing bars in air than it is to test them in beams, a number of authors have suggested that the fatigue strength may differ in the two cases. The literature on this is somewhat contradictory.

To understand the effect of concrete encasement on the fatigue behavior of reinforcement, it is useful to examine the beam under flexural stresses. Since concrete is weak in tension, a small load on the beam produces cracks in the concrete tensile zone. The concrete tensile forces are fully transferred from the concrete to the steel at each crack. There is an abundance of experimental data available to show that in a fatigue test the tensile reinforcement will fracture at or very near such a crack. This can be attributed to the fact that between cracks part of the tension is carried by the concrete so that the maximum stresses in the bars occur at cracks. The variation in stress along bars in cracked concrete was studied by Washeidt (34).

Rehm (15) conducted fatigue test on smooth and deformed bars in air as well as in beam specimens. The test results showed that the fatigue strength of an embedded bar in a beam test was lower than that for the same bar tested in tension in air. Similar test results have been reported by Meyer (36).

Contrary to Rehm's findings, however, tests on ribbed TOR-STAHL bars reported by Soretz (32), showed that embedded bars in beam tests had a fatigue strength at least 10 percent higher than similar bar tested in air. He concluded that the fatigue resistance of embedded bars increases with increasing efficiency of bond and suggested that the poorer

fatigue resistance of embedded bars found in the earlier investigation was due to deficient bond. Soretz supports his test results with the following explanations:

1. The calculation of steel stresses are made assuming the fully cracked state and neglecting bond. The actual steel stresses are usually lower, as is known from several investigations. This difference increases with increasing efficiency of bond.
2. The cracks do not close after removal of the load, because small grains of material lodge between the faces of cracks. Hence the minimum steel stress in the bar will be higher than that calculated from the minimum load. This will lead to higher fatigue strength.
3. In a bar tested in air, the weakest section determines the failure, whereas in a beam failure always occurs at a crack. There is a low probability that a crack and the weakest part of the bar will coincide, and failure therefore occurs at higher stress.

Wascheidt (34) provides excellent information on the effect of embedment on the fatigue strength of plain and deformed bars in concrete prisms and beams. His test results for a variety of plain and deformed bars tested in air and embedded in concrete prisms are shown in FIGURE 2.11.

The factor f_R is defined as:

$$f_R = \frac{\text{rib area projected on a cross-section of the bar}}{\pi \text{ (bar diameter)} \text{ (rib spacing)}}$$

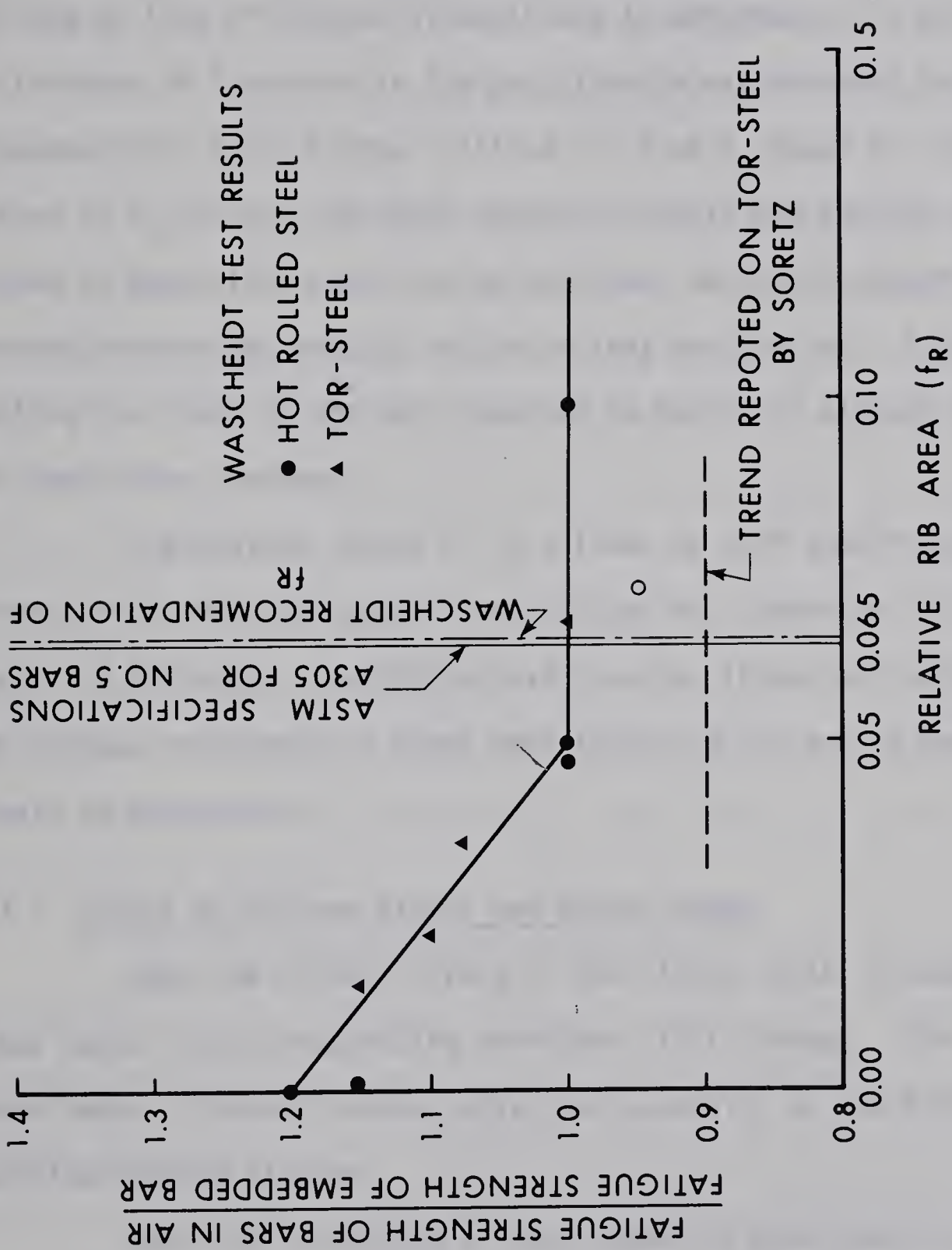


FIGURE 2.11
THE EFFECT OF CONCRETE ENCASEMENT ON FATIGUE STRENGTH
OF NO. 5 REINFORCING BARS.

FIGURE 2.11 shows that as the relative rib area is reduced below .05 the fatigue strength is reduced, presumably because the bond resistance is lower. Bars having relative rib areas, f_R , greater than .05 had no loss of fatigue strength due to embedment. In the beam tests, an increase of 6 percent in fatigue strength was observed due to concrete encasement for a bar having relative rib area f_R equal to .069. Since values of f_R for the TOR-STAHL tested by Soretz and the bar tests reported by Meyer (36) could not be obtained, no direct comparison could be made between the results of the various test series. A line representing the trend of the data reported by Soretz is plotted in FIGURE 2.11 for comparison, however.

The minimum values of f_R allowed by ASTM specification for deformations A 305 (24) ranges from .058 for No. 3 bars to .077 for No. 11 bars. On the basis of existing test results, it may be concluded that the fatigue resistance of these bars tested in air and in beam tests should be comparable.

2.3.3 Effect of Minimum Stress and Stress Range

When the minimum stress of the stress cycle is changed in fatigue tests, the corresponding endurance limit changes. The results of tests under different stress cycles can generally be correlated using a Modified Goodman Diagram.

Rehm (15) conducted a large number of experiments on beams reinforced with high strength deformed bars from which he concluded that the stress range is insensitive to the minimum stress level, unless the maximum stress approaches the yield stress. Similar conclusions were drawn by Fisher and Viest (17).

From tests of hot rolled bars of various yield strengths in beams similar to those used in the present investigation Pfister and Hognestad (28) concluded that the stress range was relatively insensitive to minimum stress level. Although this was true, their data does fall close to the straight line envelopes in the Goodman Diagrams plotted in FIGURE 2.12, 2.13 and 2.14.

The results of Wascheidt's tests (34) on unembedded High-Bond steel and Rippen-TORSTAHL are summarized in FIGURE 2.15 and 2.16. These two steels differed in their manufacturing process, the High-Bond steel being hot rolled, while the Rippen-TORSTAHL was hot rolled and cold twisted. FIGURES 2.15 and 2.16 differentiate between the fatigue behavior of these two steels.

The type of behavior illustrated in FIGURE 2.16 corresponds to that reported by Rehm (15) and Fisher and Viest (17). This type of behavior is not common in general metal fatigue, but it seems to occur more frequently in cold worked steels, where the yield strength is close to the tensile strength.

For high strength reinforcing steels of the types covered by the ASTM A 431 and A 432 specifications it appears that the fatigue strength for different stress cycles should vary according to a Goodman Diagram of the type shown in FIGURES 2.12 to 2.15. For this reason design rules for high strength bars in fatigue loading should not be specified in terms of a constant stress range because such a rule could become unsafe if the minimum stress increases.

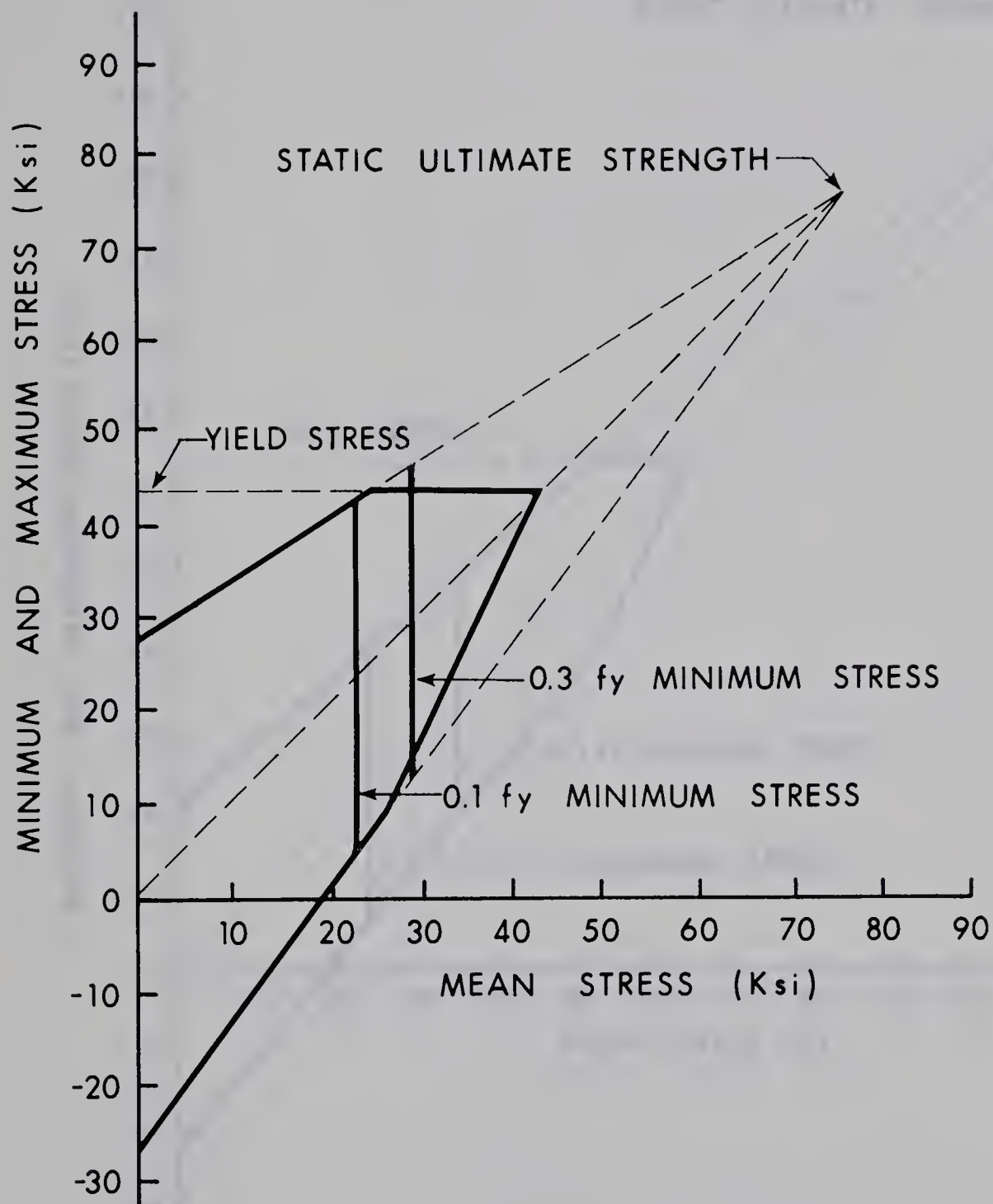


FIGURE 2.12

MODIFIED GOODMAN DIAGRAM FOR NO. 8 ASTM
A-15 BARS AT 2 MILLION CYCLES
(DATA FROM PFISTER AND HOGESTAD)

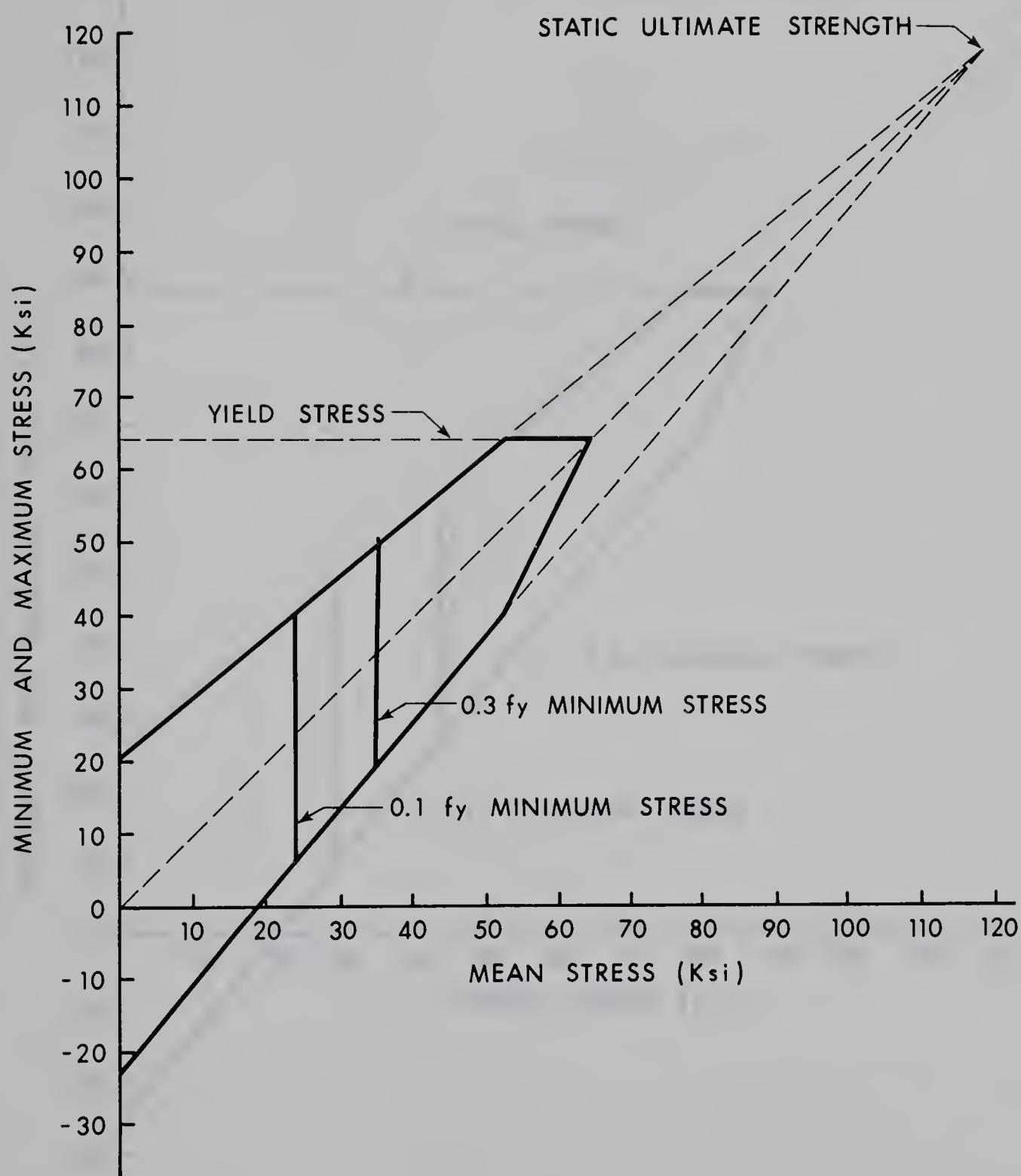


FIGURE 2.13

MODIFIED GOODMAN DIAGRAM FOR NO. 8 ASTM A-432 AT
2 MILLION CYCLES (DATA FROM PFISTER AND HOGNESTAD)

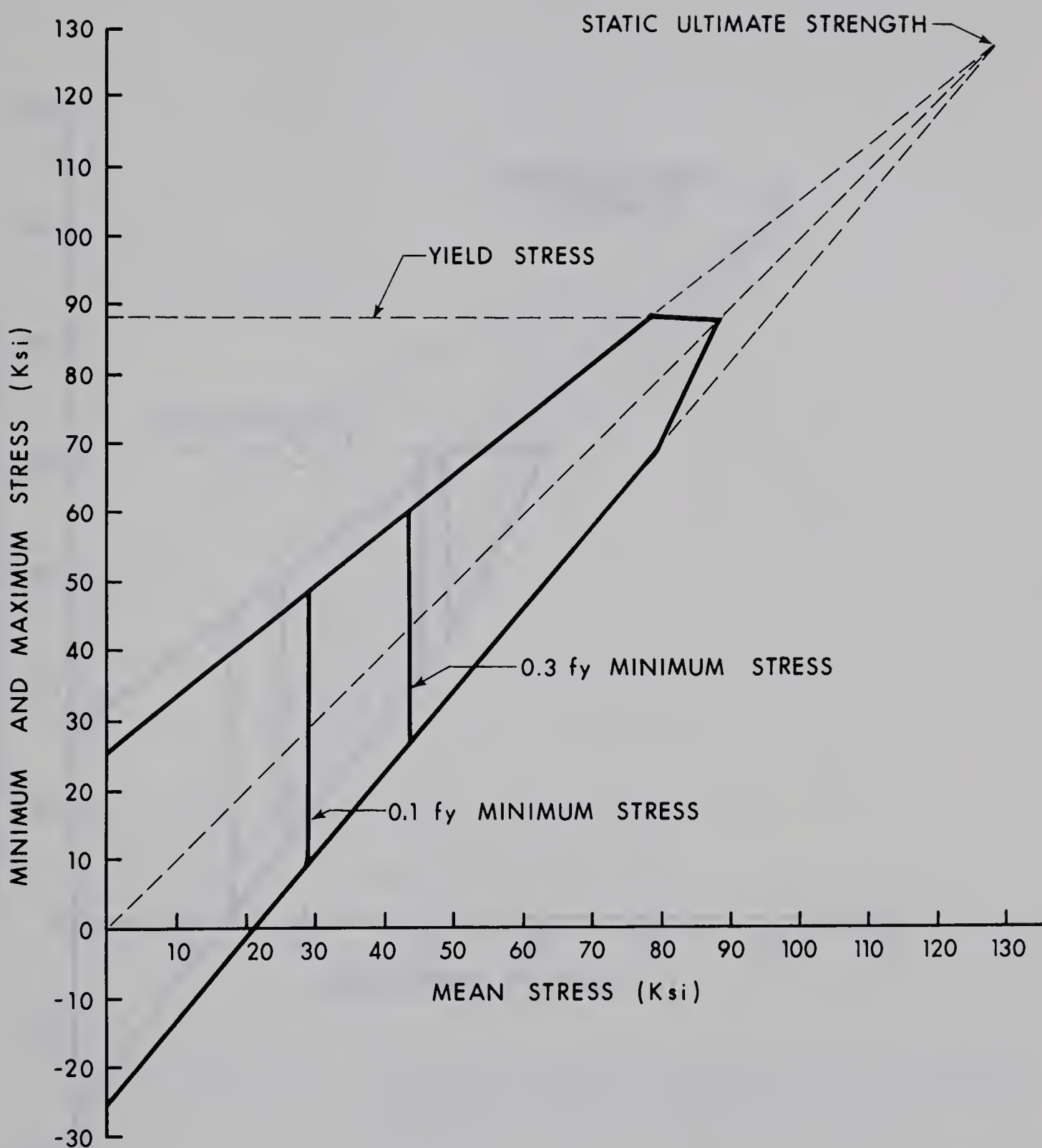
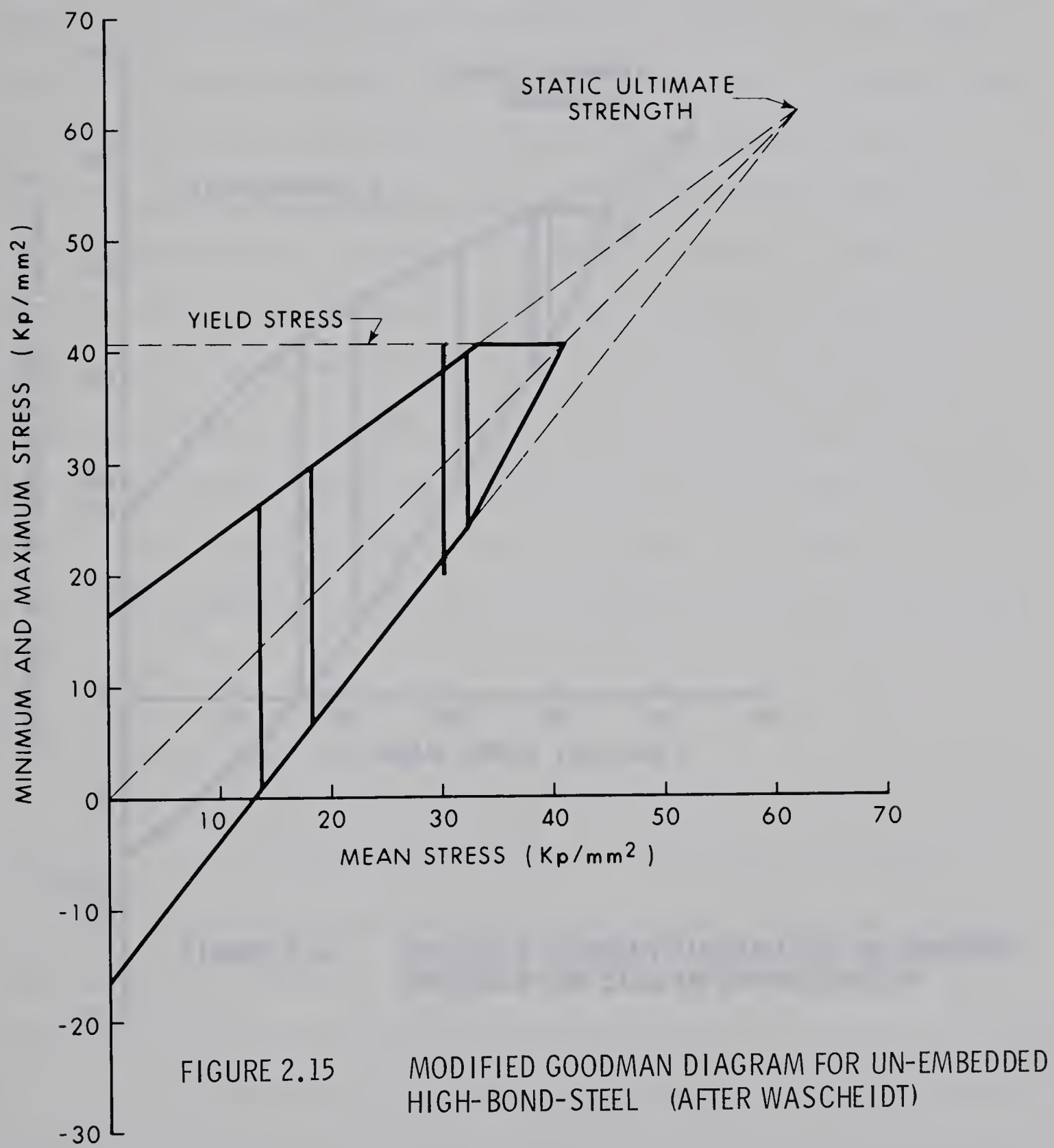
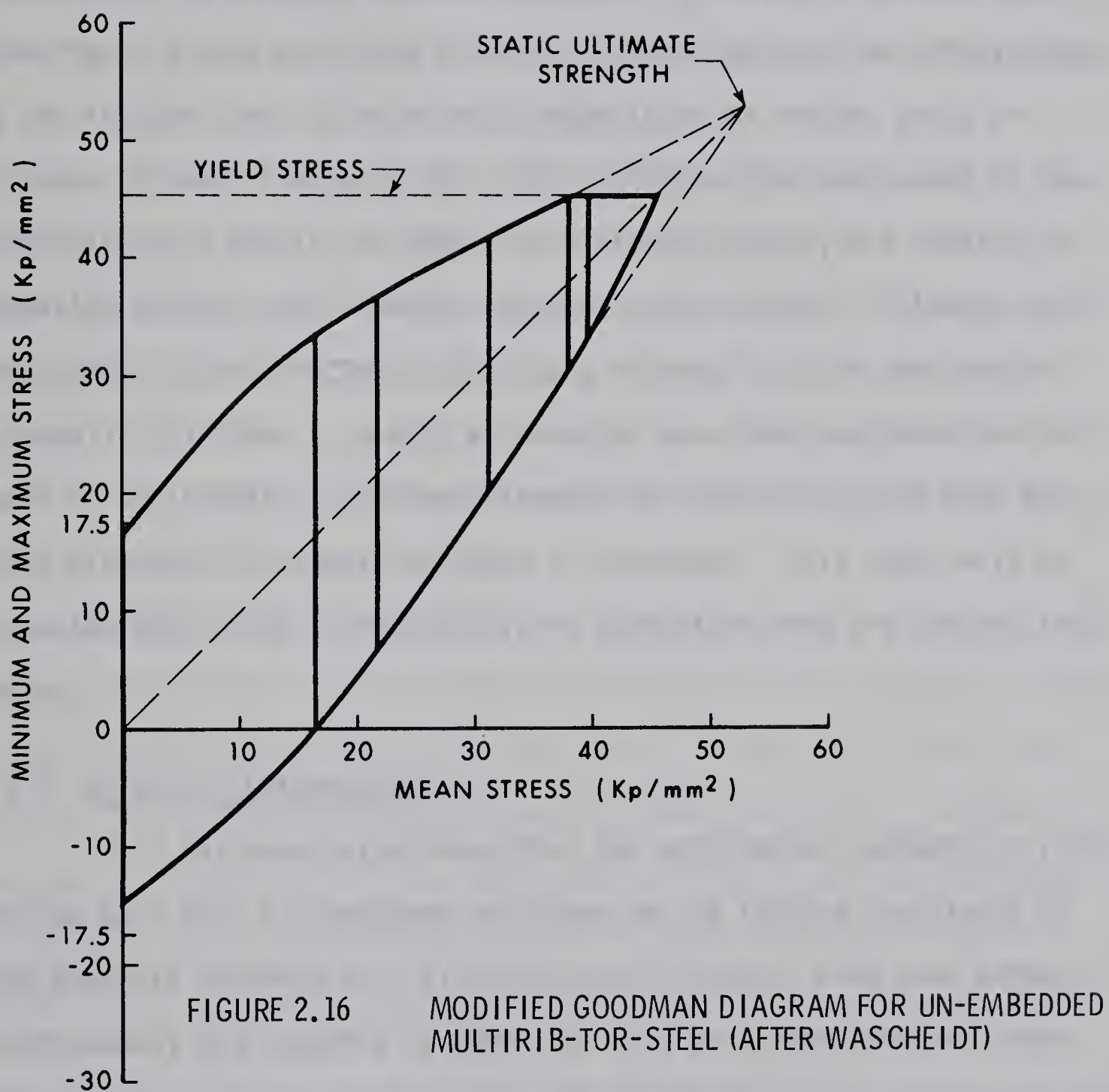


FIGURE 2.14 MODIFIED GOODMAN DIAGRAM FOR No. 8 ASTM A-431 BARS AT 2 MILLION CYCLES (DATA FROM PFISTER AND HOGNESTAD)





2.3.4 Effect of Yield and Ultimate Strength

In the preceding discussion of the fatigue of metals it has been seen that fatigue strength depends upon the yield strength or more commonly on the ultimate tensile strength. In contrast to this, most investigators have concluded that for reinforcing bars the stress range at the fatigue limit is relatively insensitive to the bar yield or ultimate strength (28,33,34,40). This inference has been drawn by comparing the test results of steels of different grades, but similar deformation pattern, bar diameter and beam cross-section. Although this conclusion is contradicted by test data reported by Lash, Macleod and Blackwell (31) there is enough evidence to show that designers can not count on an increase in fatigue strength of reinforcing bars when the yield strength or ultimate strength is increased. This topic will be discussed more fully in Section 5.2 in connection with the present test series.

2.3.5 Effect of Deformations

It has been established that the deformation patterns on reinforcing bars have a pronounced influence on the fatigue resistance of high strength deformed bars (15,28,32,33,34,39,40). Good bond between reinforcement and concrete is important in a reinforced concrete beam if the two materials are to work together in the manner assumed in design. As a result, the deformation patterns currently in use in North America were designed on the basis of good bond resistance and ease in the manufacturing process. However, the deformations, which, on one hand are responsible for superior bonding properties, act as stress-raisers on the other hand. Under normal stress conditions, the static strength of de-

formed bars is not significantly affected by the stress concentrations because local yielding leads to a redistribution of stresses in the regions of high stress. Under a cyclic loading, however, the fatigue strength will be decreased by the stress concentrations. This effect should be more pronounced in the case of high strength steels which generally are more notch-sensitive (see Section 2.2.2).

Investigations of the effects of the deformation pattern on the fatigue strength of reinforcing bars have been carried out in the United States, Germany, Japan and Austria. In these investigations bars having some deformation patterns had up to 85 percent higher fatigue strength than others. In general, the fatigue strength decreased as the severity of the deformation pattern was increased with plain bars generally having the best fatigue strength.

These investigations suggest that the geometrical details of deformations play an important role in establishing the fatigue strength of reinforcing bars. On the basis of stress concentration theory and observations on the fatigue failures of reinforcing bars, it appears that the radius at the base of the lugs, the lug height, the angle between lugs and the bar axis, and the intersection of transverse and longitudinal lugs significantly influence the fatigue characteristics of deformed bars.

2.3.5.1 Effect of Lug Base Radius and Lug Height

It is well known that regions of high stress concentrations are points of metal fatigue weakness. Deformed reinforcing bars have a variable cross-section along their length and stress peaks are produced at the discontinuities. In Section 2.2.3, it was seen that the stress concentration due to a projecting lug was a function of the radius at the base

of the lug, its height and width, and the angle of its faces. Of these factors, the radius at the base of the lug had the major effect, with the stress concentration increasing as the radius is decreased. This is illustrated in FIGURE 2.5.

The stress concentration theory has been partially supported by the fatigue test results on reinforcing bars. Deformed reinforcing bars provided with a smooth transition curve at the lug bases were found to be superior in fatigue resistance compared to bars with an abrupt change in slope at the lug base (40). In addition it has been seen that an increase in the ratio of the lug base radius to lug height leads to an increase in the fatigue resistance of reinforcing bars (39,40).

Kokubu and Okamura (40) have reported stress concentration measurements on a variety of hot rolled deformed bars produced in Japan. The strain measurements were made at the lug bases using electric strain gauges under static load. The test program included 14 varieties of deformation patterns having lug base radii ranging between 1 to 9 times the lug height. Strain measurements at the lug bases under static load showed a decrease in the stress concentration with an increase in the lug base radius.

The effect of the ratio of the base radius to the height of the deformation lugs was found to be a significant variable in these tests. This variable is discussed in Section 5.4 in connection with the present test series. In Kokubu and Okamura's tests of 50 ksi yield strength bars the fatigue strength increased from 35 percent of the tensile strength for a base radius to lug height ratio of 0.1 to about 48 percent for a ratio of 1.0 or greater.

Any attempt to minimize the reduction in fatigue strength due to deformations will necessitate an increase in the ratio of lug base radius to the lug height. On the other hand, this will significantly reduce the bonding properties of the deformed bars. In pull out tests by Komubu and Okamura (40) the bond strength of deformed bars having lug base radii ranging from 2 to 5 times the lug height was 40 to 54 percent lower than for bars having lug base radii smaller than the lug height.

2.3.5.2 Effect of Lug Inclination

The angle of inclination between the lugs and the bar axis may influence the stress concentration produced by the lugs. When the lugs are perpendicular to the bar axis, the lug bases which are points of fatigue weakness are concentrated at the same cross-section. As a result their damaging influence is concentrated at one cross-section. A decrease in the angle between the lug and the bar axis should improve the fatigue strength of reinforcing bars by spreading the stress concentration along some length of bar. Perhaps equally important is the fact that a decrease in the angle between the lug and bar axis would lead to an increase in the effective radius at the base of the lug when this is measured parallel to the axis of the bar.

In fatigue tests on cold worked TOR-STAHL (32), it was observed that a decrease in the inclination of the helical ribs to the bar axis improved the fatigue resistance of the bars. Similar observations have been made on hot rolled steel by Kokubu and Okamura (40). Their test program included deformed bars having lug inclinations of 30° to 90°

to the bar axis. The test results are summarized in FIGURE 2.17. The fatigue strength of bars having an abrupt change in the slope at the lug bases increased with a decrease in the angle between the lug and the bar axis. On the other hand, the fatigue strength of bars having smooth transition arcs at the lug bases with radii between 2 to 5 times the lug heights were unaffected by the variation in the inclination of the lugs to the bar axis. This observation may be explained on the basis of relatively small stress concentration due to large base radii, such that the effect of concentration of fatigue weakness at the same cross-section may not be significant.

By providing large radii at the bases of the lugs and decreasing the inclination of the lugs to the bar axis of bonding properties of the bar will be reduced but the fatigue resistance will increase. Since the fatigue resistance of the bars with a ratio of base radius to lug height greater than 2 was found to be unaffected by the inclination of the lug to the bar axis, it would be desirable to keep the maximum inclination of the lugs to the bar axis for better bonding properties.

2.3.5.3 Effect of Intersection between Longitudinal and Transverse Lugs

A complex state of stress exists in the reinforcing bar where the transverse lugs merge into a longitudinal rib. The influence of such a junction on fatigue strength of reinforcing bars is indefinite in the literature.

In the AASHO Road Test (17), it was observed that fatigue cracks generally started at the points where two intersecting lugs merged into longitudinal ribs. Similar failures were observed by other investigators (30,37), especially when the longitudinal ribs were placed in a

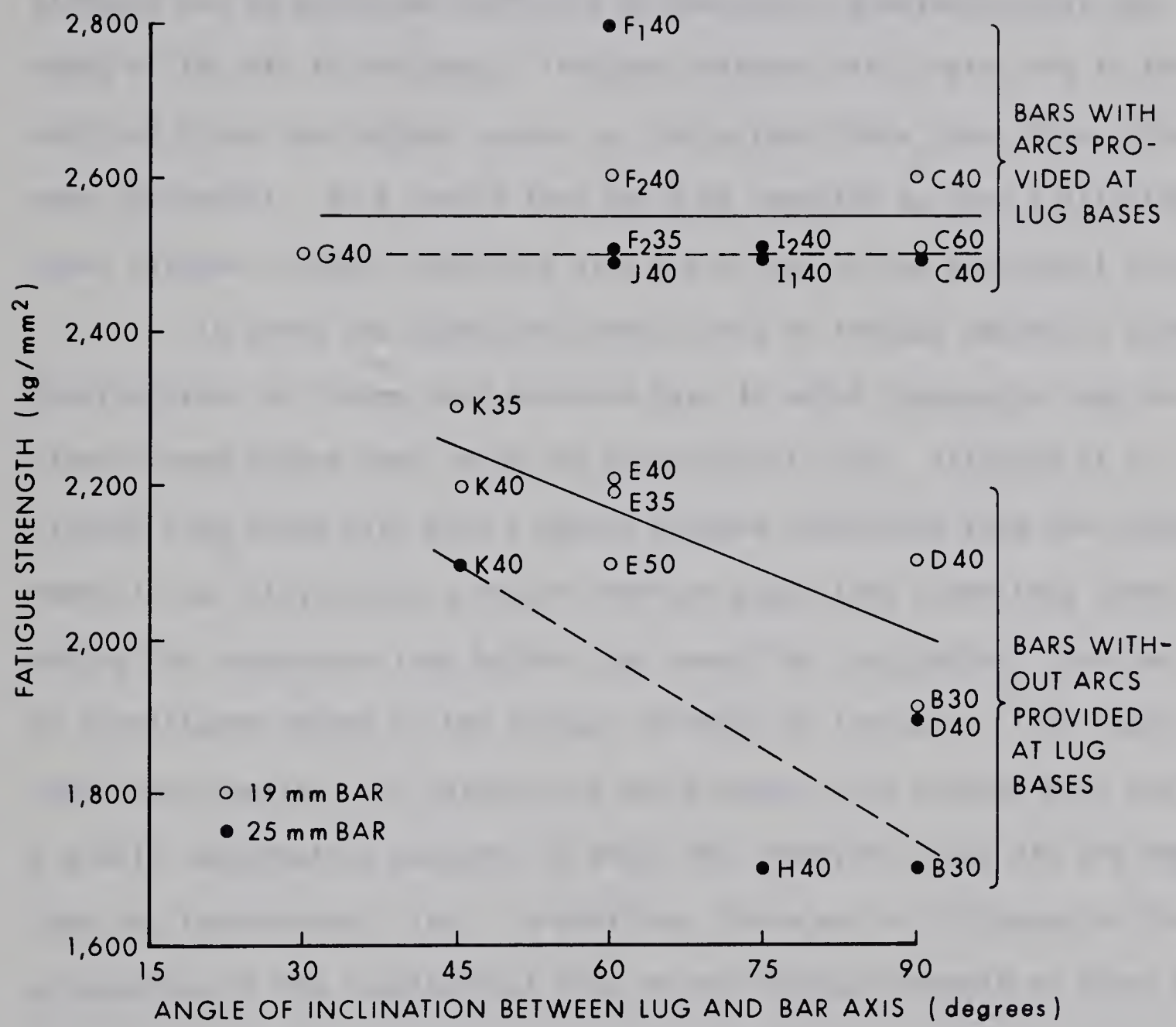


FIGURE 2.17 THE EFFECT ON FATIGUE STRENGTH OF INCLINATION OF LUGS TO BAR AXIS (AFTER KOKUBU AND OKAMURA)

vertical plane. These bars had 5 to 7 percent less fatigue strength when the longitudinal ribs were in a vertical plane than they did with the ribs in the horizontal plane (30)*. This reduction in fatigue strength can be explained partially by the strain gradient across the depth of the bar in the beam. The bars oriented with their ribs in the vertical plane have bigger stress in the extreme fibre than if the ribs were horizontal. As a result they would be expected to show a slightly lower fatigue strength than bars with their ribs in the horizontal plane.

To avoid the above mentioned source of fatigue weakness, several manufacturers in Europe have produced bars in which transverse lugs are discontinued before they reach the longitudinal ribs. Although it is claimed that these bars have a better fatigue resistance than the typical American bar (15,32,34), a recent American study (39) found that terminating the transverse lugs before they reach the longitudinal ribs had no significant effect on the fatigue strength of the bars. This study considered American hot rolled bars and European cold twisted bars having a similar deformation pattern, in which the transverse lugs did not merge into the longitudinal ribs. In addition, there was no influence of the orientation of the longitudinal ribs on the fatigue strength of these bars.

2.3.6 Effect of Diameter of Bar

The influence of the diameter of reinforcing bars on their fatigue strength has not yet been thoroughly investigated. In section 2.2.2 it was seen that for machined metal specimens the fatigue strength tended to go down as the size of specimen increased. However, the effects

*In reference 30 these data are reported in terms of fatigue life rather than fatigue strength.

of size, shape and stress gradient were found to be closely related.

The test data reported by Wascheidt (34) and Komubu and Okamura (40) show a slight decrease in strength with an increase in bar size. This topic will be discussed more fully in section 5.3 in connection with the present test series.

CHAPTER III

TEST SPECIMENS, MATERIALS AND TESTING EQUIPMENT

3.1 Description of Test Program

This investigation was a study of the fatigue behavior of intermediate and high strength reinforcing bars. Three major variables; minimum stress level, bar size and grade of steel, were investigated. The program included tests on bars of intermediate, A 432 and A 431 steel and bar sizes Nos. 5, 8 and 10. The tests on reinforcing bars were divided into the following groups -

1. Flexural fatigue tests on reinforced concrete beams containing bars of intermediate, A 432 and A 431 reinforcement and bar sizes Nos. 5, 8 and 10.
2. Rotating beam fatigue tests on standard and filleted fatigue specimens, machined from No. 8 bars of intermediate, A 432 and A 431 steel.
3. Hardness and metallurgical investigations of No. 8 bars of intermediate, A 432 and A 431 steel.

The first group of tests forms the major part of the test program. In these tests the reinforcing bar stresses simulated field conditions. The remaining test groups were designed to investigate the strength and fatigue behavior of the base metal in the bars. The fabrication and testing procedure for these tests will be discussed in this chapter.

3.2 Properties of Reinforcement

The reinforcement used in this program was of three grades, meeting ASTM specifications: A 15 (Intermediate Grade), A 432 and A 431*. All the bars of any one size and yield stress were selected from the same heat, the heats being chosen on the basis of similar yield stress for the three sizes of any one grade.

In each case the reinforcing bars were rolled from new billets. The A 15 and A 432 reinforcement came from the Edmonton plant of the Steel Company of Canada. These bars were produced in a continuous casting steel mill from steel scrap remelted in an electric furnace. The A 431 reinforcement was produced at the Hamilton plant of the Steel Company of Canada from an open hearth process. The chemical composition of the nine types of steel, obtained from mill test reports is presented in TABLE 3.1.

Photographs of all the nine types of reinforcing bars used in this investigation are shown in FIGURE 3.1. The reinforcement used had two longitudinal ribs and parallel transverse lugs inclined at about 75° to the bar axis. In all cases the transverse lugs merged into the longitudinal ribs. FIGURE 3.2 shows the mid lug profiles, obtained by sectioning the bars along their longitudinal axis. The bar diameter, lug height and lug spacing on the bars were measured with a micrometer. The radii at the bases of lugs and the enlarged photographs of the mid lug profiles shown in FIGURE 3.2 were obtained using an optical comparator. The average values of diameter, lug height, lug spacing and lug base

*At the time the reinforcement was purchased ASTM Specifications A 15, A 432 and A 431 were in effect. These were replaced in 1968 by ASTM A 615-68 Grade 40, Grade 60 and Grade 75, respectively.

TABLE 3.1

PROPERTIES OF REINFORCING BARS

BAR SIZE	NO. 5				NO. 8				NO. 10			
	A 15	A 432	A 431	A 15	A 432	A 431	A 15	A 432	A 431	A 15	A 432	A 431
Grade of Steel	50.0	67.7	89.4	52.7	65.6	84.4	49.7	64.2	83.0			
Yield Strength, ksi	76.3	109.2	122.1	83.1	109.0	123.5	83.1	110.5	109.5			
Ultimate Strength, ksi												
Elongation, percent	21.7	14.8	11.9	20.8	15.0	15.0	21.2	15.8	12.5			
Content in percent:												
Carbon	0.32	0.52	0.38	0.32	0.49	0.41	---	---	0.43	0.42		
Manganese	0.57	0.74	0.95	0.49	1.24	1.48	---	---	1.26	1.15		
Sulphur	0.032	0.039	0.031	0.042	0.033	0.031	---	---	0.028	0.032		
Phosphorus	0.015	0.025	0.008	0.015	0.025	0.012	---	---	0.024	0.008		
Silicon	--	--	0.22	--	--	0.21	---	---	--	0.12		
Vanadium	--	--	0.09	--	--	0.09	---	---	--	0.06		

TABLE 3.2

PROPERTIES OF REINFORCING BARS

BAR SIZE	NO. 5				NO. 8				NO. 10			
Grade of Steel	A 15	A 432	A 431	A 15	A 432	A 431	A 15	A 432	A 431	A 15	A 432	A 431
Unit Weight 1bs/ft	1.13	1.12	1.12	2.67	2.69	2.66	4.26	4.5	4.32			
Diameter-inches	0.586	0.580	0.597	0.935	0.930	0.966	1.225	1.230	1.210			
Half Width of Lugs - inches	0.071	0.080	0.083	0.120	0.120	0.110	0.170	0.165	0.150			
Height of Lugs - inches	.042	.055	.032	.065	.065	.060	.076	.075	.074			
Spacing of Lugs - inches	0.298	0.297	0.306	0.428	0.426	0.436	0.55	0.55	0.555			
Face Angle of Lugs - degrees	56	56	42	41	45	43	44	43	45			
Radius of base of Lugs - inches												
Steeper side - Average	.0125	.014	.0235	.02	.016	.0.02	.0317	.028	.019			
Standard deviation	.0025	.0025	.004	.003	.003	.005	.0001	.0003	.003			
Other Side - Average	.0195	.0305	.042	>.075	.032	.061	>.075	.045	.038			
Standard deviation	.0047	.0062	.0062	--	.019	.010	--	.0017	.002			

TABLE 3.3
OUTLINE OF TESTING PROGRAM

A. REINFORCED CONCRETE BEAM SPECIMENS

Series	Bar Size	Type of Reinforcement	Minimum Stress Level
1	8	Intermediate	$0.1 f_y$
2	8	A 432	$0.1 f_y$
3	8	A 431	$0.1 f_y$
4	8	Intermediate	$0.4 f_y$
5	8	A 432	$0.4 f_y$
6	8	A 431	$0.4 f_y$
7	5	Intermediate	$0.1 f_y$
8	5	A 432	$0.1 f_y$
9	5	A 431	$0.1 f_y$
10	10	Intermediate	$0.1 f_y$
11	10	A 432	$0.1 f_y$
12	10	A 431	$0.1 f_y$

B. ROTATING BEAM FATIGUE SPECIMENS

			Type of Specimen
A	8	Intermediate	Plain
B	8	A 432	Plain
C	8	A 431	Plain
D	8	Intermediate	Filletted
E	8	A 432	Filletted
F	8	A 431	Filletted



FIGURE 3.1 DEFORMATION PATTERNS ON REINFORCING BARS
(Shown half size)

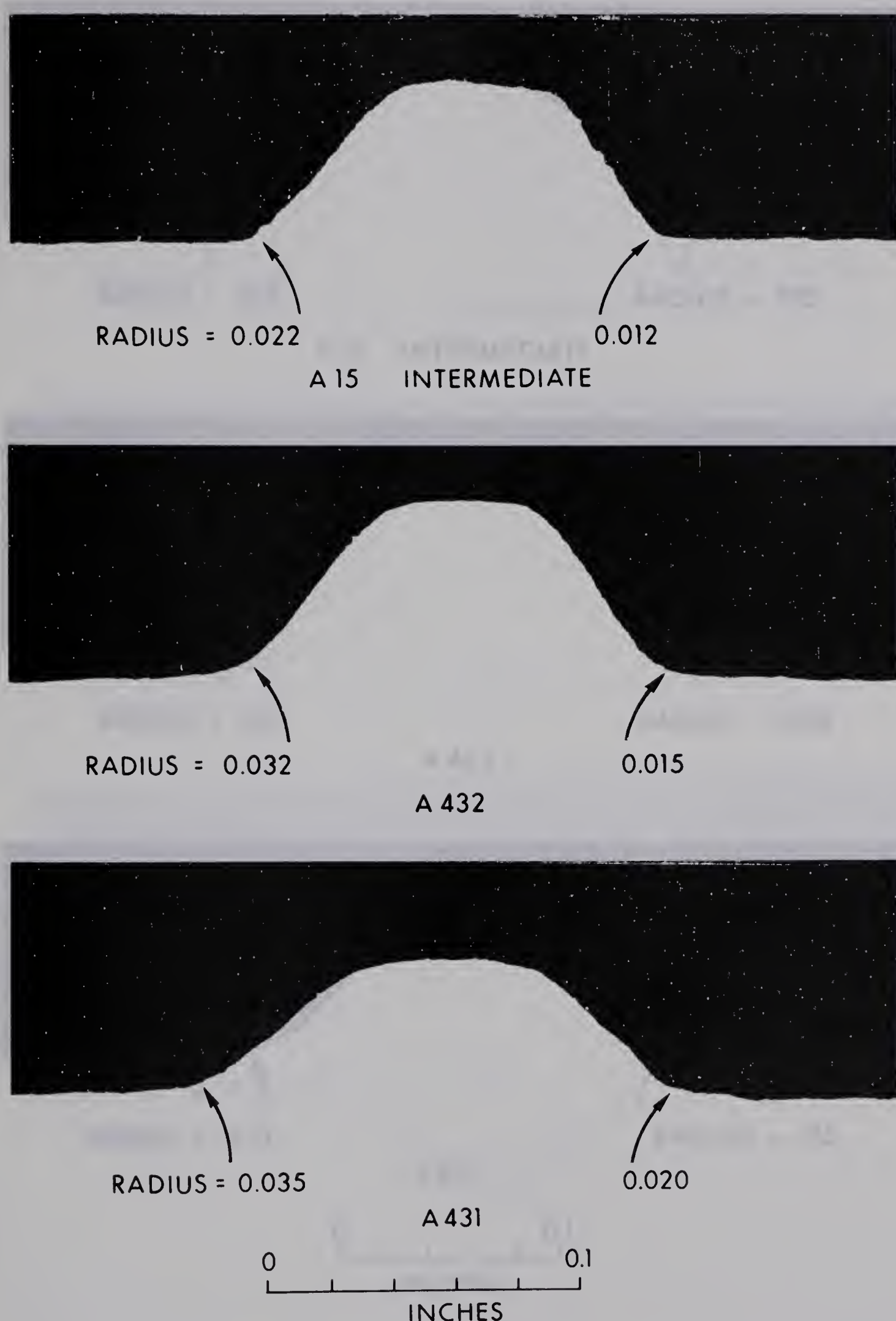


FIGURE 3.2(a) MID LUG PROFILES FOR NO. 5 BARS



RADIUS = .015

RADIUS = .075

A 15 INTERMEDIATE



RADIUS = .015

RADIUS = .038

A 432



RADIUS = .027

RADIUS = .05

A 431

0 0.1
INCHES

FIGURE 3.2(b) MID LUG PROFILES FOR NO. 8 BARS

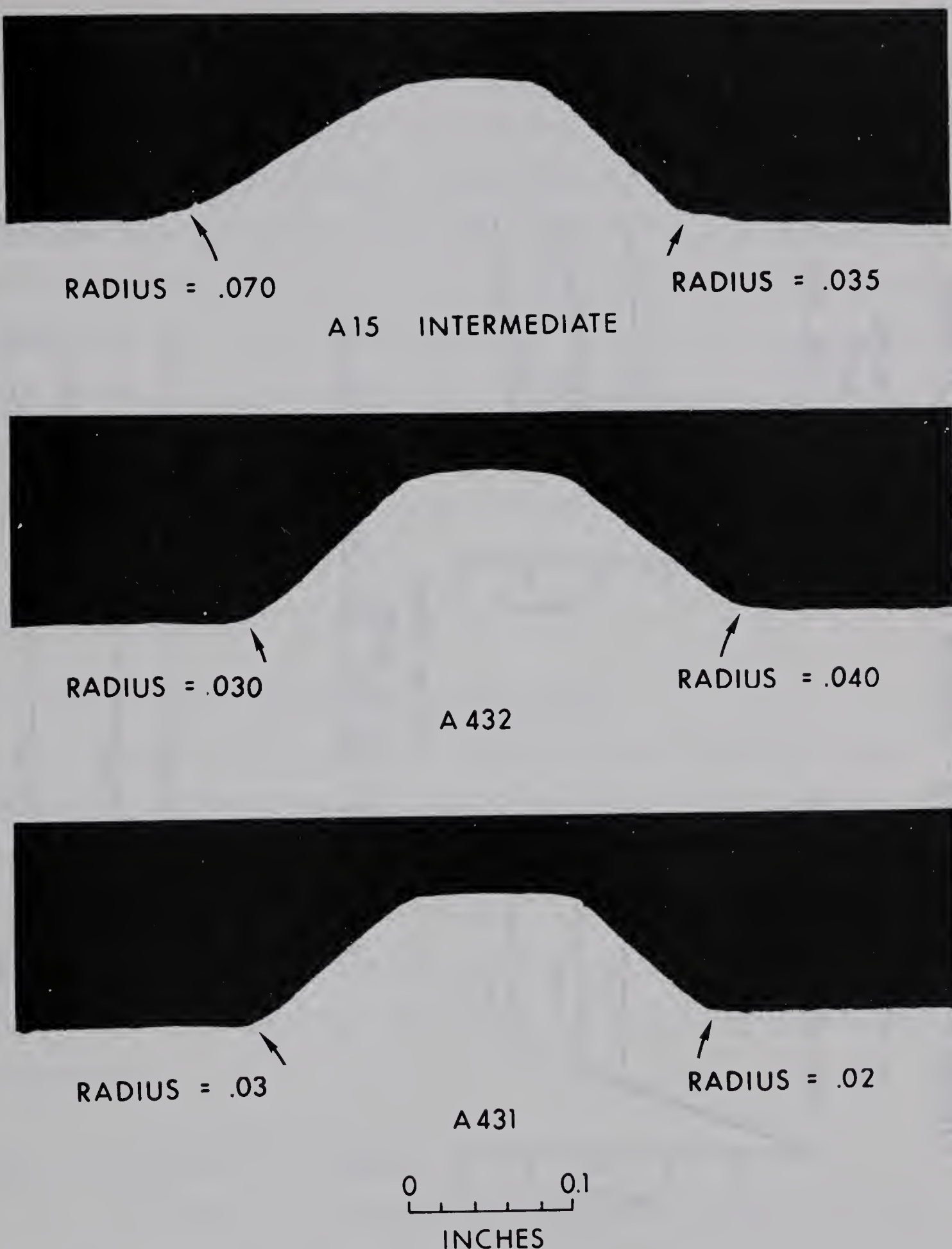


FIGURE 3.2(c) MID LUG PROFILES FOR NO. 10 BARS

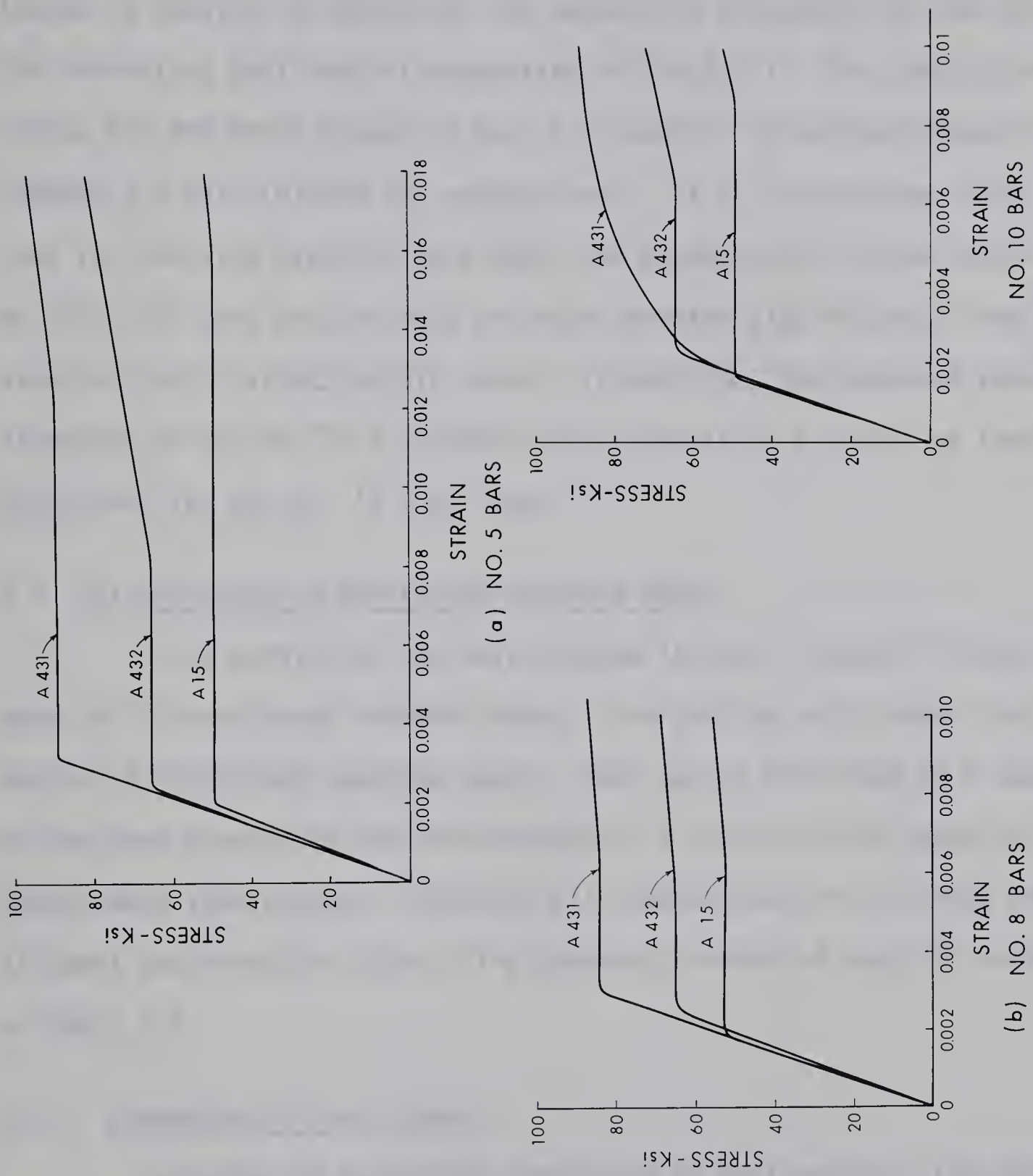


FIGURE 3.3 STRESS - STRAIN CURVES FOR TEST BARS

radii for each bar are given in TABLE 3.2.

Two reinforcing bars of each size in each grade of steel were tested in tension, to determine the mechanical properties of the bars. The laboratory test data is summarized in TABLE 3.1. The stress-strain curves for the three grades of Nos. 5, 8 and No. 10 bars are shown in FIGURES 3.3 (a), (b) and (c) respectively. It is interesting to note that for the nine types of bars used, the stress-strain curve for the No. 10 A 431 bars was the only one that deviated significantly from an elastic-plastic stress-strain curve. In addition, the measured tensile strengths of the No. 10 A 431 bars were essentially the same as those determined for the No. 10 A 432 bars.

3.3 Fatigue Tests on Reinforced Concrete Beams

This portion of the test program included flexural fatigue tests of 72 reinforced concrete beams. The testing was divided into 12 series of reinforced concrete beams. Each series consisted of 6 beams of the same dimensions and reinforcement. A total of nine types of steels were investigated, including all combinations of the three grades of steel and three bar sizes. The complete program of tests is outlined in TABLE 3.3.

3.3.1 Dimensions of Test Beams

In order to facilitate comparison of test results, the beams in this investigation were designed to be geometrically similar to those used in previous tests carried out by the Portland Cement Association Laboratories (28). The beams reinforced with No. 8 bars were identical to those described in References 28, 30, 37 and 39. The nominal dimensions

of the test beams investigated in this program are shown in FIGURE 3.4. The actual dimensions of the beams, measured at the time of testing are listed in TABLE A-1. Each test beam was reinforced with a single reinforcing bar in the tensile zone and two No. 3 bars in the compression zone. The beams can be classified into three groups on the basis of reinforcing bar diameters.

Holes of 1-1/8 inch diameter were provided through the beam directly over the supports, 3 inches below the top of the beam to permit installation of clamping bolts for the end supports. Lifting hooks were provided at the third - points of the span.

Group I (Series 1-6)

The beams in this group had a nominal cross-section of 12 by 14 inches. These beams contained one longitudinal No. 8 reinforcing bar with a clear cover of 1 inch from the bottom of the beam. The longitudinal reinforcement ratio in these beams varied from .0051 to .0053. The beams were 80 inches long and were simply supported with a span of 72 inches. No. 3 double leg stirrups were provided at 6 inches on center. These bars were supported by two No. 3 bars as shown in FIGURES 3.4 and 3.5.

Group II (Series 7-9)

These beams contained one No. 5 bar as longitudinal reinforcement, and had nominal rectangular cross-section of 7-1/2 by 10-1/4 inches. The beams were 50 inches in length and were placed at clear cover of 1 inch. In these beams the longitudinal steel ratio varied from .0046 to .0047. No. 3 double leg stirrups were provided at 4.5 inches on center.

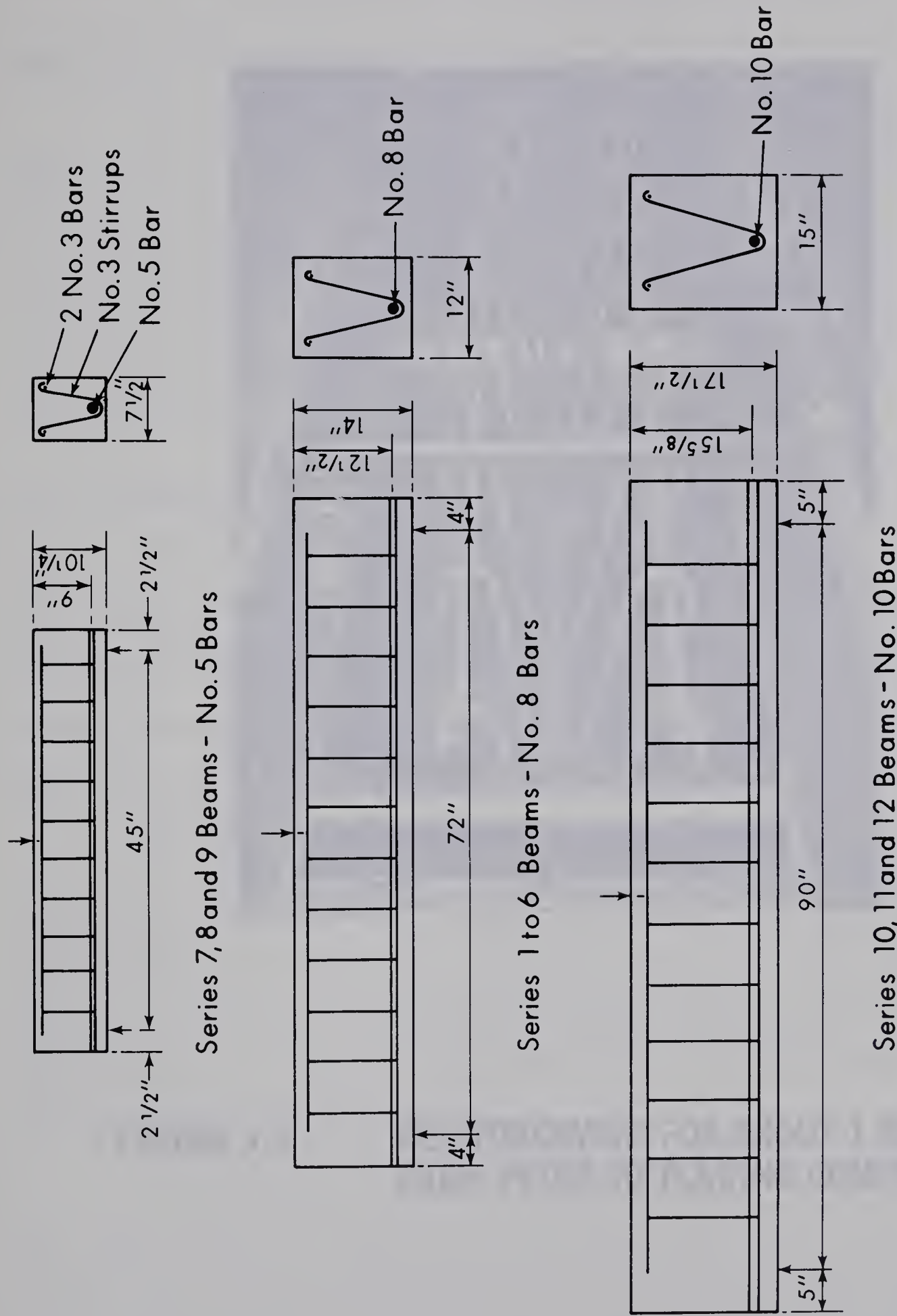


FIGURE 3.4 DETAILS OF BEAM SPECIMENS

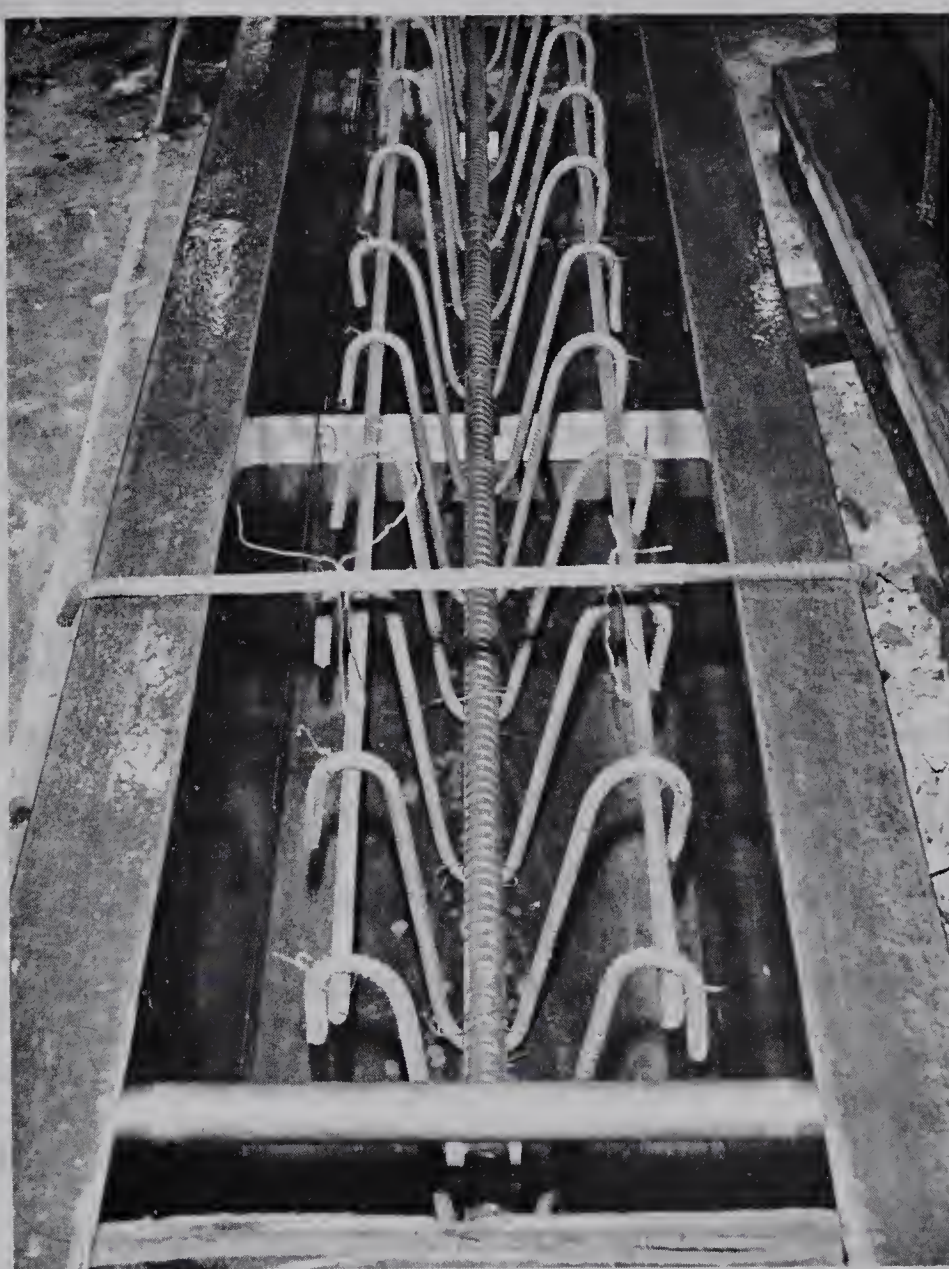


FIGURE 3.5 REINFORCEMENT FOR GROUP I BEAM IN FORM PRIOR TO PLACING CONCRETE

These were supported by two No. 3 bars as shown in FIGURE 3.4.

Group III (Series 10-12)

The beams were reinforced with a single No. 10 bar at a clear cover of 1-1/2 inches. These beams had rectangular cross-section of 15 by 17-1/2 inches, and steel ratios ranging from .052 to .053. The beams were 100 inches long and were simply supported over 90 inches. No. 3 double leg stirrups were provided at 7 inches on center. These were supported by two No. 3 bars as shown in FIGURE 3.4.

3.3.2 Properties of Concrete

The concrete in the test beams in Series 1 to 6 was mixed in the laboratory using Type III high early strength Portland Cement, washed sand and 3/4-inch maximum size aggregate. The average mix proportions by weight were: cement - 12.7 percent; sand - 32.8 percent; coarse aggregate - 47.8 percent; and water - 6.7 percent.

The concrete was mixed in a nine cubic foot capacity Eirich pan type mixer. Three batches of concrete were used to make each group of two beams in series 1 to 6. The first batch made up the lower third of both the beams, while the second and third batches were each used to make the upper two thirds of one of the beams. The slump measurements ranged between 2-3/4 and 3-1/2 inches.

The concrete in the test beams in Series 7 to 12 was supplied by a local transit mix supplier in 1-1/4 cubic yard lots. Each lot was used to cast two beams containing No. 10 bars and two beams containing No. 5 bars. The concrete was ordered as 4500 psi concrete made with Type III high early cement. The aggregates used came from the same pit

pit as those used in the beams cast in the laboratory.

In all cases the beams were vibrated using an electric immersion type vibrator. Two 6 x 12 in. test cylinders were cast according to ASTM specification No. G192-62T from the concrete used in the top of each beam. For the first two days after casting, the beams and cylinders were covered with saturated burlap and Polyethelyne sheets. After two days the forms were removed and the beams and cylinders were stored in the laboratory until testing.

The cylinders for each beam were tested for compressive strength the day the beam was placed in the testing frame. The strength of concrete was taken as the average of the strengths derived from two 6 x 12 inch cylinders. The age at testing and the average compressive strength of the test cylinders together with actual dimensions of the beams are summarized in TABLE A-1.

3.3.3 Form Work

The forms for the beams were built up using three steel channels bolted together to form a box. The forms were oiled before casting and rods were positioned in holes through the channels to form the end support holes. These rods were heavily oiled and wrapped in Polyethelyne to help in their removal.

A strip of 3/8 inch thick wood was placed in the form at the mid span before casting. This was done to initiate a flexural crack at the point of maximum stress in the beam. The wooden strip was oiled to facilitate removal before testing. During casting the reinforcing cage was supported on the crack initiator and on two small pieces of wood placed near the ends of the beam. FIGURE 3.5 shows a reinforcement

cage for a Group I beam in the form prior to casting.

3.3.4 Testing Equipment

Testing was performed using Amsler equipment consisting of a hydraulic pulsator and jacks of 22, 55 and 110 kips dynamic capacity. The Amsler hydraulic jack was mounted in a steel loading frame anchored to the test floor of the University of Alberta Structural Engineering Laboratory. The pulsator was operated at 500 cycles per minute.

The Amsler testing equipment is capable of applying a sinusoidal stress cycle varying between two limits. The maximum and the minimum stress limits is set on two separate dials. A reset-counter indicates the number of stress cycles applied. The machine is stopped automatically when it reaches a preset number of cycles; when a preset decrease in the minimum load or increase in the maximum load occurs; or when the machine or the test specimen starts to vibrate significantly. All three controls assist in obtaining relatively undisturbed fractured beam specimens.

The load dials on the pulsator panel are calibrated in divisions representing one percent of the full capacity of the jack in use. It is possible to estimate the dial readings to nearest 0.1 to 0.2 percent of the full capacity. Amsler jacks of 22, 55 and 110 kips dynamic load capacity were used for the tests of beams containing No. 5, No. 8 and No. 10 bars respectively. For the three beam sizes the possible error in the bar stress due to error in estimating the pulsator dial readings was of the order of 0.16 ksi for No. 5 bars, 0.18 ksi for No. 8 bars and 0.22 ksi for No. 10 bars. About half of the beams in series 10 to 12 were tested using an Amsler jack of 55 kips load capacity for better accuracy in estimating the load dial readings. For these beams the

possible error in the bar stress due to errors in estimating the pulsator dial reading for No. 10 bars was reduced to about 0.11 ksi.

The calibration of the Amsler equipment was checked at the beginning and end of each test series as described in paragraph 3.3.5. A 50 ton capacity load cell was calibrated throughout the range of the Amsler equipment in a calibrated Baldwin testing machine, and this load cell was then used to calibrate the Amsler equipment.

The general arrangement of the testing equipment along with the beam under fatigue loading is shown in FIGURE 3.6. The test beams were supported by two large concrete reaction blocks placed at 45, 72 and 90 inch centres for the three beam sizes. These blocks were fastened to the test floor. A roller support was placed on the other reaction block to complete the simple support system. The rollers were mounted in a housing and a rocker bar was fastened on the top of the housing. The details of the roller support are illustrated in FIGURE 3.7.

As shown in FIGURES 3.6 and 3.7, the two ends of the beams were held in special end clamps designed to prevent the tendency of the beam to "walk" laterally or longitudinally under repeated loadings. The end clamps each consisted of a 2-inch steel base plate with a machined groove which rested on the rocker bars on the supports. Bars were placed across the ends of the grooves to stop the support from sliding off the rocker bars. Side plates were welded to the base plate to form a box into which the beam fitted. A 1-inch diameter bolt was passed through holes in the side plates and the beam to hold the beam in place. Pads of 1/4 inch neoprene were placed between the steel clamps and the concrete beam

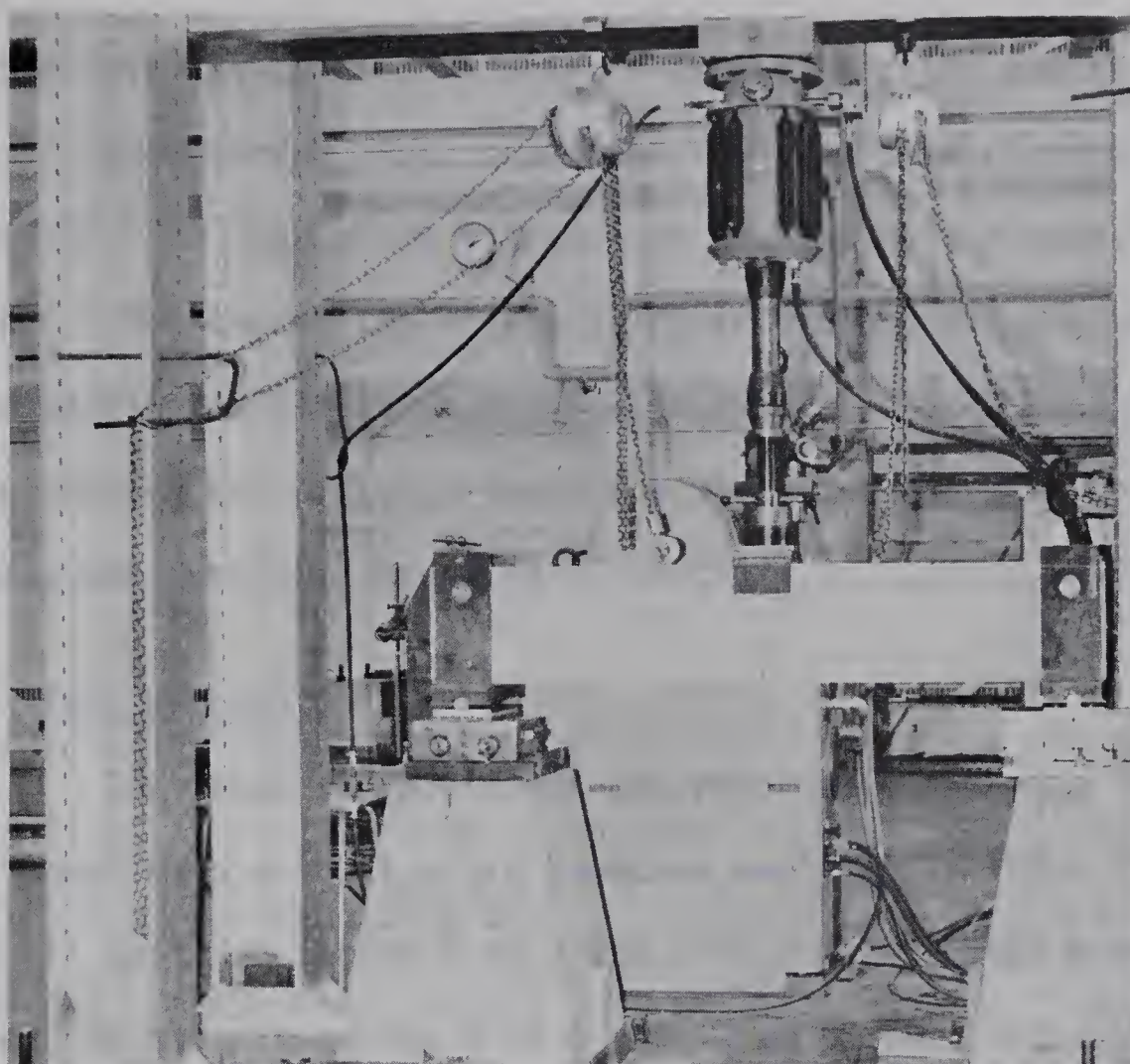


FIGURE 3.6
OVERALL VIEW
OF TESTING
ARRANGEMENT.



DETAIL OF ROLLER
END SUPPORT AND
BEAM CLAMP.

to distribute the bearing stresses from the reaction forces.

The bearing plate under the load was a 1-1/2 inch thick plate with small side lugs which fitted over the top of the beam to stop side slippage. Mounted on top of the 1-1/2 inch plate was a second plate with a machined indentation to provide a seat for the head of the jack. A neoprene pad was placed between the plate and the beam to eliminate slippage and localized crushing of concrete.

3.3.5 Test Procedure

The tests of reinforced concrete beams included 12 series of beams comprising a total of 72 beams as outlined in TABLE 3.3. The first six beams in series 1 to 3 and 7 to 9 were tested before starting another series. In series 4 to 6 and 10 to 12 the tests alternated from series to series until all the beams had been tested.

Prior to testing a beam, it was loaded with a small load to remove the wooden strip inserted as a crack initiator. The actual dimensions including the clear cover to the reinforcing bar were then measured. The calculations of the stresses in the reinforcing bars were made using the actual dimensions of each beam before it was tested.

The minimum loads on the beam were set to provide a minimum bar stress of either 0.1 or 0.4 times the yield stress of the reinforcing bar. The maximum load was varied in a manner designed to produce an S-N curve for each series. The fluctuating loading cycles were applied to the beams until failure occurred or 5 million cycles had been applied. The beams which sustained 5 million cycles without failure, were retested at a higher maximum load.

In all cases the reinforcement stresses were computed using

the straight line theory of flexure assuming the modulus of elasticity of concrete as given in the ACI Standard 318-63 (23) and that of steel as 29,000 ksi. Throughout the calculations nominal areas of 0.31, 0.79 and 1.27 sq. inch were used for the Nos. 5, 8 and 10 bars respectively. According to straight-line theory calculations the No. 3 stirrup support bars affected the calculated steel stress by less than 0.4 percent and they were ignored in calculating the steel stresses in the beams.

The Amsler pulsator was operated at 500 cycles per minute for the entire test program. The initial load setting on the pulsator varied slightly in the first 12 hours or so and minor load adjustments were required during this period. The Amsler pulsator dials were calibrated at the beginning, middle and end of each group of test specimens using a 50 ton load cell. The change in calibration ranged between 0 to 2 percent. A linear correction was applied to the test loads to account for the change in calibration.

The effect of the forced vibration on the steel stresses was approximated by assuming that the load would over run the top and bottom of the cycle set on the machine by two percent of the stress range in the cycle. This was calculated using formulas provided in the Amsler Instruction Manual (41).

The crack patterns were marked on the beams, after a few thousand load repetitions and after failure. After collapse of the beams, details of the fractured face of the reinforcing bars were recorded. Some typical fractured reinforcing bars were taken out from the beams for further examination.

3.4 Rotating Beam Fatigue Tests

The reinforcing bars tested in the reinforced concrete beam tests exhibited the combined effect of several variables. For this reason a test series was designed to investigate the fatigue behavior of the base metal in the reinforcing bars using standard rotating beam specimens machined out of No. 8 bars of the three grades of steel. The test specimens were divided into series A to F including standard un-notched specimens and filleted notched specimens as outlined in TABLE 3.3.

3.4.1 Details of Rotating Beam Specimens

The design and details of un-notched specimen shown in FIGURE 3.8 was taken from the "Instruction Manual" supplied with the fatigue testing machine (42). One No. 8 reinforcing bar was taken from each grade of steel and twelve pieces of the required size were cut from each bar. The test specimens were turned on a precision automatic lathe following a template. The rotating beam specimens came from the centre of reinforcing bar pieces.

In each case the surface of the specimen was polished using 0, 00 and 000 emery paper, successively in the longitudinal direction. Care was taken to make sure that surface finish was free from nicks, scratches and tool marks.

Notched specimens were tested to investigate the effect of stress concentration and the notch sensitivity of the various grades of steels. A fillet was chosen because of its similarity to the deformations on the reinforcing bars. The dimensions of the filleted specimen were chosen arbitrarily to give a known stress concentration. Twelve

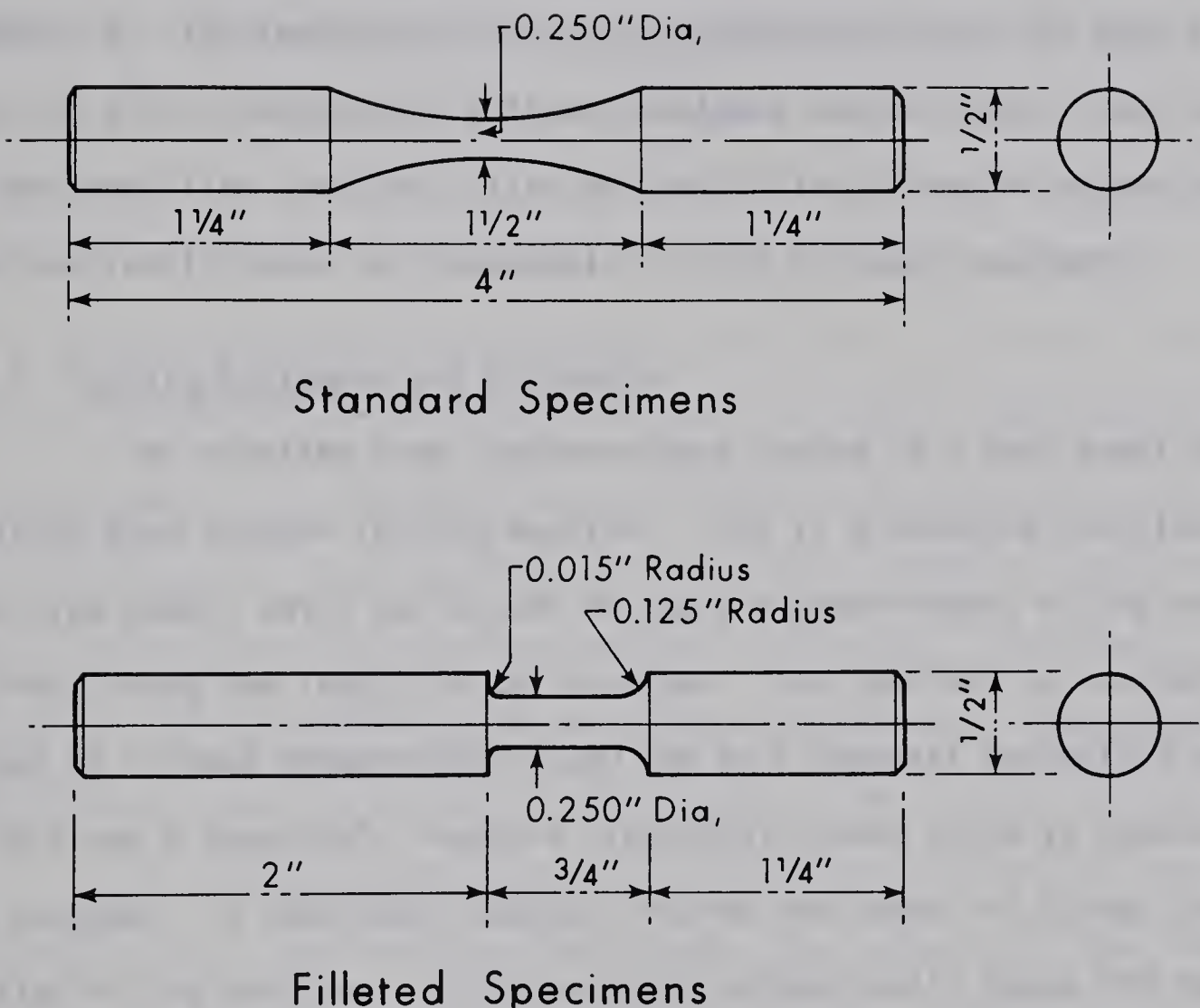


FIGURE 3.8 DETAILS OF ROTATING BEAM FATIGUE SPECIMENS

identical specimens were turned from the centre of No. 8 bars of each grade. These specimens were prepared and polished by similar procedure as described for un-notched specimens.

The details of the filleted specimen are illustrated in FIGURE 3.8. The theoretical stress concentration factor for this fillet was 1.85 (11). Unfortunately these specimens had accidental tool marks at the transition from the fillet to the 1/4 inch diameter segment and the test results were not dependable for the filleted specimens.

3.4.2 Testing Equipment and Procedure

The rotating beam specimens were tested in a Budd Model RBF-200 Rotating Beam Fatigue Testing Machine. This is a rotating cantilever beam type model, which can be set to apply a given moment at the section half-way along the length of the specimen. The specimen is rotated under a load at a speed between 500-12,000 rpm by a rheostat controlled motor. In this way a completely reversed sinusoidal stress cycle is applied to the specimen. A resettable counter records the number of stress cycles applied to the specimen. A micro-switch automatically shuts off the machine, when the stiffness of the specimen changes significantly due to fatigue cracking.

Cyclic loads were applied to the specimen until it developed a fatigue crack or had sustained 10 million cycles. The specimens which endured 10 million cycles were retested at higher alternating stresses. The loads were selected to establish S-N curves with a well defined fatigue limit.

3.5 Hardness Tests and Metallographic Investigation

In general, the fatigue strength of plain machined specimens increases with an increase in the yield strength, while that of reinforcing bars stays constant. This may be due to in part to an uneven distribution of material strength and properties across the member. Hardness and metallographic observations were undertaken to study this possibility. The hardness tests were made using Vicker's Pyramid Hardness (V.P.H.) tests.

The hardness tests indicated a variation in the metal tensile strength in the bar cross-section and for this reason, metallographical investigation of the bar metal was undertaken to explain this variation. The metallographic investigations were oriented towards the observation of the general macro and micro-structure of the metal, non-metallic inclusions and the micro-structure of metal at points of high stress concentration near the roots of deformations on the surface of the bars.

The hardness tests and metallographical observations were confined to No. 8 bars of the three grades since these bars were the bars which had been tested in rotating beam tests. The bars were sliced in the longitudinal and transverse directions to observe metal structure in both planes. Bar specimens approximately 3/4 inch long were cut by an abrasive cut-off saw. The bars were kept submerged in a cooling agent to avoid any change in metal structure due to the heat produced due to cutting. To facilitate polishing and metallographical observations the sliced bar specimens were mounted in Araldite blocks.

The polishing of the specimens was done in four gradual stages, using silicon carbide belts, silicon carbide discs, diamond abrasive and

alumina coated discs. The final finish of the surface was approximately .05 microns.

The specimens sliced along the longitudinal direction were used for observing micro-structure and the non-metallic inclusions. This plane of observation was preferred, because the inclusions were oriented in this plane and the banded structure of the metal could be seen better. The macroscopic observations were made on the surface transverse to the bar axis. These specimens were also used for hardness tests.

CHAPTER IV

TEST RESULTS

4.1 Reinforced Concrete Beam Specimens

4.1.1 Descriptions of Failures

All the reinforced concrete beam specimens failed due to fatigue failure of the tension reinforcement. Prior to the beam failure an essentially symmetrical pattern of flexural and shear cracks was observed in all the beams. In general, three major cracks appeared in a beam, at the initial loading. The central crack started at the crack initiator and extended approximately as far as the neutral axis of the beam. The other two cracks were symmetrical and their distance from the central crack varied with the size of beams. As the number of cycles increased the cracks became more distinctly visible. No attempt was made to measure the crack width. Longitudinal cracks were noted on the bottom of the beam below the bar. These cracks extended each way from each of the three flexural cracks about half a crack space in each direction. On removing the bars from the beams, however, the bond between the bar and the concrete was found to be excellent in this region.

FIGURE 4.1 illustrates a typical crack pattern on beam specimen 8-50-11 after failure.

In most cases the fatigue fracture of the reinforcement occurred at the performed crack at mid-span. The location and a description of the fracture of the reinforcement in the beams is given in TABLE A-2. In four cases out of the 72 beams, the reinforcement fractured just over the stirrup nearest to mid-span. In these cases there were distinct

marks of rubbing between the reinforcement and the stirrup. Six beams failed at the first major inclined crack in the shear span at a distance ranging from 2 to 9-5/8 inches from mid-span.

In 34 of the 36 beams containing No. 8 bars, the fractures originated at the base of a transverse lug at a point near the bottom of the bar. In the remaining two beams, failure appeared to have originated at the base of a transverse lug, where the lug merged into the longitudinal rib. It should be noted that the longitudinal ribs were in the horizontal plane in all beams.

With three exceptions the fractures in the 18 beams containing No. 5 bars originated along the base of transverse lug at a point near the bottom of the bar. In two beams, the fracture started at the bottom of the bar midway between two transverse lugs, while in the third the crack appeared to have started at the intersection of the longitudinal and transverse lugs.

Of the 18 beams containing No. 10 bars in series 10-12, seven beams failed due to bar fractures which initiated at the intersection of transverse and longitudinal lugs. In the remaining eleven beams, the fracture started at the base of a lug near the bottom of the bar.

The details of the fractures in the reinforcing bars in all test series have been summarized in TABLE A-2. FIGURES 4.2(a), (b) and (c) respectively show typical failures due to cracks which started at the base of a lug at the bottom of the bar, midway between the bottom and rib, and at the intersection of lugs. On removal of the bars from beam 8-50-9 and 10-50-6 fatigue cracks were observed along the base of the lug adjacent to the one at which the final fracture occurred. These

cracks have been shown in FIGURE 4.3. In the whole investigation no definite trend of fracture along the steeper side of the lug was observed.

4.1.2 Presentation of Test Data for Reinforced Concrete Beams

The computed bar stresses and the number of load cycles applied to the beam specimens are presented in TABLE A-3 for the 12 test series. The test results have been plotted on S-N curves in FIGURES 4.4 to 4.7. Each of these figures presents and compares the S-N curves for the three grades of steel in each bar size. The lines in these curves were fitted by observation. The fatigue strengths at five million cycles obtained from these curves are listed in TABLE 4.1.

The maximum stresses corresponding to a complete reversal stress cycle (mean stress = 0) have been estimated for No. 8 bars using the Goodman Diagrams presented in section 5.1 of this report and are summarized in column 8 of TABLE 4.1. The corresponding stresses listed for the No. 5 and No. 10 bars were also obtained from Goodman Diagrams drawn with straight-line envelopes.

4.2 Presentation of Test Data for Rotating Beam Tests

The data for rotating beam series A, B and C for plain specimens and D, E and F for filleted specimens is listed in TABLE A-4. The stresses reported in this table were calculated from the diameter and applied moment assuming a linear distribution of stresses across the section of minimum diameter. The effects of stress concentrations at the root of the fillet were not considered in this computation. The theoretical stress concentration factor (K_t) for the notched specimens was 1.85 ignoring the effect of tool marks at the base of the fillet.

The test data is shown on S-N diagrams in FIGURES 4.8 and 4.9 for plain and filleted specimens respectively. Each of these figures presents and compares the S-N curves for the three grades of steel. The curves in these figures were fitted to the data by observation. In the case of specimens which were retested, the strengths were discounted by five percent for each retest to account for the coaxing effect when drawing the lines. The fatigue strength at five million cycles for the plain and filleted specimens was obtained from FIGURES 4.8 and 4.9 and is summarized in TABLE 4.2.

Two standard rotating beam specimens of each grade of steel were tested in tension. The shape of the specimens made it impossible to accurately determine any property except the ultimate tensile strength, which is recorded in column (4) of TABLE 4.2.

The data for the filleted specimens shows a great deal of scatter. Part of this may be due to tool marks on specimens at the transition between the fillet and the one-quarter inch diameter part of the bar. FIGURE 4.10 shows an enlargement of this portion of two specimens. The tool marks can be seen in both photographs and a fatigue crack can be seen in one specimen. For this reason, this data has not been considered in the discussion of the tests presented in Chapter V.

4.3 Hardness Test Results and Metallographic Observations

The test data from the Vickers Pyramid Hardness (V.P.H.) tests is summarized in FIGURE 4.11 for the A 15, A 432 and A 431 No. 8 bars. Eleven hardness tests were carried out on each bar at uniformly spaced points along two perpendicular diameters. From a standard hardness conversion chart the equivalent tensile strengths of the three bars

were found to be: A 15 - 85 to 101 ksi with an average value of 92 ksi, A 432 - 110 to 125 ksi with an average value of 119 ksi, and A 431 - 105 to 135 ksi with an average value of 125 ksi. The average strengths determined in this way agree very well with the tensile strengths determined from tensile tests on the rotating beam specimens as listed in TABLE 4.2. None of the hardness tests were made in the decarburized surface layer.

The macroscopic observations on the etched bar cross-sections of A 15, A 432 and A 431 steel are shown in FIGURE 4.12. The non-uniformity of the metal structure in the bar cross-section may be seen from these metallographs. The A 15 and A 431 bars showed evidence of segregation in the ingot. This effect might lead to variable fatigue properties of the metal in the bar cross-section. The A 15 bar also showed an appreciable amount of unhomogeneous metal structure in the center of the bar. This effect might have been responsible for a large scatter in test results for the A 15 plain rotating beam specimens. The A 432 bar showed some black spots in the center of the bar cross-section, which on microscopic examination were found to be phosphorus and carbon rich zones. The chemical analysis provided by the manufacturer further confirmed this inference, since the A 432 bars had higher percentage of phosphorus present than either the A 15 or A 431 bars (TABLE 3.1).

The general macro-structure of the metal in three steels can be seen in FIGURE 4.13. These metallographs were taken on the longitudinal etched sections of the bars. The non-homogeneous ingotized structure in the A 15 bar is shown by the wide banding near the center of the bar. Phosphorus segregation in A 432 bar is indicated by the

longitudinal white lines in this photograph. A few ghost-like bands due to phosphorus concentrations can be seen in the center of the A 431 bar but these tend to disappear as one moves toward the surface.

The micro-structure of the bar metal in the central core of the bars is shown in FIGURE 4.14 and that at the surface near the base of a lug is shown in FIGURE 4.15. The A 15 steel had a banded or wrought structure in the central core which essentially disappeared as the outside of the bar is approached. The A 431 steel had a higher carbon content and had a finer grain structure than the other two steels.

The zone of decarburization at the surface of all the three bars is visible in FIGURE 4.15, the depths of penetration of this zone is evident from the white finer grain structure at the boundary. The presence of this zone may significantly lower the fatigue strength of the reinforcing bars since the decarburized zone is largely made up of low-strength ferrite crystals. The decarburization zone seems to be thinner in the A 432 bars than in the others. An oxidized layer is also visible on all three bars in FIGURE 4.15. In no case were cracks observed in the surface of the bars.

The microscopic inclusions in the bar samples are shown in FIGURE 4.16. These metallographs were taken on un-etched specimens at 100 magnification. The metallographs show longitudinal discontinuous inclusions which were primarily carbon. The intensity of the inclusions seems to be uniform in all the steels. These inclusions when compared to standard ASTM charts, may be classified as C⁺ (background classification). The inclusions present are not excessive, and their influence on fatigue strength may not be significant since they are oriented in the direction of stress.

TABLE 4.1

CHARACTERISTICS AT FATIGUE LIMIT IN REINFORCED CONCRETE BEAM TESTS

ASTM Standard	(2) Yield Strength Ksi	(3) Ultimate Strength Ksi	Computed Applied Stress - ksi			
			(4) Minimum Stress Level	(5) Minimum Maximum*	(6) Maximum*	(7) Range
(8) Maximum Stress for complete Reversal**						
NO. 8 BARS						
A 15	52.7	83.1		5.2	35.8	30.6
A 432	65.6	109.0	0.1 f_y	6.8	36.4	29.6
A 431	84.4	123.5		8.3	38.7	30.4
						19.0
NO. 8 BARS						
A 15	52.7	83.1		21.2	46.8	25.6
A 432	65.6	109.0	0.4 f_y	28.2	53.7	25.5
A 431	84.4	123.5		34.4	59.2	24.9
						19.0
NO. 5 BARS						
A 15	50.0	76.3		5.0	36.5	31.5
A 432	65.8	109.2	0.1 f_y	6.6	38.6	32.0
A 431	89.4	122.1		8.9	45.4	36.5
						31.0
NO. 10 BARS						
A 15	49.7	83.1		5.0	35.2	30.2
A 432	64.2	110.5	0.1 f_y	6.4	34.9	28.5
A 431	83.0	109.5		8.3	37.3	29.0
						17.8

*Corresponding to five million stress cycles.

**From Modified Goodman Diagrams assuming straight-line envelopes.

TABLE 4.2
CHARACTERISTICS AT FATIGUE LIMIT
- ROTATING BEAM FATIGUE TESTS

(1) ASTM Standard	(2) Yield Strength of Bar (Ksi)	(3) Ultimate Tensile Strength of Bar (Ksi)	(4) Ultimate Tensile Strength of Specimen (Ksi)	(5) Nominal Stress Range* (Ksi)	(6) Un-notched Filletted
A 15	52.7	83.1	94.0	92.5	57.0
A 432	65.6	109.0	119.0	111.5	69.5
A 431	84.4	123.5	128.0	137.0	94.5

*Corresponding to ten million cycles, computed for minimum diameter ignoring effect of stress concentration.

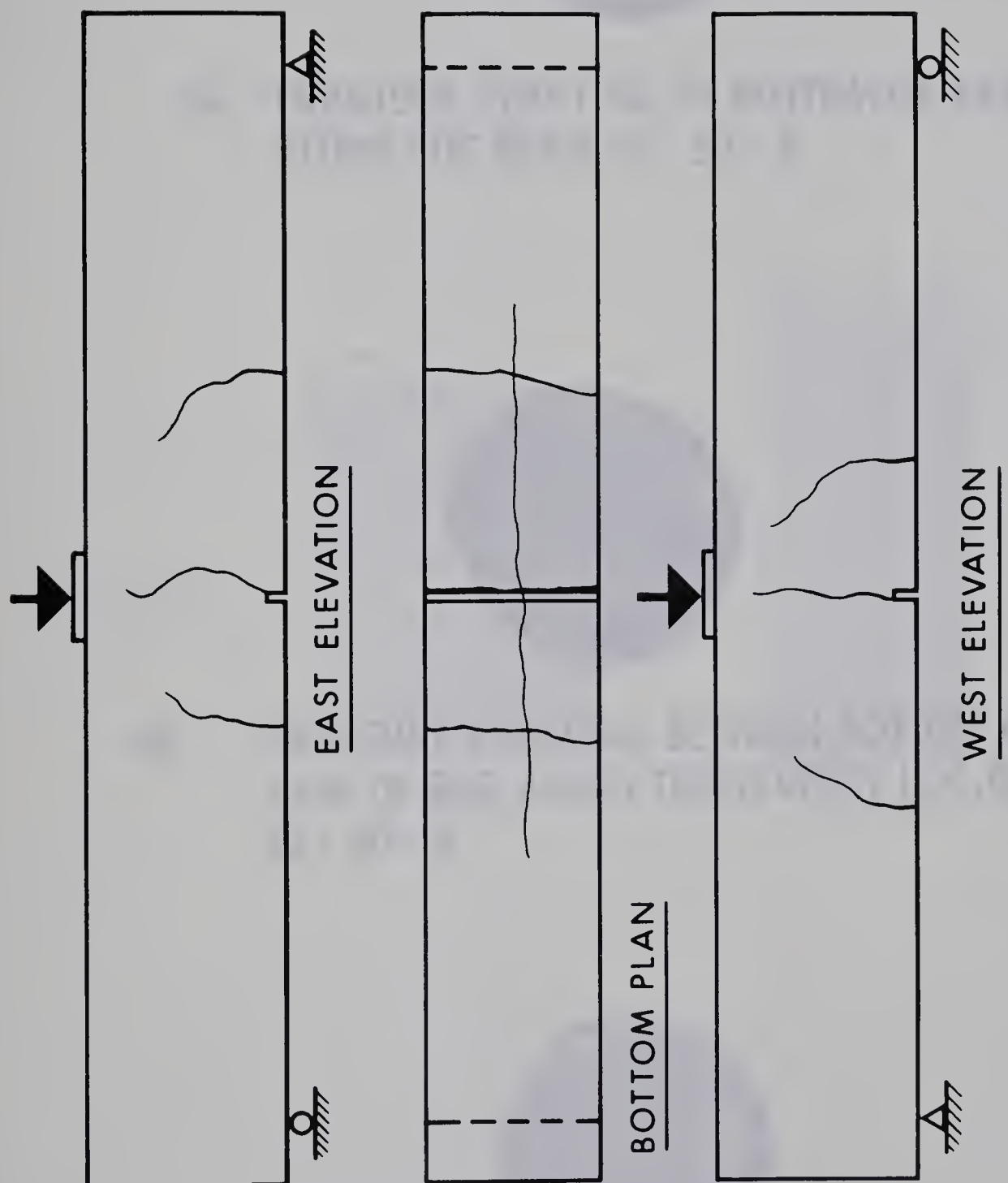
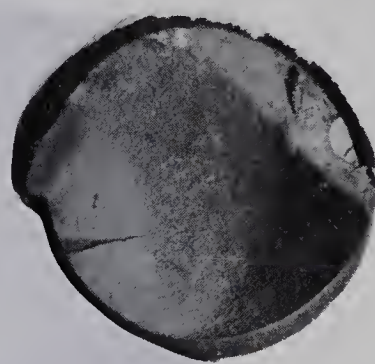


FIGURE 4.1 TYPICAL CRACK PATTERN IN BEAM SPECIMEN
AFTER FAILURE .

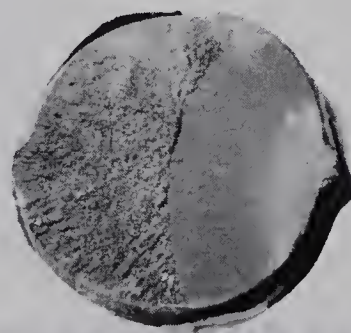
FIGURE 4.1



(a) FRACTURE STARTING AT BOTTOM OF BAR
ALONG LUG,BEAM 10 - 50 - 4



(b) FRACTURE STARTING BETWEEN BOTTOM AND
SIDE OF BAR ALONG TRANSVERSE LUG,BEAM
10 - 60 - 6



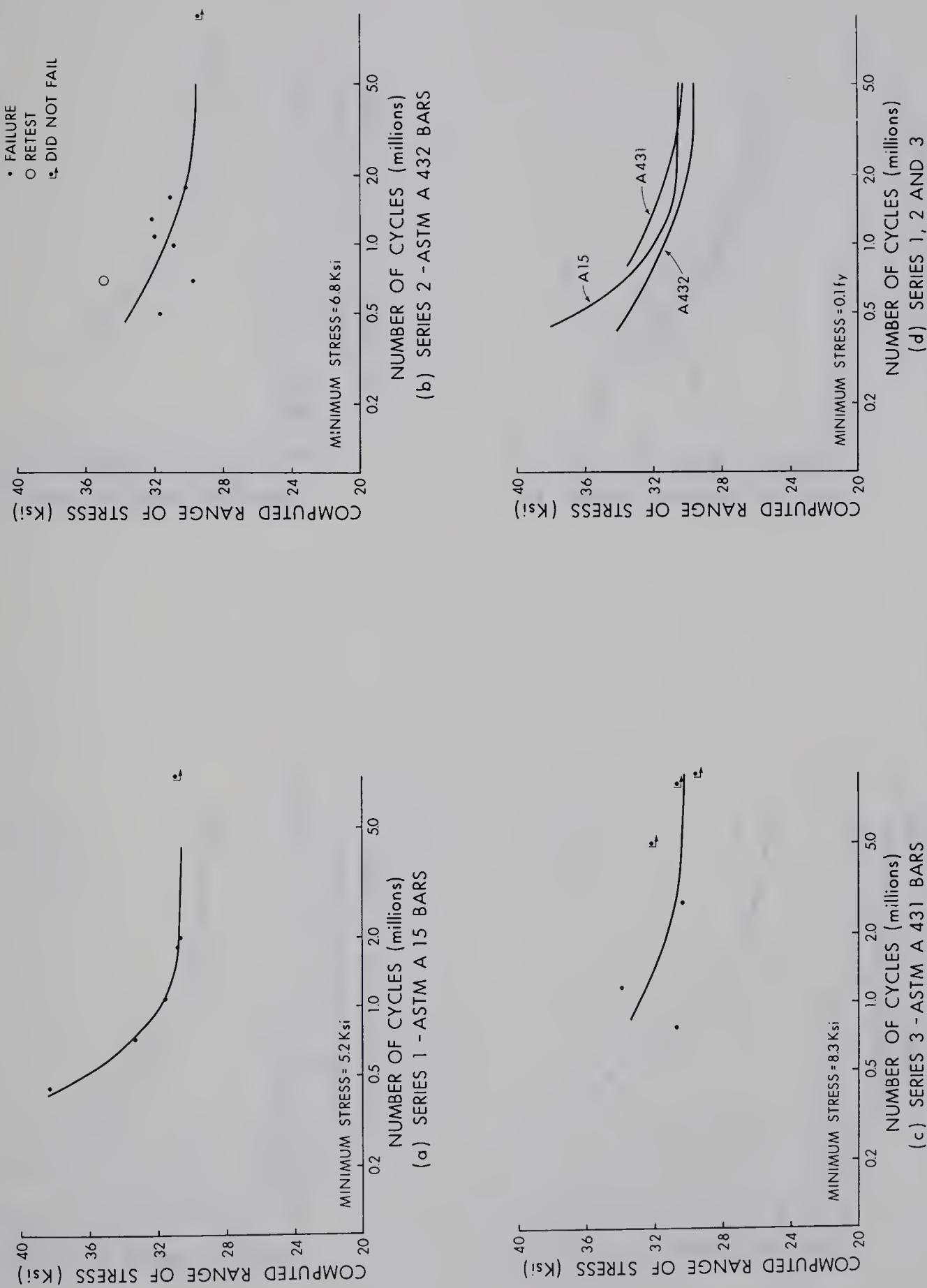
(c) FRACTURE STARTING AT INTERSECTION OF LUG
AND RIB,BEAM 10 - 75 - 5

FIGURE 4.2 TYPICAL FRACTURE SURFACES



FIGURE 4.3 FATIGUE CRACKS AND FATIGUE FAILURE OF BARS.

FIGURE 4.4 S-N CURVES FOR No. 8 BARS MINIMUM STRESS = 0.1 fy



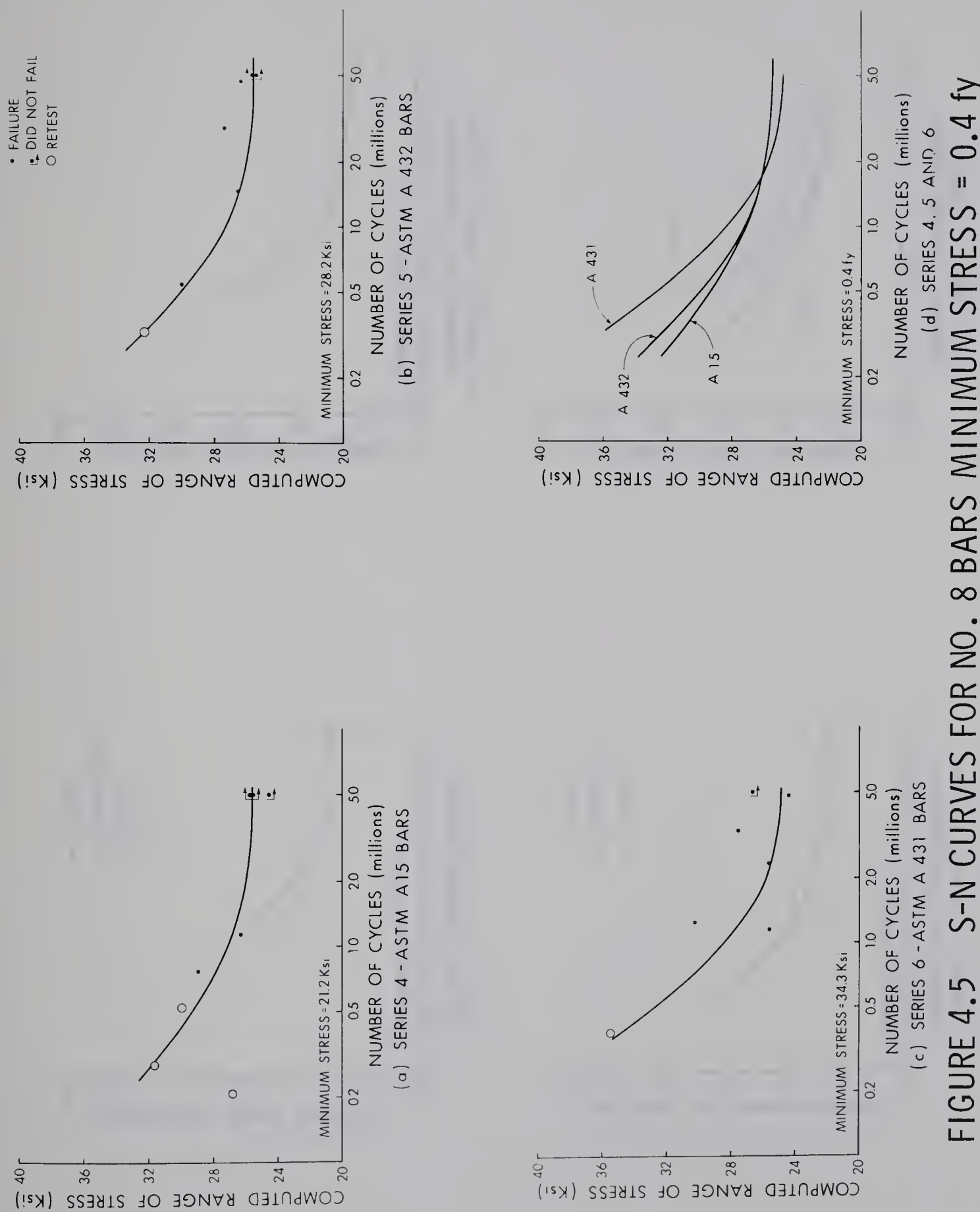


FIGURE 4.5 S-N CURVES FOR NO. 8 BARS MINIMUM STRESS = 0.4 fy

FIGURE 4.6 S-N CURVES FOR NO. 5 BARS MINIMUM STRESS = 0.1 fy

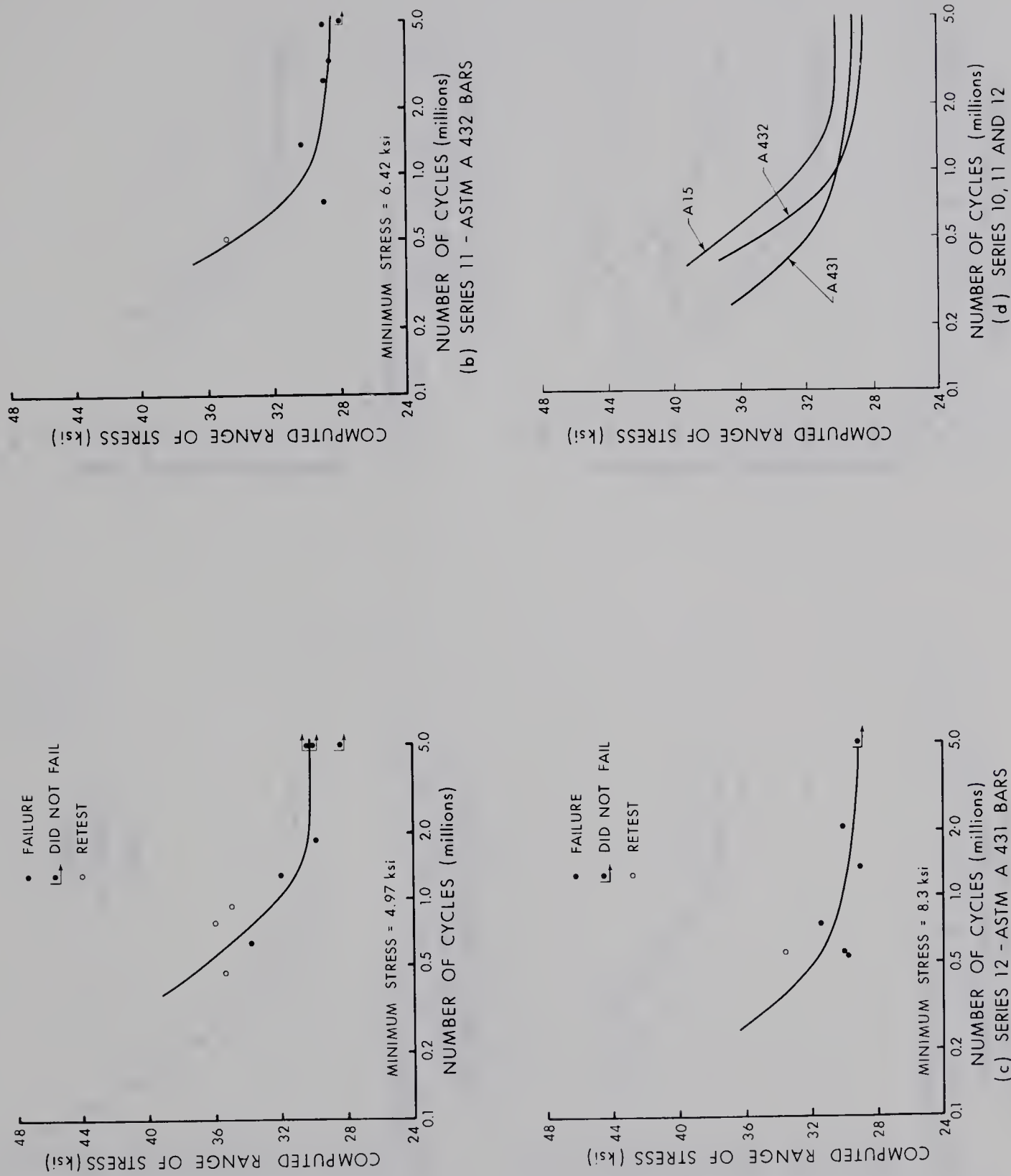


FIGURE 4.7 S-N CURVES FOR No. 10 BARS MINIMUM STRESS = 0.1 fy

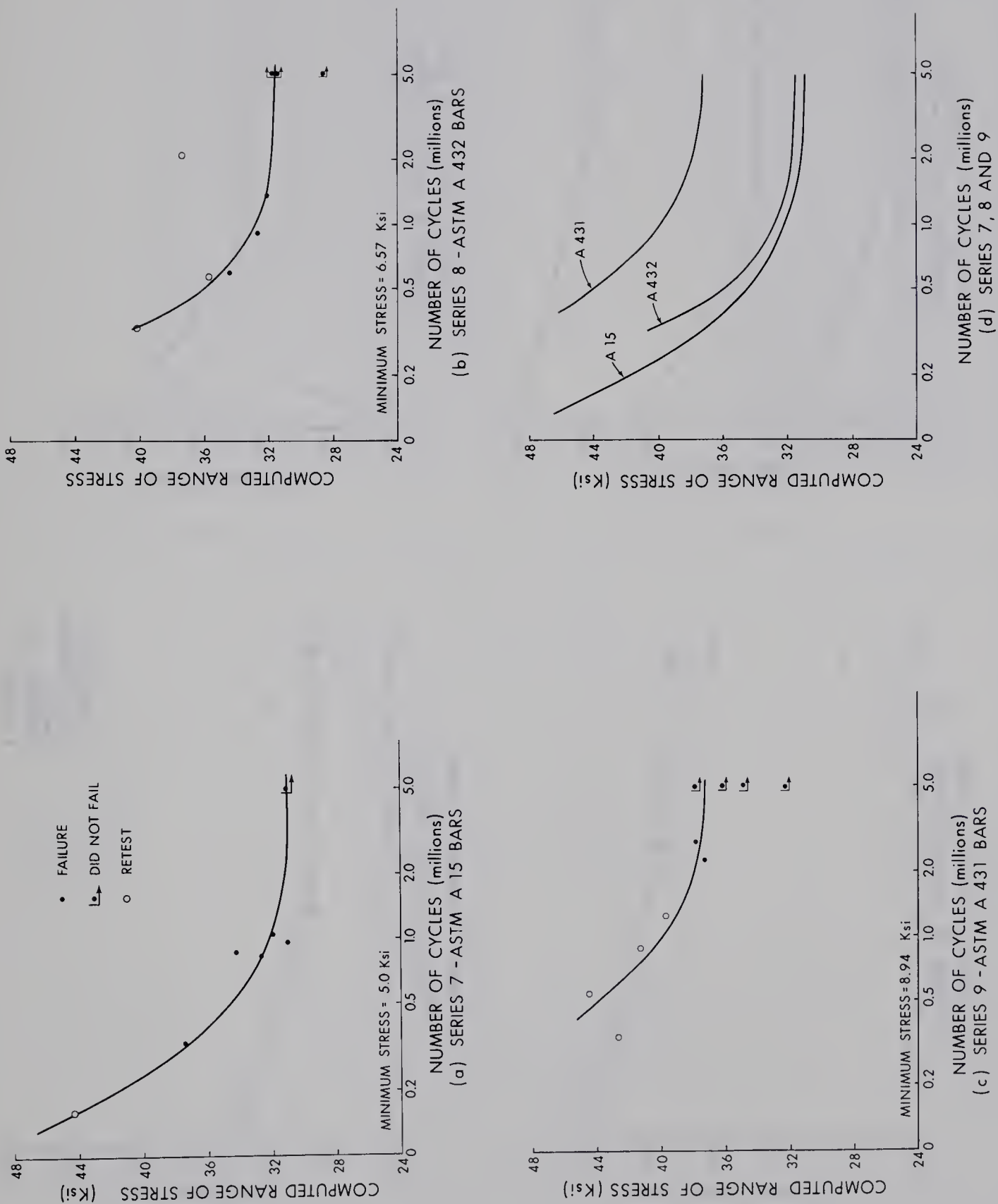
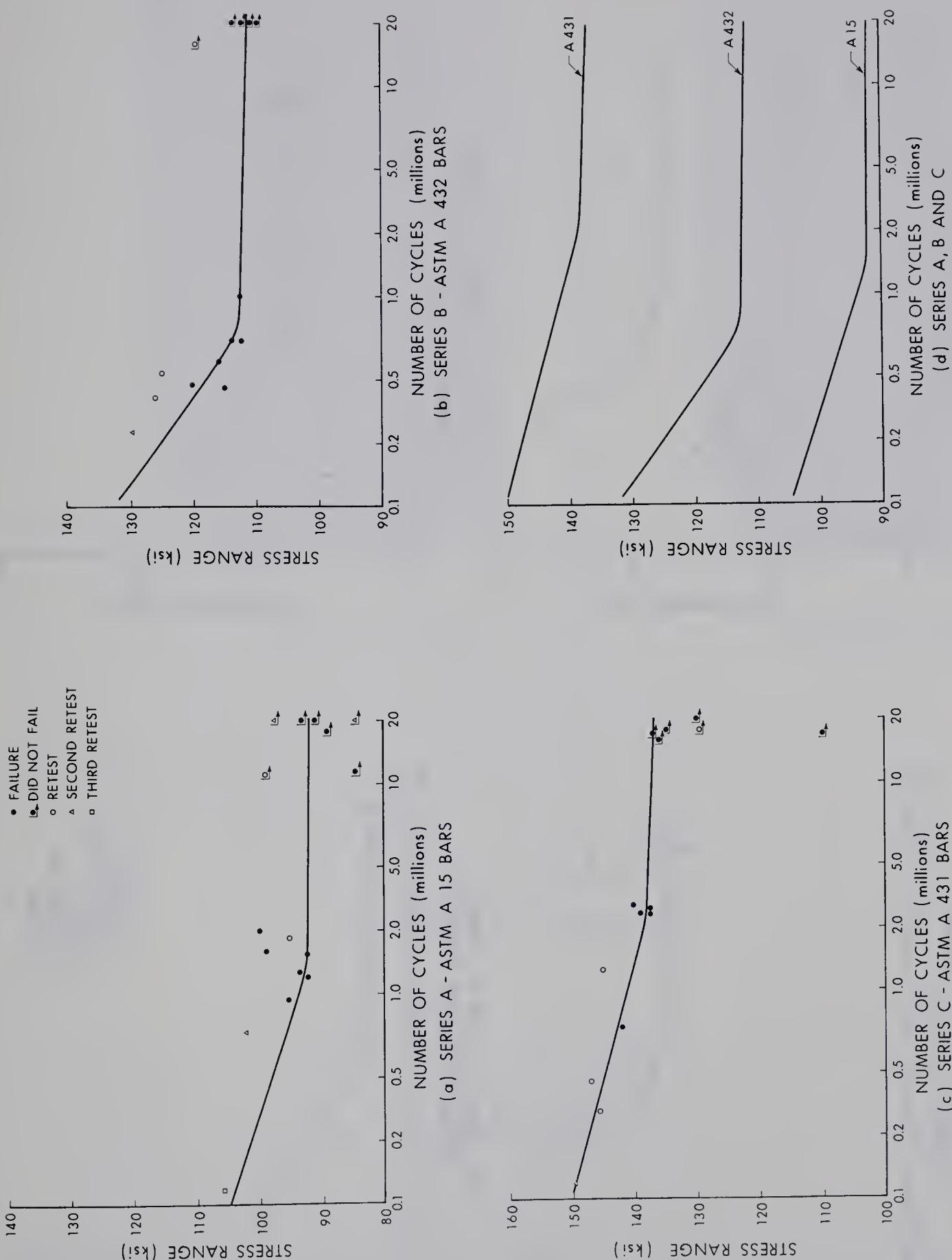


FIGURE 4.8 S-N CURVES FOR PLAIN ROTATING BEAM SPECIMENS



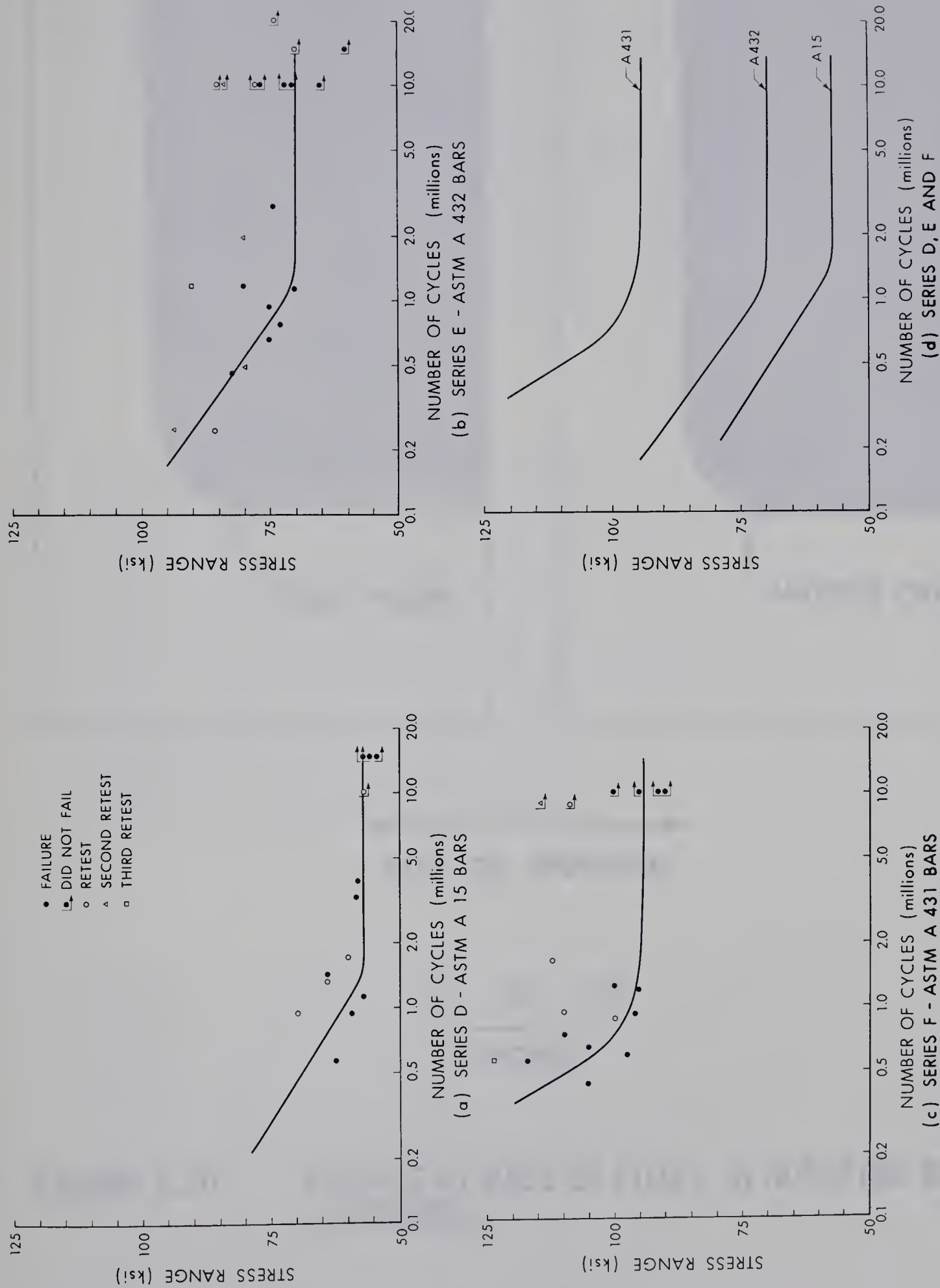


FIGURE 4.9 S-N CURVES FOR FILLETED ROTATING BEAM SPECIMENS

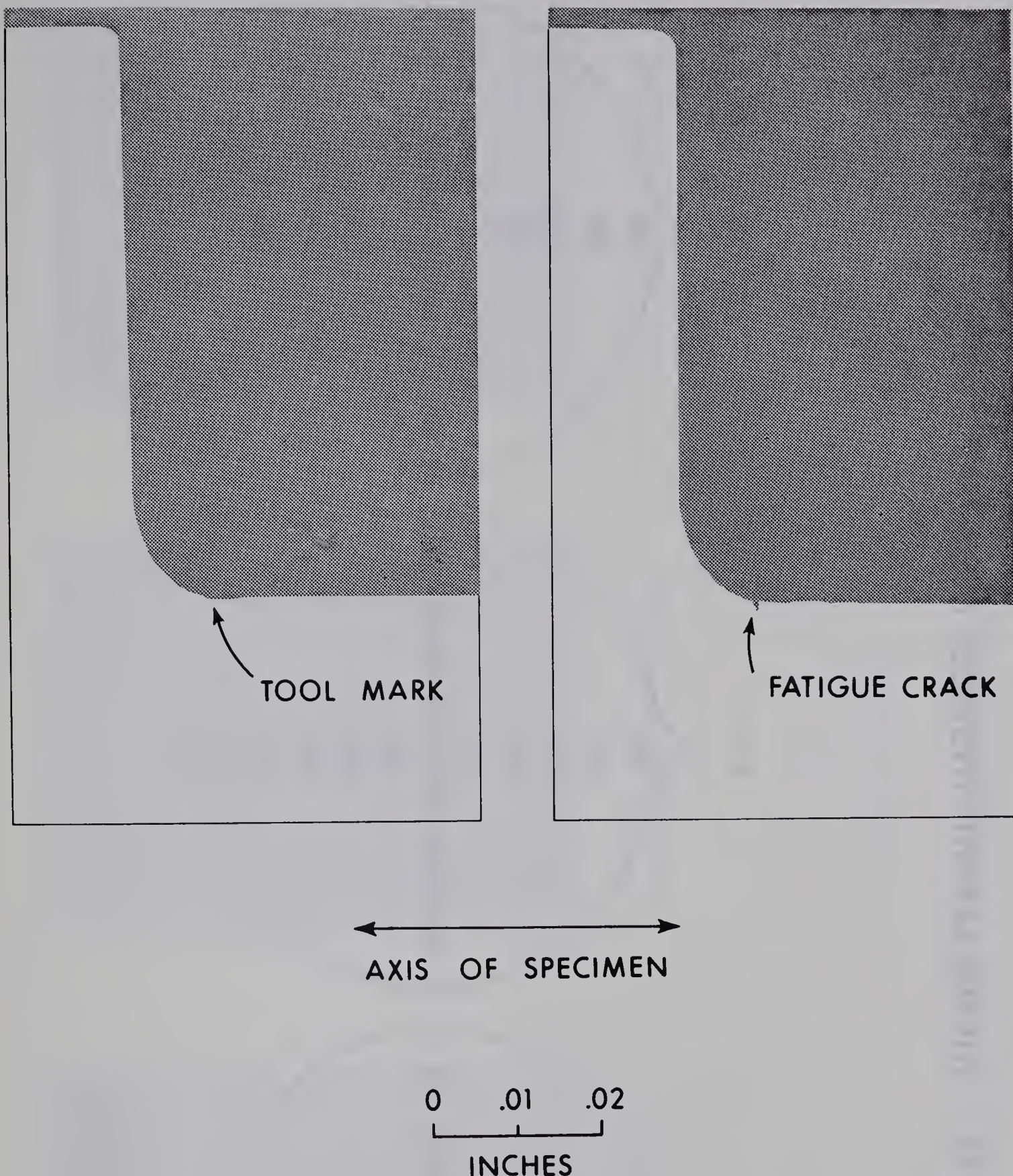


FIGURE 4.10

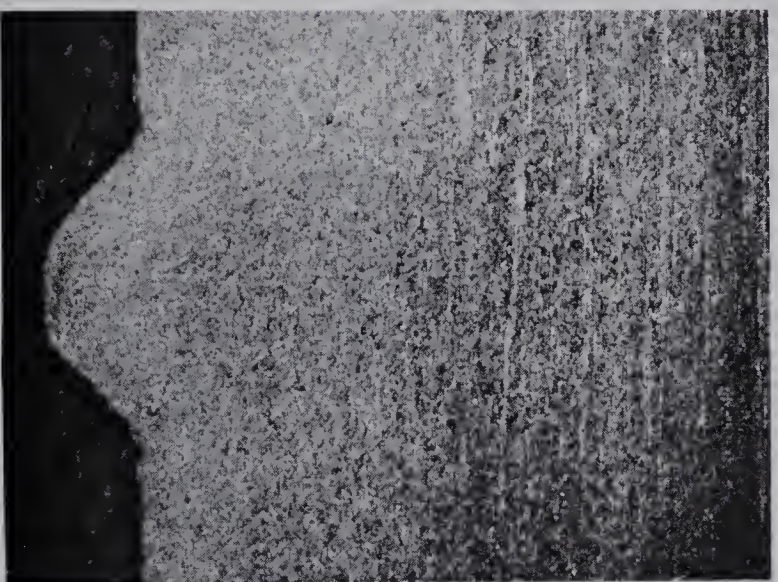
PROFILE AT BASE OF FILLET IN ROTATING BEAM SPECIMENS.



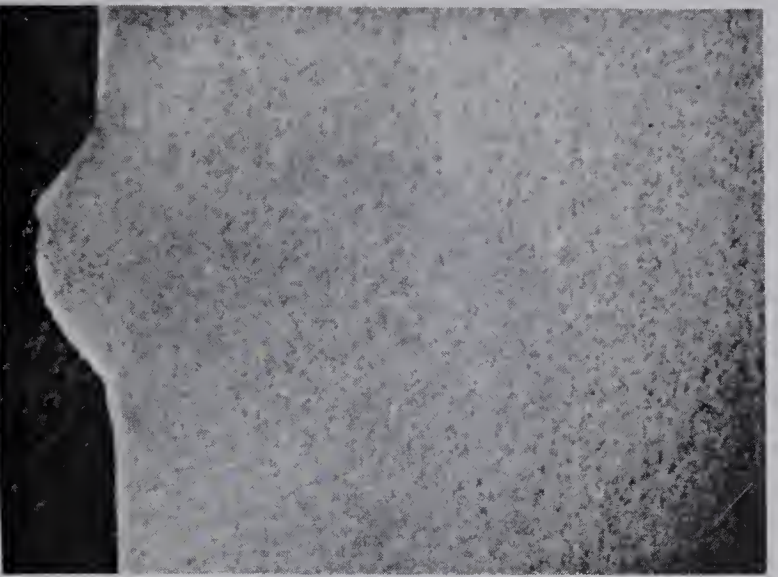
FIGURE 4.11 VICKER PYRAMID HARDNESS VALVES NO. 8 BARS



(a) ASTM A15 BAR



(b) ASTM A432 BAR



(c) ASTM A431 BAR

FIGURE 4-12 MACRO-STRUCTURE OF NO. 8 REINFORCING BARS.



(a) ASTM A15 BAR
(b) ASTM A432 BAR
(c) ASTM A431 BAR

SCALE - INCHES

0 0.1 0.2

FIGURE 4.13 MACRO-STRUCTURE OF NO.8 REINFORCING BARS

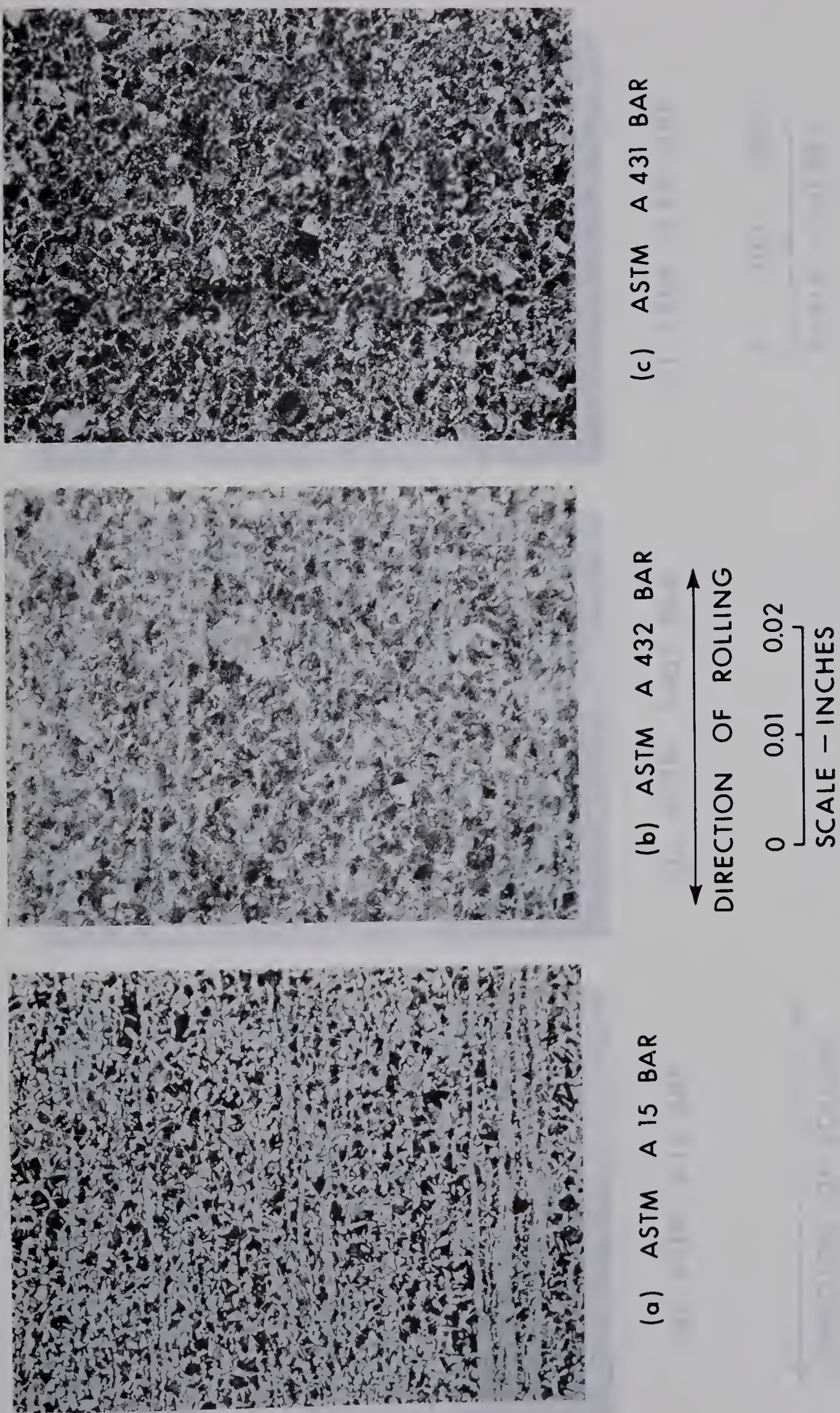
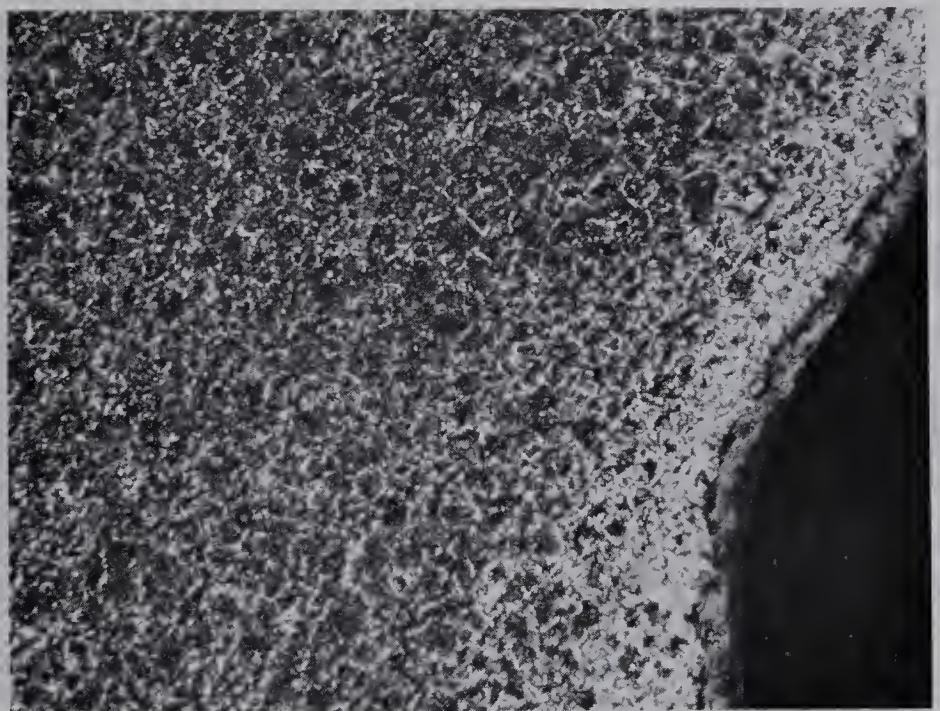


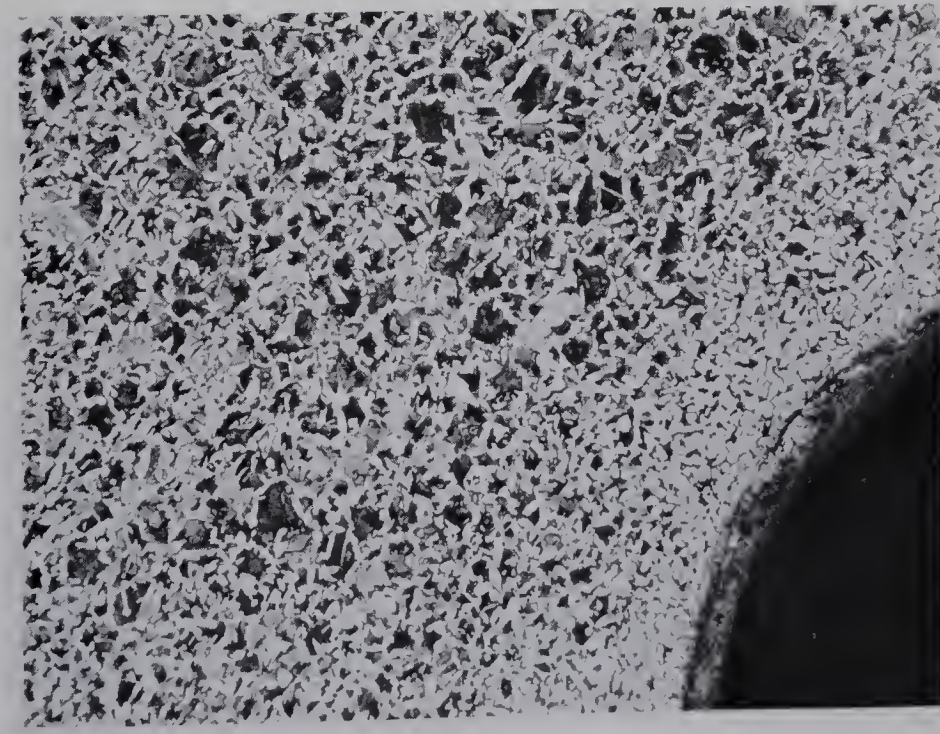
FIGURE 4.14 MICRO-STRUCTURE OF LONGITUDINAL SECTIONS OF No. 8 REINFORCING BARS.



(c) ASTM A 431 BAR



(b) ASTM A 432 BAR



(a) ASTM A 15 BAR

→
DIRECTION OF ROLLING

0 0.01 0.02
SCALE — INCHES

MICRO-STRUCTURE OF NO. 8 REINFORCING BARS
AT BASE OF DEFORMATION LUG.

FIGURE 4-15

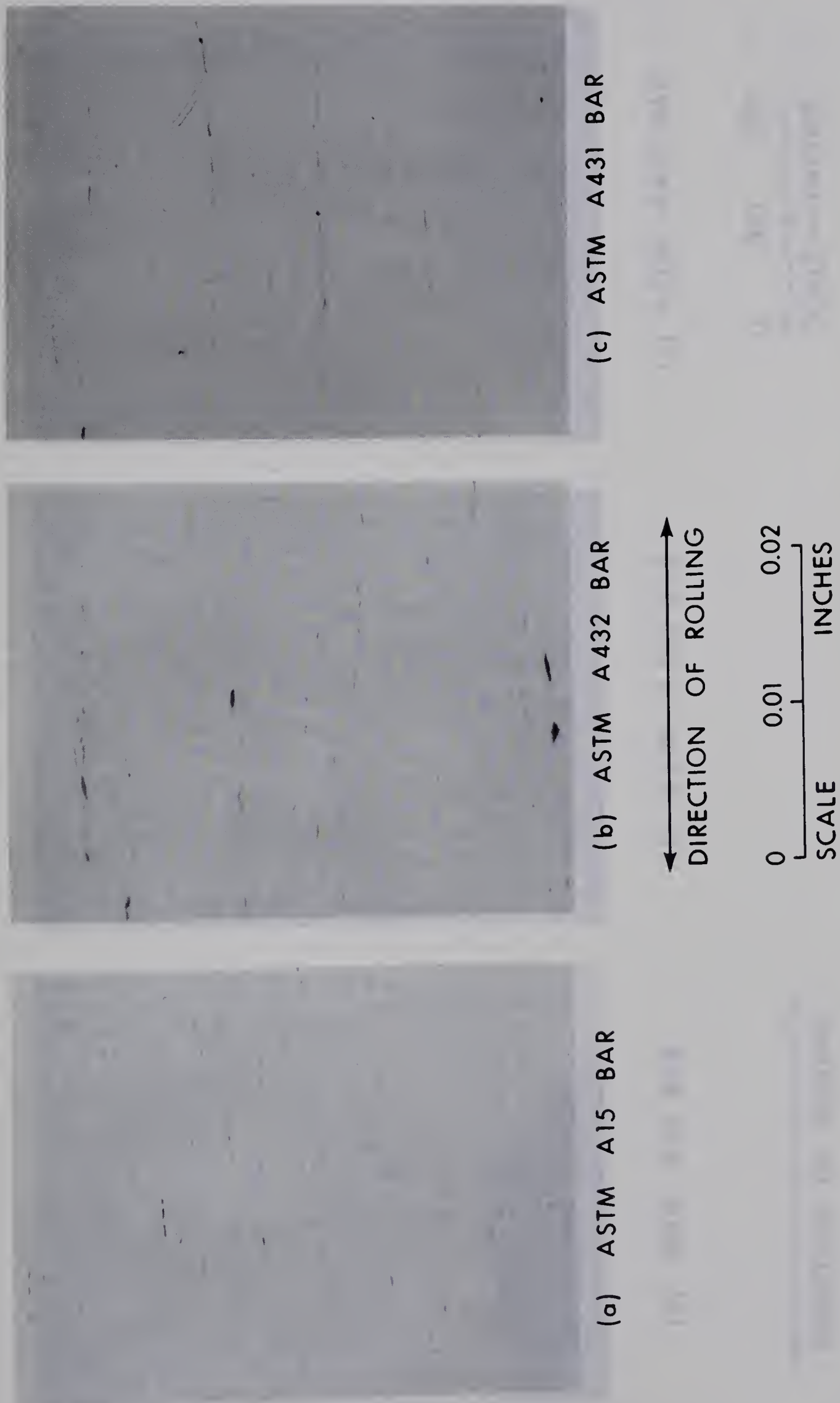
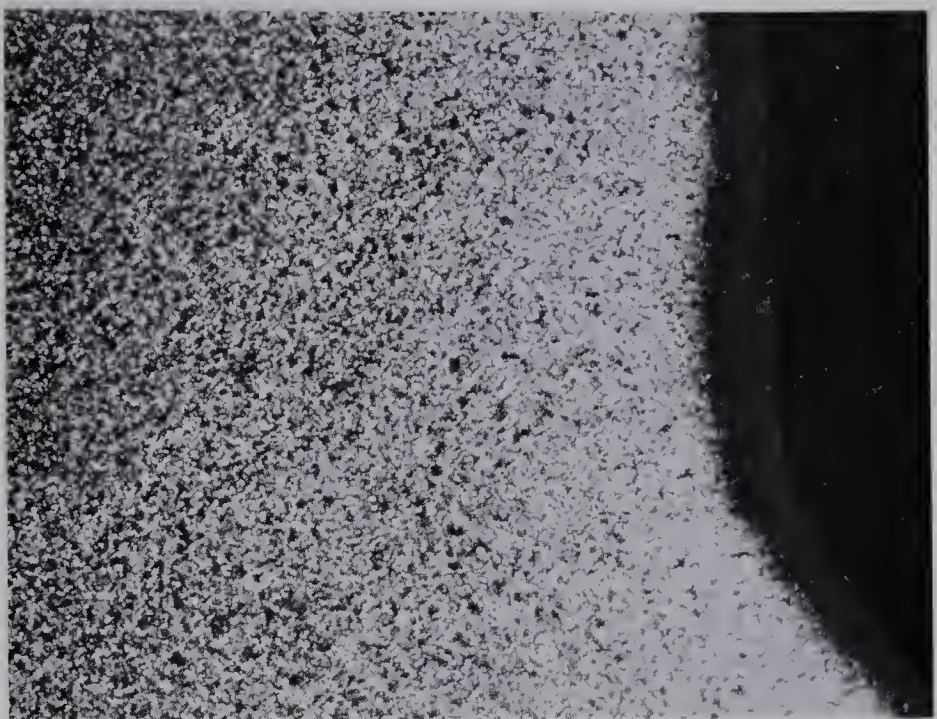


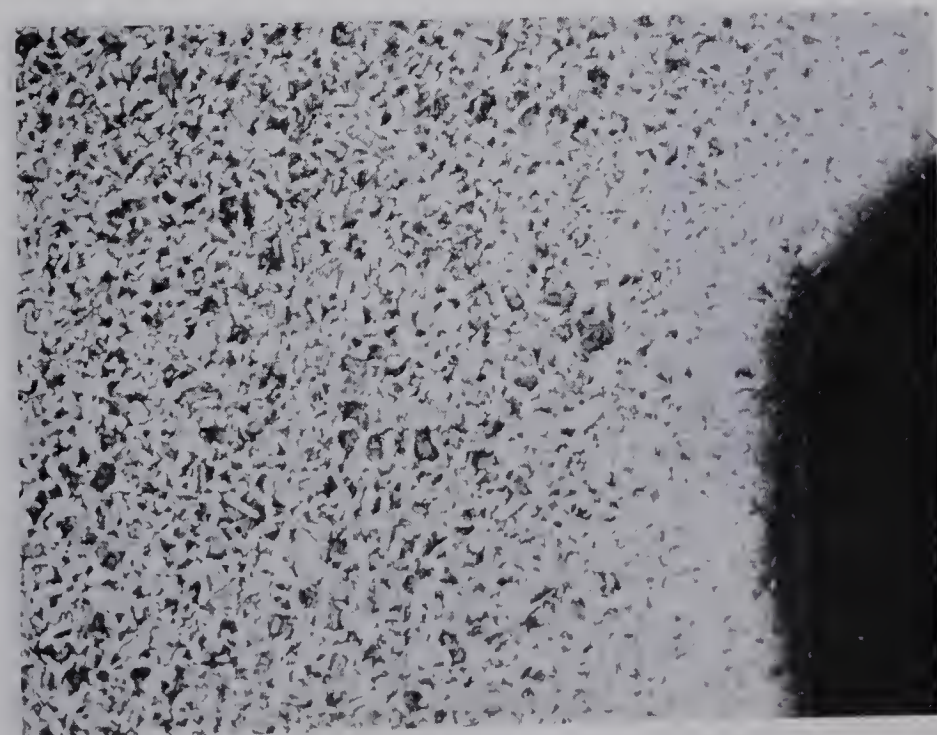
FIGURE 4-16
NON-METALLIC INCLUSIONS IN LONGITUDINAL SECTIONS
NO. 8 REINFORCING BARS.



(a) ASTM A15 BAR



(b) ASTM A432 BAR



(c) ASTM A431 BAR

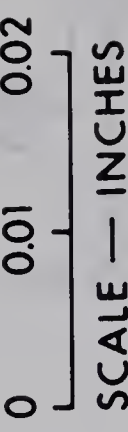
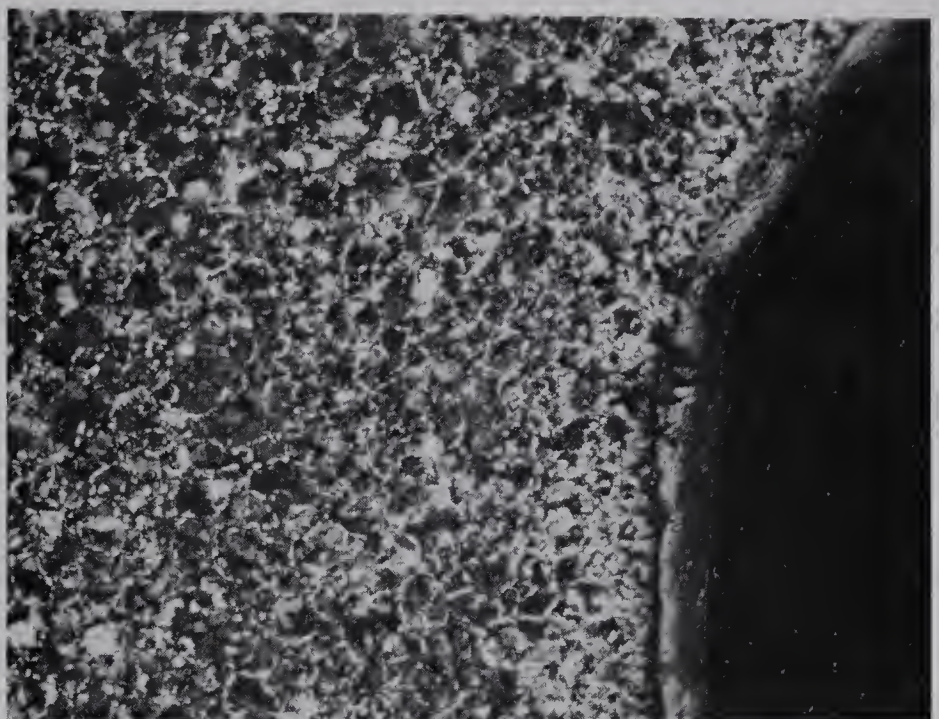
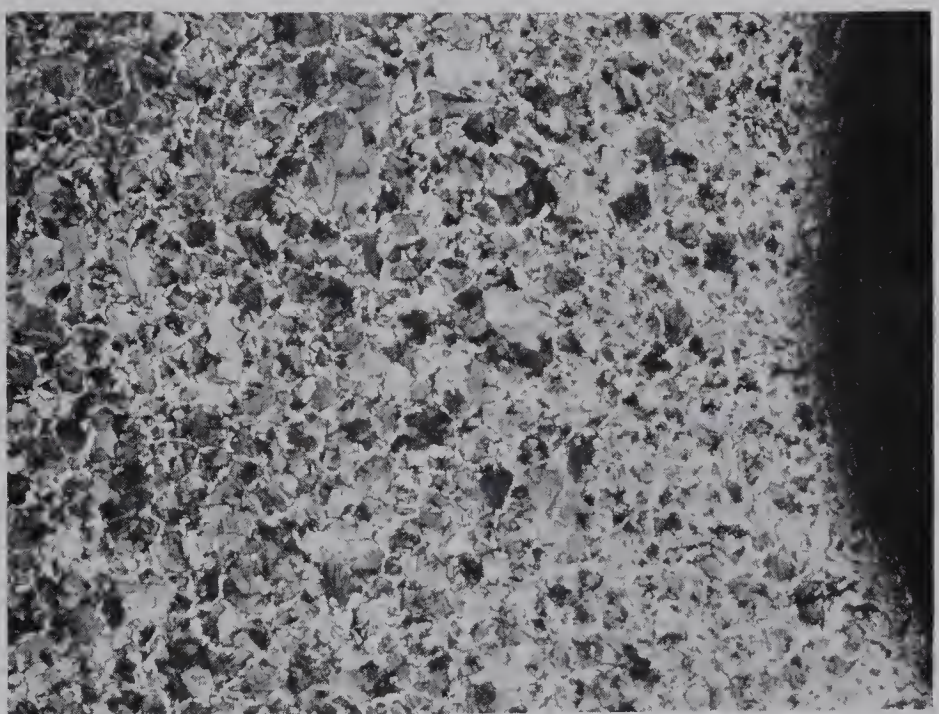


FIGURE 4 - 17 MICRO-STRUCTURE OF NO. 5 REINFORCING BARS
AT BASE OF DEFORMATION LUG.



(c) ASTM A 431 BAR



(b) ASTM A 432 BAR



(a) ASTM A 15 BAR

→
DIRECTION OF ROLLING

0 0.01 0.02
SCALE — INCHES

FIGURE 4 - 18 MICRO-STRUCTURE OF No. 10 REINFORCING BARS
AT BASE OF DEFORMATION LUG.

CHAPTER V

DISCUSSION OF TEST RESULTS

The test series presented in this report considered three main variables; the bar diameter, the grade of steel in the bar and the minimum stress level used in the tests. In addition, the deformations differed in height and base radius although the deformation pattern was similar in all the bars tested. Each of these variables will be discussed in this chapter. The implications of the metallurgical observations will also be discussed briefly.

5.1 Effect of Minimum Stress

The fatigue strength of metals at various minimum stress levels is related to the type of metal and the applied stress function. The fatigue test data of ferrous metals under direct and bending stresses, when plotted on an R-M diagram as shown in FIGURE 2.10, generally fall between the Gerbers parabola and Modified Goodman line as discussed in Section 2.2.5. The test results from hot-rolled deformed reinforcing bars tend to fall along the Modified Goodman line as shown in FIGURES 2.12 to 2.15 while the data from tests of cold worked deformed bars agrees more closely to the Gerber parabola as illustrated in FIGURE 2.16. In general, for reinforcing bars the stress range corresponding to any given fatigue life decreases with an increase in the minimum stress of the cycle. This effect seemed to be more pronounced for hot rolled steels than for cold worked steels.

The limiting stress range of No. 8 bars at a minimum stress of $0.1 f_y$ and $0.4 f_y$ can be compared using the Modified Goodman Diagram

shown in FIGURES 5.1 to 5.3. These figures are plotted for stress cycles corresponding to the fatigue strength at five million cycles as determined from the S-N curves in FIGURES 4.4 and 4.5. In a Goodman Diagram the average stresses in the cycles are plotted horizontally and the maximum and minimum stresses in the cycles are plotted vertically. The envelopes to the test data in FIGURES 5.1 to 5.3 can be represented with straight lines. The stress ranges reported in column 8 of TABLE 4.1 were obtained from these and similar Goodman Diagrams.

These test diagrams suggest that the test data for different grades of hot rolled reinforcing bars tested at various minimum stress levels may be approximated by the Modified Goodman Law. Although this conclusion differs from that reached by several other investigators (15, 17,28), it is supported by Goodman Diagrams such as those in FIGURES 2.12 to 2.15 for data from other investigations of hot rolled reinforcing bars (28,34). For cold worked reinforcing bars there is evidence that this conclusion is not valid (see FIGURE 2.16).

5.2 Effect of Yield and Ultimate Strength

The effect of yield and ultimate strength on fatigue strength of reinforcing bars may be discussed from two points of view. First, it is possible to consider the effect of the grade of steel on the fatigue strength of the metal in the bar and then, by means of the study of the effective stress concentration produced due to deformations and bar size effect, to combine these effects to determine the fatigue strength of reinforcing bars. Second, it is possible to compare the fatigue strength of two reinforcing bars of different grade but having identical deformations, bar size and used in beams of similar cross-

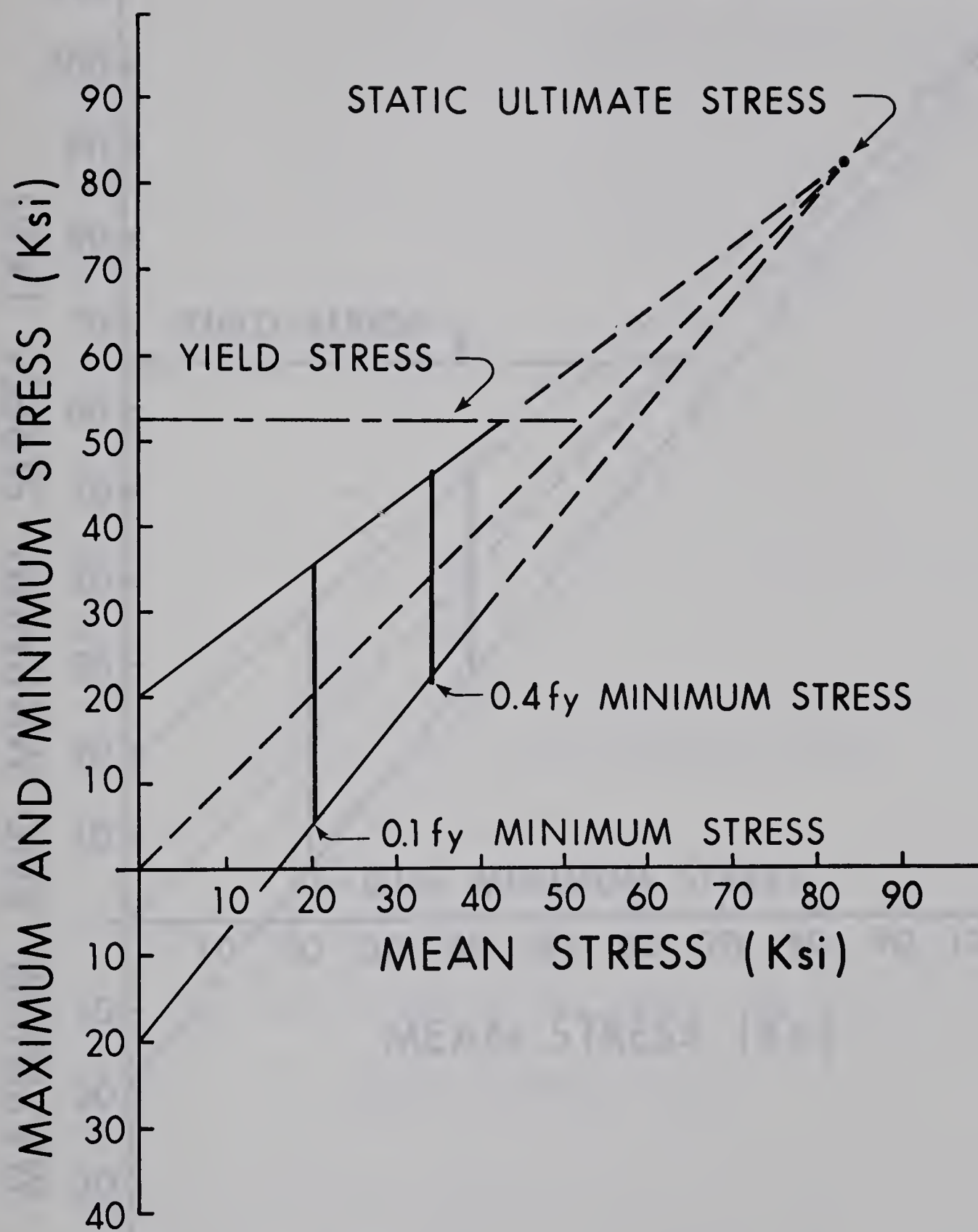


FIG. 5.1 MODIFIED GOODMAN DIAGRAM
FOR NO 8 ASTM A15 BARS

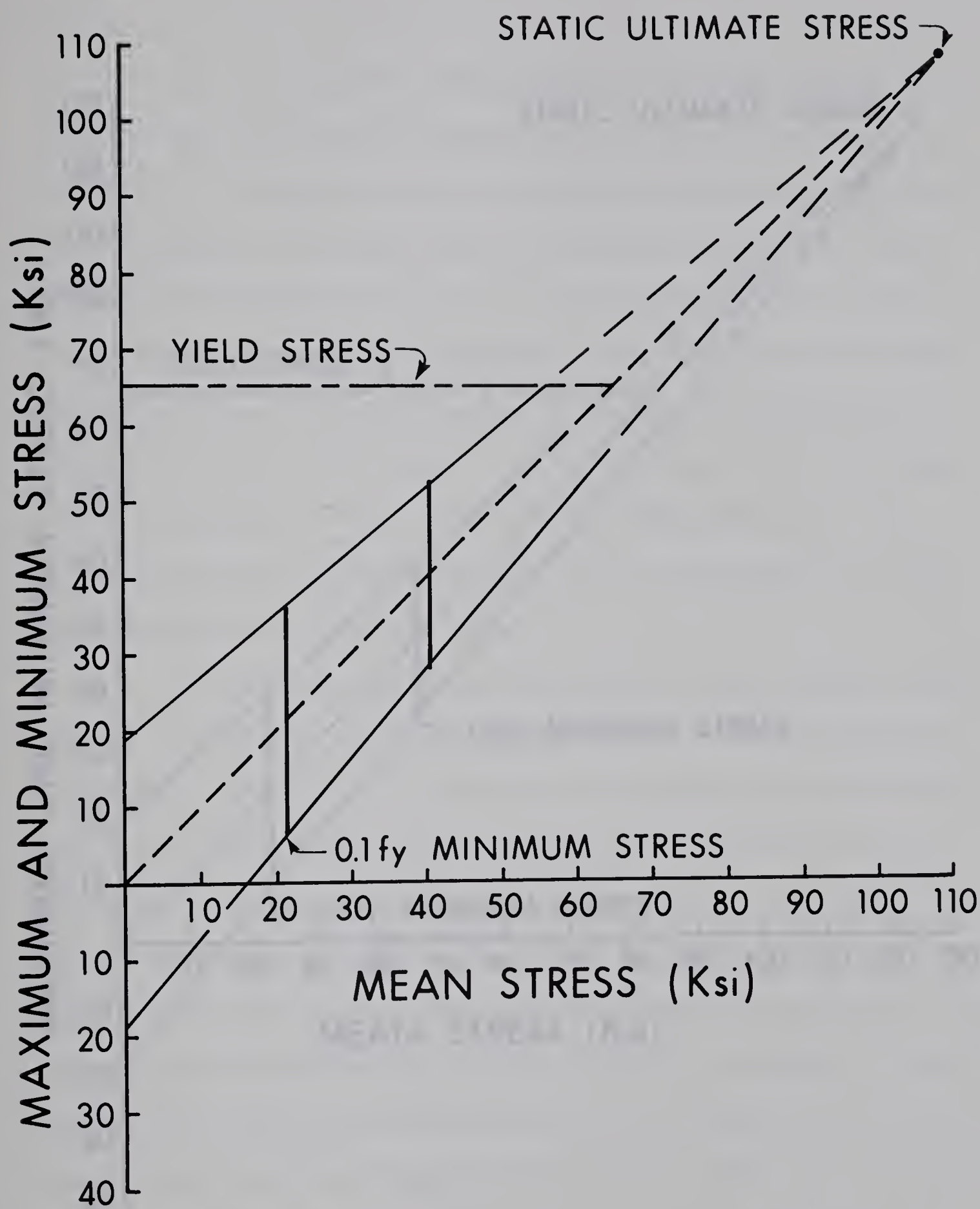


FIG. 5.2 MODIFIED GOODMAN DIAGRAM
FOR NO 8 ASTM A 432 BARS

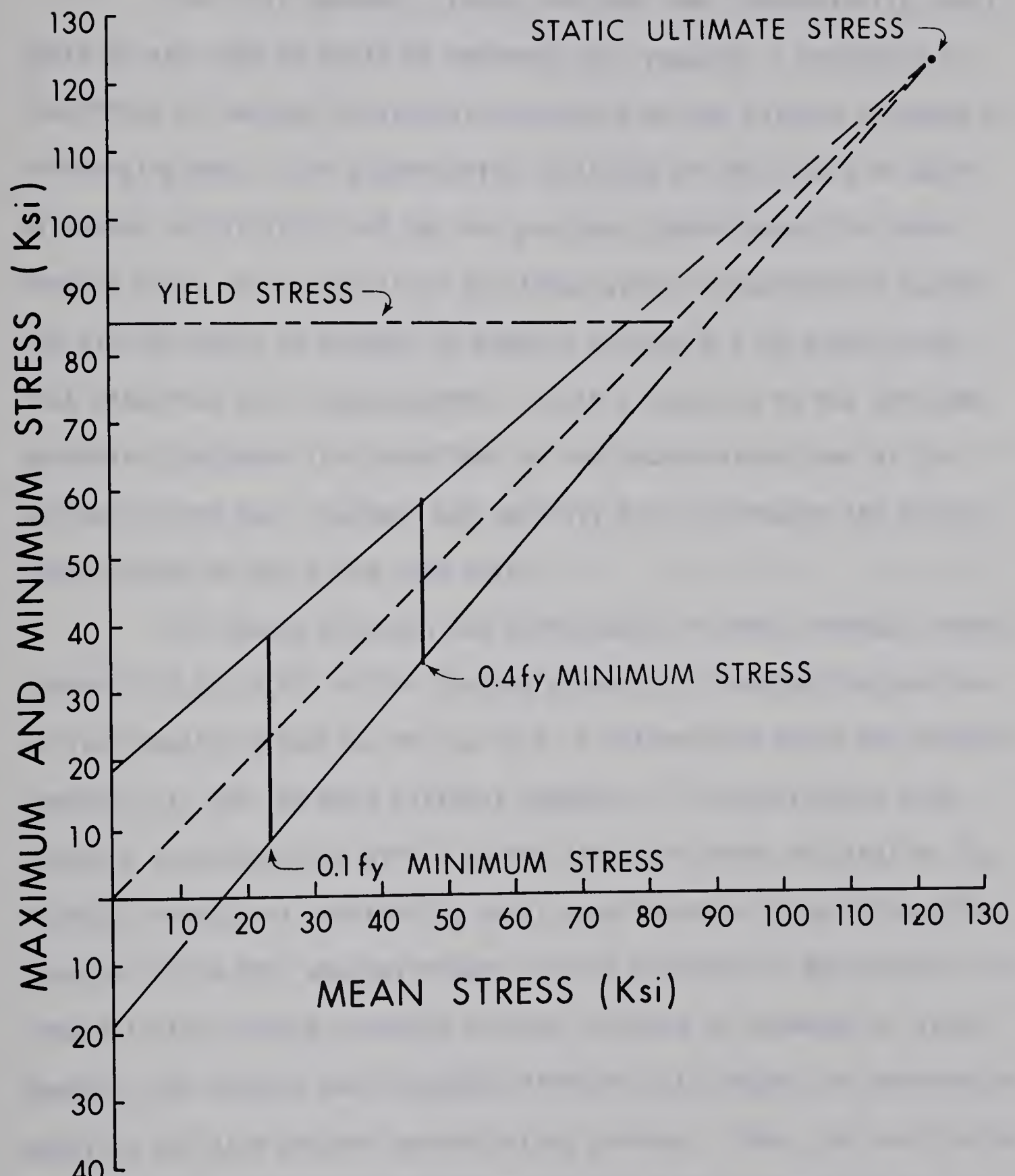


FIG. 5.3 MODIFIED GOODMAN DIAGRAM
FOR NO 8 ASTM A 431 BARS

section.

The first approach, though rational and theoretically applicable to any type of plain or deformed bar, requires a knowledge of the effect of various individual parameters on the fatigue strength of reinforcing bars. The quantitative isolation of the effect of each parameter is difficult and has not yet been investigated for reinforcing bars. On the basis of published stress concentration factors and similar data, an attempt is made in Section 5.4 to explain the test data from this investigation. In this analysis it has not been possible to account for the effect of the decarburized zone at the surface of the bar, however, and possibly for this reason the calculated values do not agree with tests.

The second approach has been adopted in most previous investigations (28,31,34,40) of the fatigue strength of reinforcing bars due to its simplicity and due to the lack of information about the factors necessary to use the more rational approach. The conclusions from previous investigations differ on the effect of grade of steel on the fatigue strength of reinforcing bars; some found an insignificant influence (28,34,40), whereas others (31,34) observed an appreciable increase in the fatigue strength with an increase in strength of steel. However, the various test programs differed with respect to deformation details, bar size and bar manufacturing process. Thus, the conclusions derived for one deformation pattern and bar size, though true for a particular set of parameters, may not apply to another set of variables, since the fatigue response of a bar should change with the grade of steel (see section 2.3.4), the deformation pattern (2.3.5) and the bar size (2.3.6).

The fatigue strength of plain standard rotating beam specimens cut from No. 8 bars tested in this investigation increased almost linearly with the increase in the strength of the steel, as shown in FIGURES 5.4 (a) and (b). In these tests, the metal in the center of the bars could resist fatigue stresses ranging from 51 to 55 percent of the tensile strength of the bars. This indicates that the metal in the higher grade steel bars has the ability to resist higher fatigue stresses and the fatigue strength at complete reversal is about 50 percent of the tensile strength of the metal. It should be noted in this respect that the rotating beam specimens were cut from the center of the bars and the hardness and metallographical observations revealed that the metal properties were not uniform across the bar cross-sections.

In contrast to plain rotating beam specimens, the fatigue strength of reinforcing bars in reinforced concrete beam tests was found almost constant for eight out of nine bars investigated as shown in TABLE 4.1 and FIGURE 5.4. The exception was the A 431 No. 5 bar which showed an increase of about 15 percent in the stress range at 0.1 f_y minimum stress as compared to A 15 and A 432 steel bars of the same size. On further examination it was found that the ratio of the radius at the base of the deformations to the height of the lugs was about three times than that for the A 15 and A 432 steel bars. This will be discussed more fully in section 5.4.

The variation in fatigue strength plotted in FIGURES 5.4(a) and (b) may be affected by at least four factors:

1. The yield strength or ultimate tensile strength of the bars.
2. The surface condition of the bars. The two dashed lines in

each figure refer to specimens having machined surfaces.

The top curve represents specimens that were relatively free of stress concentrations. The three solid lines refer to bars having a rolled surface with deformations and varying degrees of oxide coating and decarburization.

3. The size of the bars. The two dashed lines represent specimens 1/4 inch in diameter at the section of failure. The diameter of reinforcing bar specimens plotted with the solid lines was 5/8, 1 and 1-1/4 inches, respectively from top to bottom.
4. The type of loading cycle. The two types of specimen shown with dashed lines were tested in completely reversed bending cycles while the other specimens were tested in cycles varying from a minimum to maximum tension which was almost axially applied.

FIGURES 5.4 (a) and (b) suggest that for practical purposes the fatigue strength of the deformed bars investigated was between 17.5 and 20 ksi for completely reversed stress cycles, regardless of the size or strength of the bar.

FIGURES 5.5 (a) and (b) compares the test results of this investigation with the available test data on deformed bars (28,31,33,34,40). In plotting these figures, Goodman Diagrams were used to adjust all data to a stress cycle with minimum stress equal to zero. The Alberta tests are shown by the solid lines in these figures. In general it may be concluded that the ratio of fatigue strength to yield or tensile strength decreases with an increase in the yield or tensile strength of deformed bars.

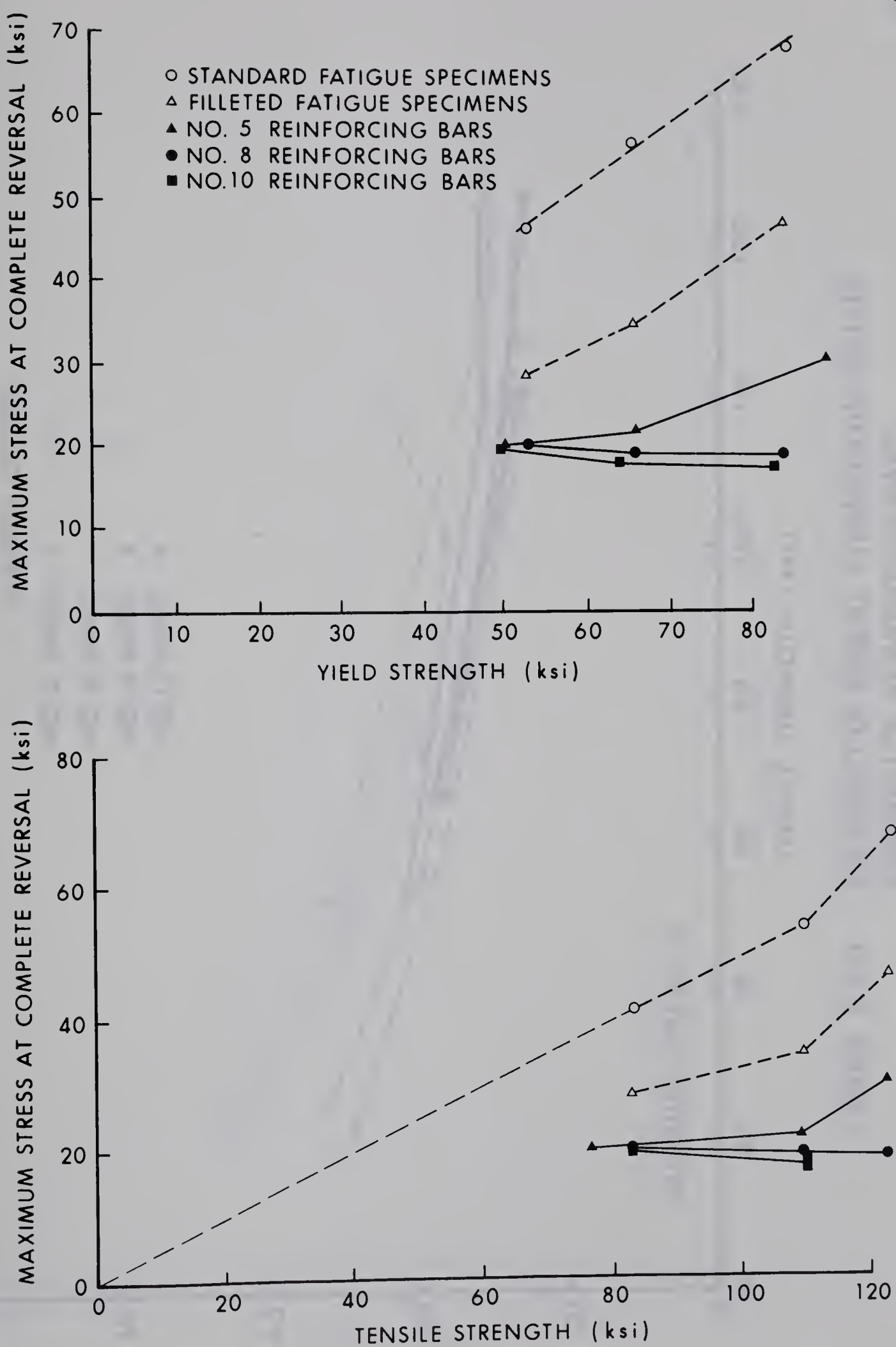


FIGURE 5.4

EFFECT OF YIELD AND TENSILE STRENGTH ON
FATIGUE STRENGTH - ALBERTA TESTS.

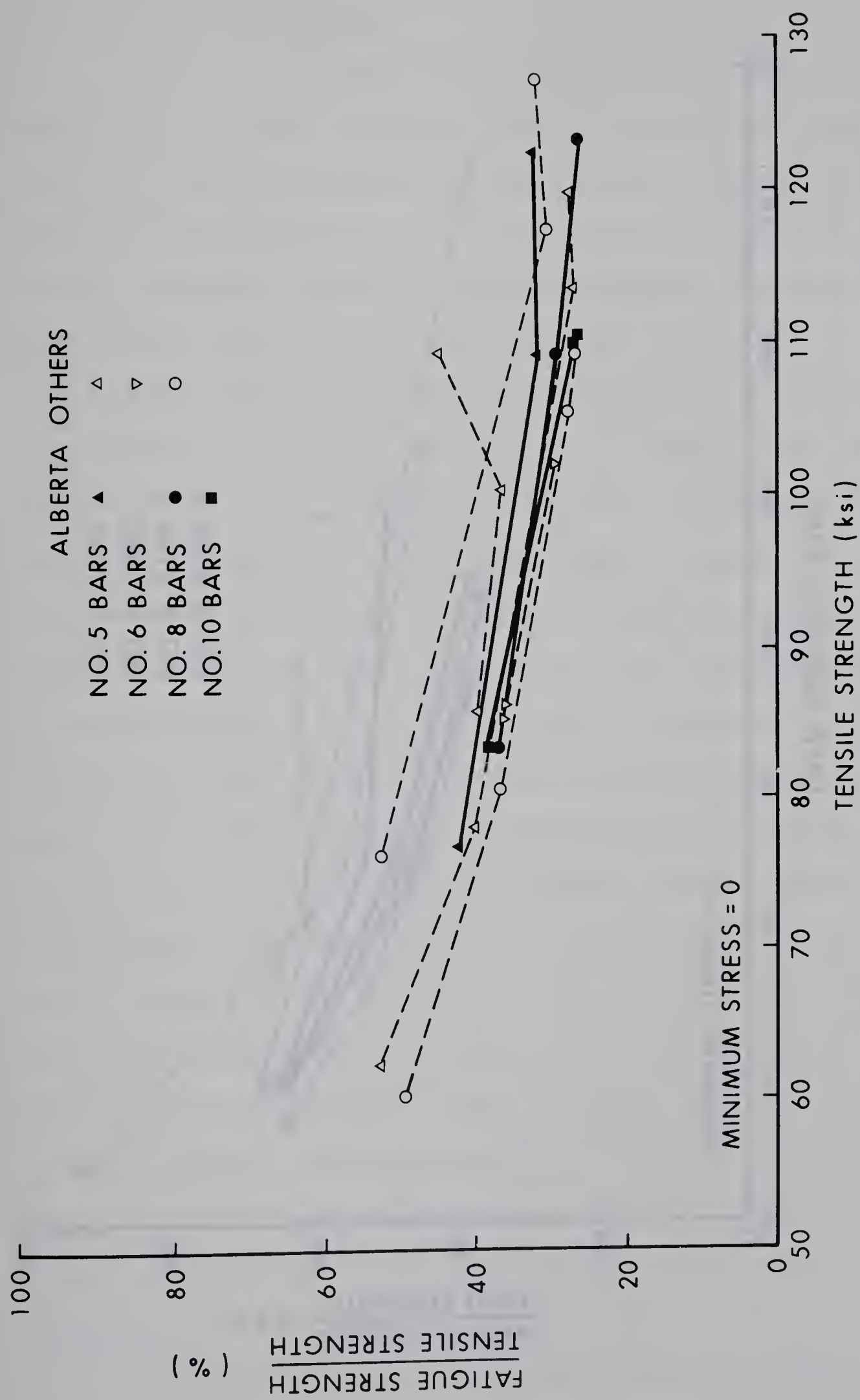


FIGURE 5.5(a) THE EFFECT OF TENSILE STRENGTH ON FATIGUE STRENGTH OF REINFORCING BARS

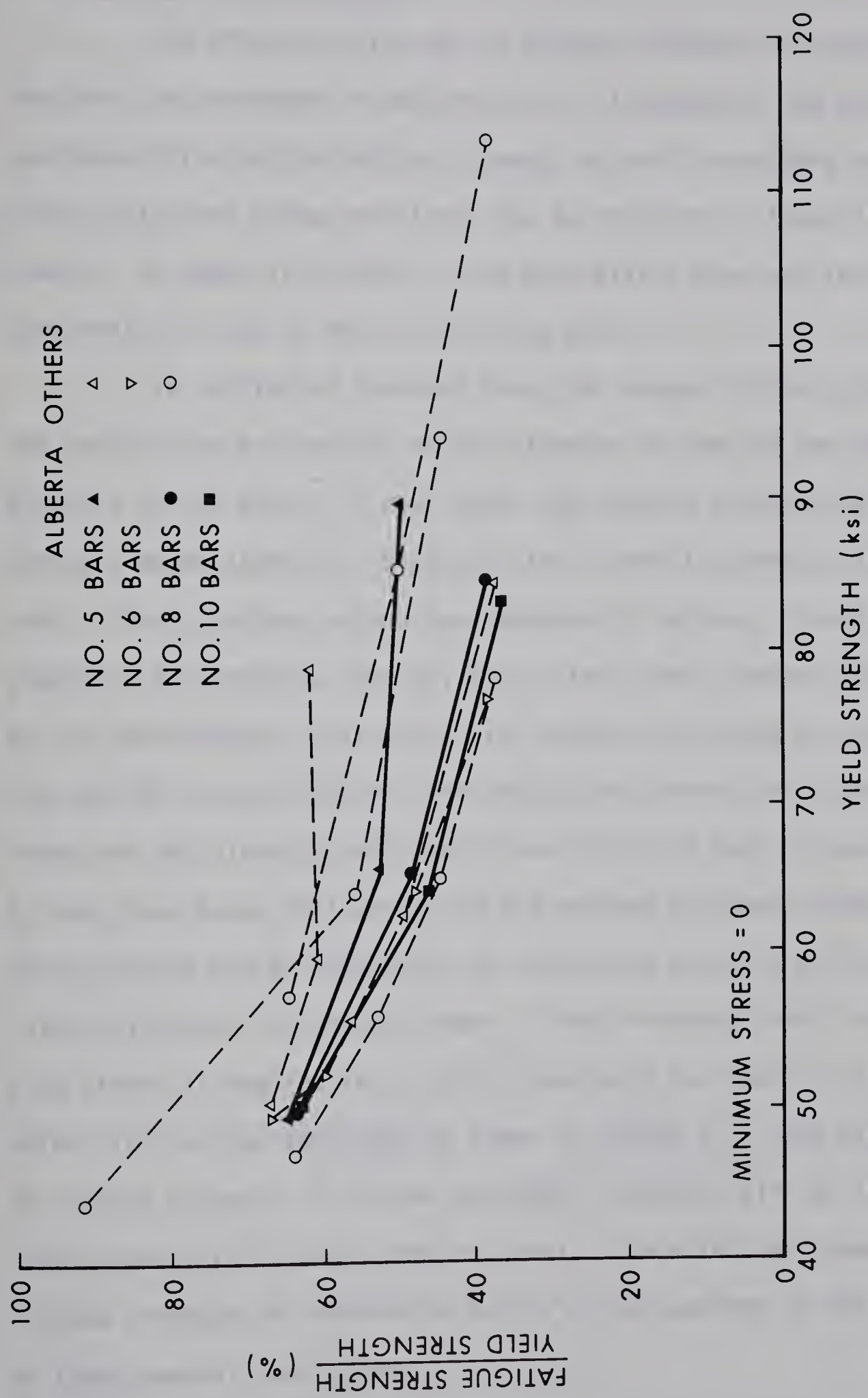


FIGURE 5.5(b) THE EFFECT OF YIELD STRENGTH ON FATIGUE STRENGTH OF REINFORCING BARS

5.3 Effect of Bar Diameter

The effect of size on the fatigue strength of machined steel specimens was reviewed in section 2.2.2. In general, the size of the specimens affected the fatigue strength of small specimens and specimens with significant stress gradients due to notching or flexural loading. However, as shown in FIGURE 2.3 the size effect dies out for specimens comparable in size to most reinforcing bars.

In reinforced concrete beams the overall stress gradient in the reinforcing bar depends on the diameter of the bar and the stress gradient in the beam. In most cases the tensile reinforcing bars in concrete beams approach a state of direct tensile stress, with only a small stress gradient across the diameter of the bar. Local stress gradients are present, however, due to the stress concentration caused by the deformations. Since the size effect in fatigue is related to the applied stress function, the conclusions drawn from rotating beam tests are not directly applicable to reinforcing bars in concrete beams. On the other hand, tests on plain and notched specimens under reversed direct stress may be comparable to the stress patterns developed in reinforcing bars in concrete beams. Under reversed direct stress the size effect is negligible for plain specimens but there is a small size effect for notched specimens as shown in FIGURE 2.3. The effect of size on fatigue strength of notched specimens increases with an increase in stress concentration and grade of steel. The effect of diameter on the fatigue strength of reinforcing bars will be examined in the framework of these general conclusions.

For hot rolled reinforcing bars of identical manufacturing

process and geometrically similar deformations, tested in air, Wascheidt (34) reports that bars equivalent to No. 8 bars had 5 to 10 percent lower fatigue strength than those equivalent to No. 5 bars. These tests were in agreement with the observations made on multi-rib TOR-STAHL by several investigators in Germany.

Recent tests in Japan (40) on hot rolled deformed reinforcing bars suggest a small decrease in fatigue strength with an increase in bar size for both plain and deformed bars. These tests were conducted on reinforced concrete beams containing bars having diameters equivalent to No. 6 and No. 8 bars. The bars of both sizes were manufactured using the same manufacturing process and had similar deformations.

The findings reported by Wascheidt (34) and by Kokubu and Okamura (40) are summarized in FIGURE 5.6 for comparison with the Alberta test data. The fatigue strengths of the deformed bars plotted in this figure show a reduction with an increase in the bar diameter or cross-sectional area. This effect seemed to be more pronounced for higher strength bars in the Alberta tests but the opposite trend was observed in Wascheidt's (34) tests as shown in the following table.

TABLE 5.1

Test Series	Nominal Yield Strength (ksi)	Ratio of Fatigue Strength to Fatigue Strength of No. 8 Bars			
		No. 5	No. 6	No. 8	No. 10
Alberta	50	1.00	--	1.00	0.99
Alberta	60	1.06	--	1.00	0.95
Alberta	75	1.28	--	1.00	0.935
Wascheidt	50	1.23	--	1.00	--
Wascheidt	60	1.08	--	1.00	--
Kokubu and	50	--	1.05	1.00	--
Okamura	60	--	1.05	1.00	--

SYMBOL	REMARK	SYMBOL	REMARK
—	ALBERTA	A	NOMINAL YIELD 50 ksi
— — —	WASCHEIDT	B	NOMINAL YIELD 60 ksi
— · · —	KOKUBU AND OKAMURA	C	NOMINAL YIELD 75 ksi

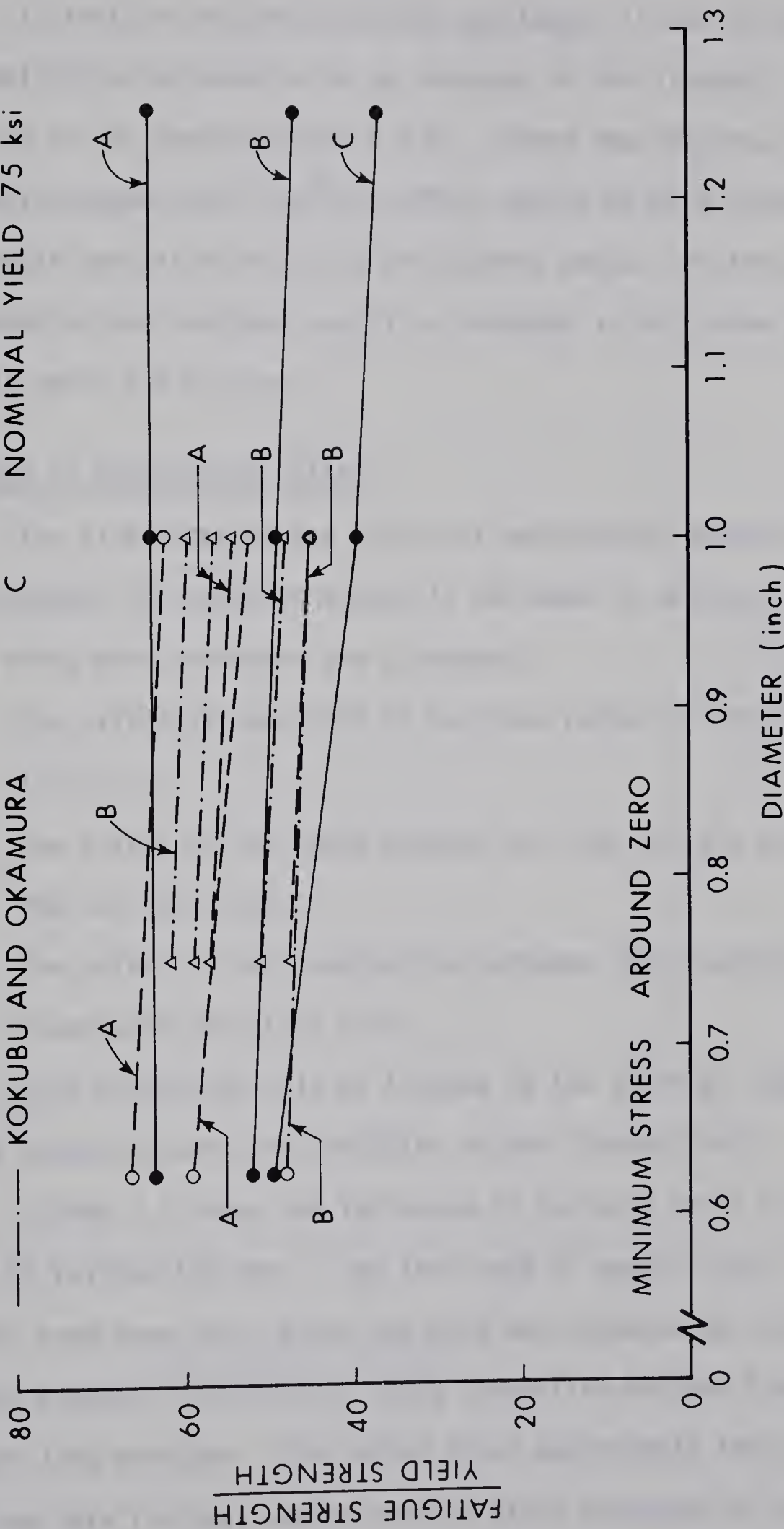


FIGURE 5.6 EFFECT OF BAR DIAMETER ON FATIGUE STRENGTH OF REINFORCING BARS.

In tests of notched machined specimens, it was seen that the notch sensitivity increased with an increase in the strength of the steel or the size of the specimen (Art 2.2.2). These two factors, taken together would suggest that the size effect should be more pronounced in high strength bars as observed in the Alberta tests. On the other hand, if the decarburized zone has a similar strength in all three grades of steel this would not be true.

5.4 Effect of Deformation Pattern

The literature on the effect of deformation patterns on the fatigue strength of reinforcing bars is reviewed in section 2.3.5. In general, three main variables are discussed:

1. The effect of the ratio of lug base radius to the lug height (2.3.5.1).
2. The effect of the angle between the lugs and the axis of the bar (2.3.5.2).
3. The effect of the intersection between longitudinal and transverse lugs (2.3.5.3).

This discussion will be limited to the first of these three since the other two were not variables in the Alberta tests.

FIGURE 5.7 shows the influence of lug base radii on the fatigue strength of reinforcing bars. The test data of several test reports (28,39,40) have been used, after the data was adjusted to correspond to a complete reversal stress cycle using a modified Goodman Diagram with a straight line envelope. The dashed lines approximate the zones containing the data for bars having nominal yield strengths of 50, 60 and 75 ksi. Two important conclusions can be drawn from the test data. First,

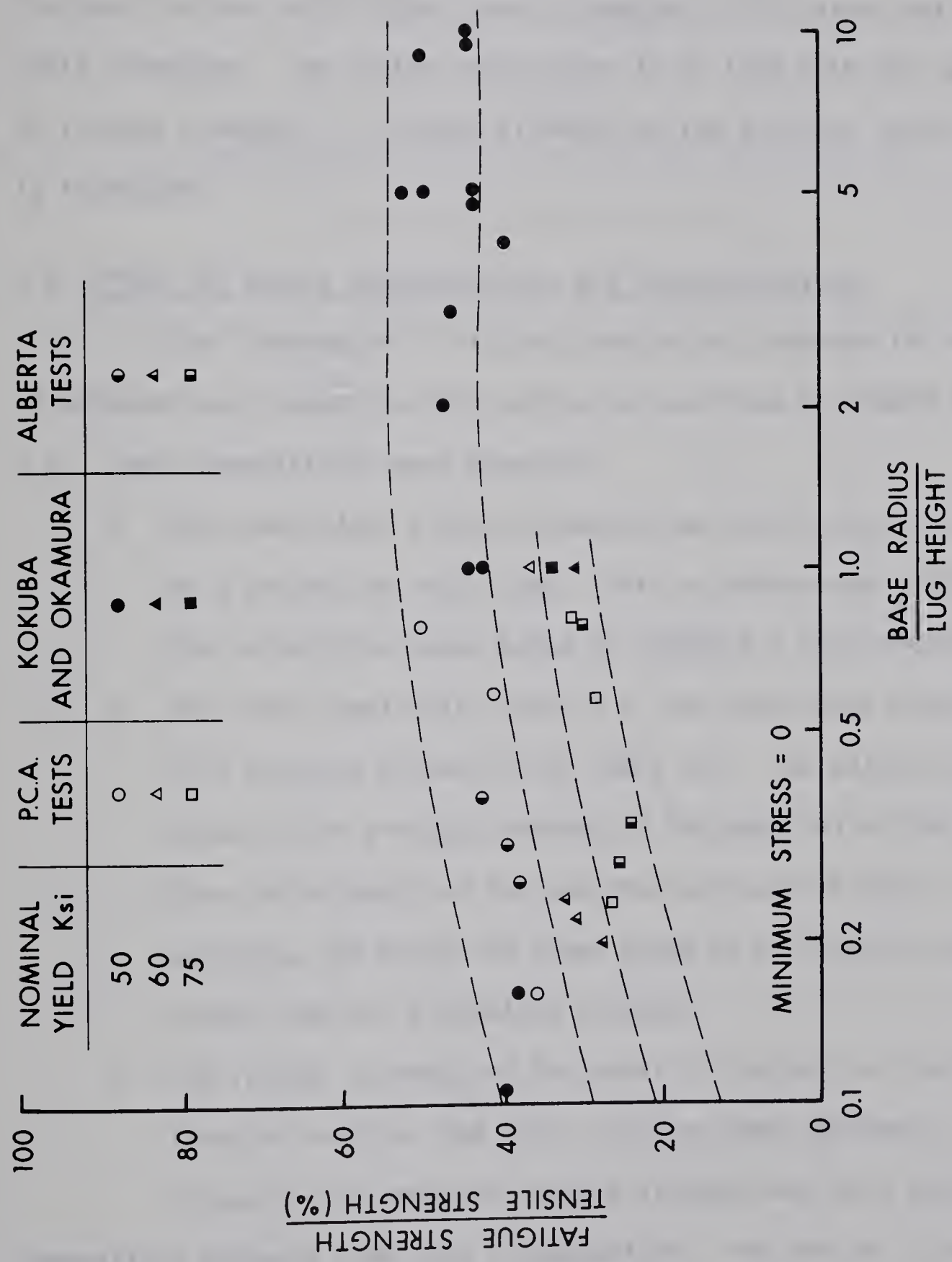


FIGURE 5.7 THE EFFECT OF LUG BASE RADIUS ON FATIGUE STRENGTH OF REINFORCING BARS.

the fatigue strength of the reinforcing bars appears to decrease with a decrease in the ratio of the lug base radius to the lug height. Second, the data for bars with higher yield strengths falls below that for lower yield strengths. The latter observation is in line with the lower ratio of fatigue strength to ultimate strength as the yield or tensile strength is increased.

5.5 Effect of Stress Concentrations and Decarburization

The "theoretical" fatigue strength was computed for nine types of deformed bars tested in this project as outlined in TABLES 5.2 and 5.3. These computations were based on:

1. The theoretical stress concentration factor, K_t , at the base of a projecting notch (38). This is determined in TABLE 5.2. The calculations were based on FIGURE 2.5 and similar graphs.
2. The notch sensitivity factor, q , for the steels considered (10) given in column (5) of TABLE 5.3. The values given were based on the average strength of the material in the bar rather than the strength of the decarburized surface layer. In addition, the graph for q was based on a fillet or notch rather than for projecting notches.
3. The fatigue strength of the metal in the bars as outlined from the tests of the plain rotating beam specimens.

In every case measured fatigue strength was less than the theoretical strength from such a computation. For the No. 5 bars the measured fatigue strength was about 55 percent of the calculated fatigue strength for the three grades. For the other two sizes the measured fatigue strengths ranged from about 55 percent of the calculated fatigue

TABLE 5.2
 CALCULATION OF THEORETICAL STRESS CONCENTRATION
 FACTORS FOR REINFORCING BARS (K_t)

Bar Size	Grade of Steel	r/w	h/w	θ	K_t
No. 5	A 15	0.176	0.59	56°	1.86
	A 432	0.175	0.69	56°	1.86
	A 431	0.284	0.39	42°	1.62
No. 8	A 15	0.167	0.54	41°	1.81
	A 432	0.133	0.54	45°	1.91
	A 431	0.182	0.54	43°	1.79
No. 10	A 15	0.188	0.45	44°	1.76
	A 432	0.170	0.45	43°	1.79
	A 431	0.127	0.49	45°	1.90

TABLE 5.3
ANALYSIS OF FATIGUE STRENGTH OF REINFORCING BARS
FOR COMPLETELY REVERSED STRESS CYCLE

Bar Size	Grade of Steel	Fatigue Strength Rotating Beam specimens (ksi)	K_t of Deformed bar	q (Kuhn & Hardrath)	Calculated K_f $= q(K_t^{-1}) + 1$	Calculated Fatigue Strength of Deformed bar (ksi)	Measured Fatigue Strength of Deformed bar	Measured/Theoretical (8)/(7)
(1)	(2)	(3)	(4)	(5)	(6)	(7)	(8)	(9)
No. 5	A 432	55.5	1.86	0.57	1.49	28.2	20.0	0.71
A 431		67.0	1.62	0.75	1.47	45.5	31.0	0.63
A 15		42.0	1.86	0.57	1.49	30.4	20.0	0.68
A 15		46.2	1.81	0.64	1.52	34.2	19.0	0.66
No. 8	A 432	55.7	1.91	0.69	1.63	43.0	19.0	0.56
A 431		68.5	1.79	0.75	1.59	43.0	19.0	0.44
A 15		45.6	1.76	0.70	1.53	29.8	20.0	0.67
No. 10	A 432	56.0	1.79	0.73	1.58	35.8	18.0	0.50
A 431		60.0	1.90	0.71	1.64	36.6	17.8	0.49

* Computed as (3)/(6)

strength for the three grades. For the other two sizes the measured fatigue strengths ranged from about 55 percent of the calculated fatigue strength for A 15 bars down to about 40 percent for A 431 bars.

One possible explanation of this phenomenon is that the metal on the outside of the bars where the fatigue cracks started was weaker than that in the interior of the bars due to decarburization of the surface of the ingot and billet. A number of investigators have reported that when the surface of steel specimens is decarburized their fatigue strength is significantly reduced (1,2,3,7,12). In FIGURE 5.8, the solid points correspond to test data for machined steel specimens of various tensile strengths tested in reversed bending. The open circles in this Figure represent companion tests which were decarburized after machining. The fatigue strength of the decarburized specimens correspond approximately to Eq. (2.6) derived from Munse's Equation for the fatigue strength of as-rolled plates (27).

The triangular points in FIGURE 5.8 represent the complete reversal fatigue strengths of the deformed bars tested at Alberta from column (8) of TABLE 5.3 multiplied by the fatigue stress concentration factor, K_f , from column (6) of this table. Thus, they approximately correspond to the fatigue strength of an as-rolled plate of the same steel. Equation 2.6 appears to form a lower bound to the reinforcing bar fatigue strengths when they are transformed in this way.

From tests of machined and tempered specimens and similar machined, tempered and decarburized specimens, Jackson and Pochapsky (7) concluded that:

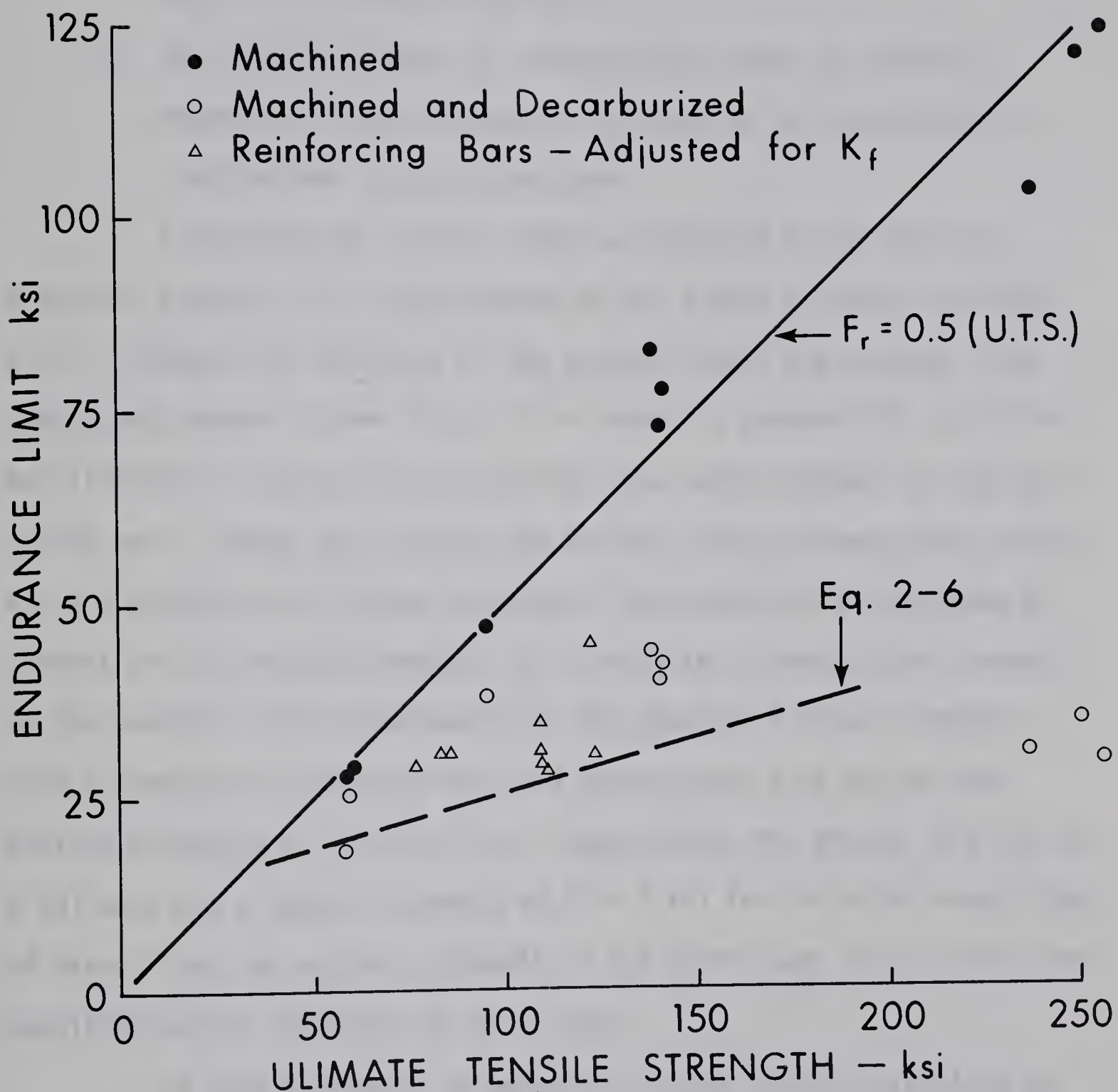


FIGURE 5.8 EFFECT OF DECARBURIZATION ON FATIGUE STRENGTH

1. The core hardness of fatigue-test pieces does not have as large an influence on the fatigue strength as does the hardness in the decarburized skin.
2. The fatigue strength of decarburized steels is primarily dependent on the strength of the ferrite in the relatively "carbon-free" decarburized zone.

A decarburized surface layer was observed in the metallographical studies of all three grades of No. 8 bars as shown in FIGURE 4.15. Although the strengths of the surface layers are unknown, they should vary between about 40 ksi if no carbon is present (4), up to the bar strength if the outer layer had the same carbon content as the rest of the bar. Taking into account the fatigue stress-concentration factor, K_f , and assuming the fatigue strength of the decarburized layer was 50 percent of its tensile strength, it is possible to compute the strength of the ferrite layer corresponding to the observed fatigue strengths. Such a computation indicates that the decarburized zone had to have tensile strengths of 70 and 90 ksi, respectively, for the No. 5 A 432 and A 431 bars and a tensile strength of 60 ± 3 ksi for the other seven types of bars. Thus the apparent strength of the outer layer falls within the possible zone of strengths for this layer.

If this hypothesis is accepted, further study is required to explain the different fatigue strengths observed for the three grades of No. 5 bars. Possible explanations could be that the decarburized zone is thinner due to more bar being rolled out of the billet or that the surface layer has been hardened by more rolling, possibly at cooler temperatures.

CHAPTER VI

CONCLUSIONS

Over the past half century, fatigue strength has been accepted as a distinct mechanical property of the metal, since a direct correlation of fatigue strength with other mechanical properties such as yield or tensile strength, hardness and ductility has been found to be uncertain. Therefore, the fatigue strength and its variation with other parameters must be determined experimentally. On the basis of the limited number of experimental results, the following conclusions may be drawn from this investigation.

1. The limiting stress range of the stress cycle is influenced by the minimum stress level of the cycle. The test data on hot rolled reinforcing bars tested at various minimum stress levels may be approximated by the Modified Goodman Law. For this reason the allowable stresses in hot rolled reinforcing bars subjected to cyclic loads should not be based on a constant limiting stress range as recommended by previous investigators (11, 20, 26).
2. The fatigue strength of the deformed reinforcing bars was found to be appreciably lower than that of the bar metal. The application of the stress concentration theory does not adequately explain this difference.
3. The fatigue test data for Nos. 5, 8 and 10 bars conforming to ASTM A 15, A 432 and A 431 indicates that the fatigue strength of deformed bars is relatively insensitive to the

yield or tensile strength of the metal.

4. There is a small decrease in the fatigue strength with an increase in the diameter of the bar. This effect increases with the increase in the strength of steel.

The large disparity between the fatigue strengths of the machined rotating beams specimens and the reinforcing bars could not be explained on the basis of stress concentration theory. This may be the result of the different surface condition of the two types of specimens. The decarburization and oxidation layer present on the surface of deformed bars probably have a significant influence on the fatigue strength of the deformed reinforcing bars. This aspect of the problem requires further investigation.

Other areas which warrant investigation are the effects of residual stresses and the effect of the environment, the latter may become more significant in the case of high strength steels.

LIST OF REFERENCES

1936 - 1950

1. Austin, C.R., "Effect of Surface Decarburization on Fatigue Properties of Steel", Metals and Alloys, Vol. 2, 1931, pp. 117-119.
2. Hankins, G.A., Becker, M.L., "Further Experiments on the Effect of Surface Conditions on the Fatigue Resistance of Steels". Journal of Iron & Steel Inst. Vol. 133, 1936, pp. 399-419.
3. McDowell, J.F., "Fatigue Endurance of Killed, Capped and Rimmed Steels", Metals and Alloys, Vol. 11, 1940, pp. 27-32.
4. Lacy, C.E. and Gensamer, M., "The Tensile Properties of Alloyed Ferrites", Trans. American Soc. of Metals, Vol. 32, 1944, pp. 88-110.
5. Miner, M.A., "Cumulative Damage in Fatigue", Trans. A.S.M.E., Vol. 67, 1945, pp. A59-A64.
6. Neuber, H., "Theory of Notch Stresses", U.S. Navy, Ann Arbor, Michigan, 1946.
7. Jackson, L.R. and Pochapsky, T.E., "The Effect of Composition on the Fatigue Strength of Decarburized Steel", Trans. American Soc. of Metals, Vol. 39, 1949, pp. 45-60.
8. Orbon, B., "High Grade Steel as Reinforcement in Concrete Beams Anchorage, Jointed Bars, Crack Formation", ACI Journal, Vol. 46, Nov. 1949, p. 235.

1951 - 1960

9. Phillips, C.E., Heywood, R.B., "Size Effect in Fatigue of Plain and Notched Steel Specimens Loaded Under Direct Stress", Proceedings Inst. Mech. Engrs., Vol. 165, 1951.
10. Kuhn, P., Hardrath, H.F., "An Engineering Method for Estimating Notch Size Effect in Fatigue Tests on Steels", Nat. Adv. Comm. for Aeronautic Tech. No. 2805, 1952.
11. Peterson, R.E., "Stress Concentration Design Factors", John Wiley, 1953.
12. Lipsitt, H.A. and Horne, G.T., "The Fatigue Behavior of Decarburized Steel", Proceedings Am. Soc. Test Materials, Vol. 57, 1957, pp. 587-599.
13. Chang, T.S. and Kesler, C.E., "Fatigue Behavior of Reinforced Concrete Beams", Proceedings ACI, Vol. 55, August 1958, pp. 245-54.
14. Stelson, T.E., and Cernica, J.N., "Fatigue Properties of Concrete Beams", Proceedings ACI, Vol. 55, August 1958, pp. 255-60.
15. Rehm, G., "Contribution to the Problem of the Fatigue Strength of Steel Bars for Concrete Reinforcement", International Association for Bridge and Structural Engineering, Sixth Congress, Stockholm (1960), Preliminary Publication, pp. 35-46.

1961

16. Metal Handbook, Vol. 1, American Society of Metals, Metal Park, Ohio (1961).

17. Fisher, J.W. and Viest, I.M., "Fatigue Tests of Bridge Materials of AASHO Road Test", Highway Research Board, Special Report 66, 1961, pp. 132-47.
18. Harris, W.J., "Metallic Fatigue", Vol. 1, Pergamon Press, 1961.
19. Kuguel, R., "A Relation Between Theoretical Stress Concentration Factor and Fatigue Notched Factor Deduced from High Stress Volume", Proc. Am. Soc. Test Mat., Vol. 61, 1961, pp. 732-48.
20. Weibull, W., "Fatigue Testing and Analysis of Results", Pergamon Press, 1961.

1962

21. Forrest, P.G., "Fatigue of Metals", Pergamon Press, 1962.
22. Verna, J.R., Stelson, T.E., "Fatigue of Small Reinforced Concrete Beams Under Repeated Loads", Proceedings ACI, Vol. 59, 1962.

1963

23. A.C.I. Committee 318, "Building Code Requirements for Reinforced Concrete (ACI 318-63)", American Concrete Institute, 1963.

1964

24. ASTM Specifications for Steel Bars for Concrete Reinforcement, American Society for Testing and Materials, Oct., 1964.
25. Hardrath, H.F., "Cumulative Damage", Fatigue - An Interdisciplinary Approach, Syracuse Univ. Press, 1964, pp. 245-61.
26. Kravshenko, P. Ye, "Fatigue Resistance", (Translated from Russian), MacMillan Company, 1964.

27. Munse, W.H., "Fatigue of Welded Steel Structures", Welding Research Council, New York, 1964.
28. Pfister, J.F., Hognestad, E., "High Strength Bars as Concrete Reinforcement", Part 6, Fatigue Tests", Journal of the PCA Research and Development Laboratories, Vol. 6, No. 1, Jan. 1964, pp. 13-23.
29. Sinclair, M.G., "Some Metallurgical Aspects of Fatigue", Fatigue - An Interdisciplinary Approach, Syracuse Univ. Press, 1964.

1965

30. Burton, K.T., "Fatigue Tests of Reinforcing Bars", Journal of the PCA Research and Development Laboratories, Vol. 7, No. 3, Sept. 1965, pp. 13-23.
31. Lash, S.D., MacLeod, N., and Blackwell, W., "High Strength Reinforcements in Reinforced Concrete Beams", Part II, Crack Widths, Deflections, Fatigue Strength, Report No. 38, Department of Civil Engineering, Queen's University, Kingston, Ontario.
32. Soretz, S., "Fatigue Behavior of High Strength Reinforcement", Concrete and Constructional Engineering, Col. 60, July 1965, pp. 272-80.
33. Kokubu, M., Okamura, H., "Fundamental Study on Fatigue Behavior of Reinforced Concrete Beams Using High Strength Deformed Bars", (English Summaries). Trans. Japan Society of Civil Engineers, No. 122, October, 1965.

34. Wascheidt, H., "Zur frage der Dauerschwingfestigkeit von Betonstahlen im Einbetonierten Zustand", (On the Fatigue Strength of Embedded Concrete Reinforcing Steels) Doctoral Thesis, Technical University of Achen, Germany, 1965.

35. "Metals Engineering - Design", A.S.M.E. Handbook, Second Edition, McGraw-Hill, 1965 (Chapter 8.4, "Decarburization").

1966

36. Mayer, M., "Dauerfestigkeit von Spannbetonbauteilen", (Fatigue Strength of Pre-stressed Concrete Structural Elements). Deutscher Ausschuss für Stahlbeton, Vol. 176, Berlin, 1966.

1967

37. Burton, K.T., Hognestad, E., "Fatigue Test of Reinforcing Bars - Tack Welding of Stirrups", Proceedings ACI, Vol. 64, May, 1967.

1968

38. Derecho, A.T. and Munse, W.H., "Stress Concentration at External Notches in Members Subjected to Axial Loadings", Engineering Experiment Station Bulletin No. 494, University of Illinois, 1968.

39. Hanson, J.M., Burton, K.T., Hognestad, E., "Fatigue Tests of Reinforcing Bars - Effect of Deformation Pattern", Journal of the PCA Research and Development Laboratories, Vol. 10, No. 3, Sept. 1968, pp. 2-13.

40. Kokubu, M., Okamura, H., "Fatigue Behavior of High Strength Deformed Bars in Reinforced Concrete Bridges", Journal of the Faculty of Engineering, Univ. of Tokyo, Vol. 29, 1968.

Miscellaneous

41. Amsler Manual, Instruction No. 122/10, Alfred J. Amsler & Co., Schaffhausen, Switzerland.
42. Instructional Manual for Fatigue Testing Machine Model RBF-200 Rotating Beam, The Budd Company, Phoenixville.

APPENDIX A
REINFORCED CONCRETE
BEAM DATA

TABLE A-1
REINFORCED CONCRETE BEAM DATA

* Beam Number	Age at Testing Days	Beam Dimensions		Concrete Strength at Testing psi
		Width Inches	Effective Depth Inches	
SERIES 1				
8-50-1	31	12.20	12.48	5,120
8-50-2	32	11.94	12.12	5,370
8-50-3	29	12.10	12.59	5,370
8-50-4	31	12.19	12.57	5,145
8-50-6	32	12.08	12.78	5,855
SERIES 2				
8-60-1	50	12.12	12.55	4,960
8-60-2	57	12.10	12.48	5,405
8-60-3	54	12.05	12.57	5,400
8-60-4	57	11.88	12.62	5,025
8-60-5	58	12.19	12.63	5,640
8-60-6	65	11.85	12.71	5,160
8-60-11	76	12.00	12.65	4,845
8-60-12	69	12.12	12.67	4,945
8-60-12	69	12.12	12.67	4,945
SERIES 3				
8-75-1	53	12.15	12.59	4,465
8-75-2	54	11.82	12.68	4,665
8-75-3	70	12.12	12.68	5,030

* The numerals in the beam number refer to the bar size, the nominal yield strength and the number of the beams in the series, respectively.

TABLE A-1 (Continued)

* Beam Number	Age at Testing Days	Beam Dimensions		Concrete Strength at Testing psi
		Width Inches	Effective Depth Inches	
8-75-4	67	12.10	12.64	5,300
8-75-5	82	12.06	12.60	4,960
8-75-6	83	12.14	12.65	4,410
SERIES 4				
8-50-7	126	12.12	12.67	5,435
8-50-8	133	12.12	12.70	5,315
8-50-9	143	12.06	12.68	4,535
8-50-10	153	12.12	12.73	4,940
8-50-11	200	12.18	12.67	5,245
8-50-12	207	12.10	12.60	5,070
SERIES 5				
8-60-7	125	12.12	12.76	5,280
8-60-8	134	12.06	12.74	5,260
8-60-9	139	12.12	12.74	4,945
8-60-10	161	12.00	12.68	5,210
8-60-13	150	12.12	12.49	4,775
8-60-14	180	12.00	12.55	4,720
SERIES 6				
8-75-7	103	12.05	12.68	3,725
8-75-8	113	12.12	12.64	3,715
8-75-9	122	12.00	12.70	4,385
8-75-10	147	12.12	12.82	5,080

TABLE A-1 (Continued)

* Beam Number	Age at Testing Days	Beam Dimensions		Concrete Strength at Testing psi
		Width Inches	Effective Depth Inches	
8-75-11	151	12.12	12.70	4,230
8-75-12	167	11.94	12.68	4,357
SERIES 7				
5-50-1	195	7.50	8.82	4,750
5-50-2	198	7.50	8.95	4,860
5-50-3	191	7.50	8.90	5,260
5-50-4	204	7.50	8.78	5,185
5-50-5	196	7.44	8.94	4,840
5-50-6	202	7.50	9.00	4,775
SERIES 8				
5-60-1	174	7.50	9.20	5,890
5-60-2	203	7.44	8.86	5,885
5-60-3	198	7.45	8.99	4,120
5-60-4	218	7.44	9.06	4,030
5-60-5	215	7.50	8.85	4,170
5-60-6	216	7.44	9.00	4,050
SERIES 9				
5-75-1	212	7.44	8.98	4,125
5-75-2	230	7.45	8.97	4,100
5-75-3	225	7.45	8.87	5,885
5-75-4	241	7.45	8.93	5,470
5-75-5	235	7.44	9.09	4,550
5-75-6	240	7.47	9.02	4,480

TABLE A-1 (Continued)

* Beam Number	Age at Testing Days	Beam Dimensions		Concrete Strength at Testing psi
		Width Inches	Effective Depth Inches	
SERIES 10				
10-50-1	312	15.62	15.71	4,750
10-50-2	319	15.38	15.86	5,100
10-50-3	326	15.50	15.80	5,300
10-50-4	348	15.50	15.61	5,080
10-50-5	356	15.44	15.77	5,020
10-50-6	369	15.50	15.82	4,880
SERIES 11				
10-60-1	293	15.50	15.81	5,600
10-60-2	302	15.50	15.35	5,700
10-60-3	316	15.50	15.84	4,200
10-60-4	340	15.62	15.56	4,100
10-60-5	341	15.68	15.48	4,110
10-60-6	365	15.44	15.80	4,175
SERIES 12				
10-75-1	277	15.44	15.68	5,400
10-75-2	297	15.48	15.76	4,190
10-75-3	304	15.44	15.60	5,860
10-75-4	324	15.50	15.74	6,050
10-75-5	337	15.50	15.58	4,760
10-75-6	349	15.50	15.72	4,580

TABLE A-2.

RESULTS OF FATIGUE TESTS ON REINFORCED CONCRETE BEAMS

Beam Mark	Distance of Bar Fracture From $\frac{1}{4}$ of the Beam (Towards)			Origin of fracture in bar		Fracture Remarks
	Hinged End (inch)	Roller End (inch)	Bottom	Intersection of Lug and Rib	Base of Lug	
Series 1						
8 - 50 - 1	3/16	—	✓		✓	 LIP
8 - 50 - 2	2 5/16	—	✓		✓	Clean Break
	—	9/16	✓		✓	Clean Break
8 - 50 - 4	—	1/4	✓		✓	
8 - 50 - 5	—	—				Beam did not fail. No retest.
8 - 50 - 6	3/4	—	✓		✓	

TABLE A-2. (CONTINUED)

Beam Mark	Distance of Bar Fracture From $\frac{1}{4}$ of the Beam (Towards)			Origin of fracture in bar			Fracture Remarks
	Hinged End (inch)	Roller End (inch)	Bottom	Intersection of Lug and Rib	Base of Lug		
Series 2							
8 - 60 - 1	—	—	✓		✓		
8 - 60 - 2	—	1/4	✓		✓		
8 - 60 - 3	1/8	—	✓		✓		
8 - 60 - 4	1/2	—	✓		✓		 BRITTLE SMALL LIP Small piece of metal was broken free
8 - 60 - 5	—	—					Beam did not fail. No retest.
8 - 60 - 6	1/8	—			✓		Small piece of metal broken free.

TABLE A-2. (CONTINUED)

Beam Mark	Distance of Bar Fracture From $\frac{1}{2}$ of the Beam (Towards)			Origin of fracture in bar		Fracture Remarks
	Hinged End (inch)	Bottom	Intersection of Lug and Rib	Base of Lug		
Series 3						BRITTLE
8 - 75 - 1	—	—	✓	✓	START	Beam did not fail. No retest.
8 - 75 - 2	—	—				SMALL BRITTLE ZONE
8 - 75 - 3	4	—	✓	✓	START	Beam did not fail. No retest.
8 - 75 - 4	—	—				Beam did not fail. No retest.
8 - 75 - 5	—	—				Beam did not fail. No retest.
8 - 75 - 6	—	—	✓	✓		

TABLE A-2. (CONTINUED)

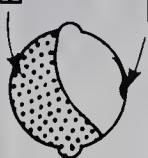
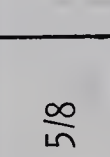
Beam Mark	Distance of Bar Fracture From ℓ of the Beam (Towards)			Origin of fracture in bar		Fracture Remarks
	Hinged End (inch)	Roller End (inch)	Bottom	Intersection of Lug and Rib	Base of Lug	
Series 4						BRITTLE
8 - 50 - 7	7/8	—	✓	✓	✓	
8 - 50 - 8	—	2 3/4	✓	✓	✓	
8 - 50 - 9R	3/4	—	✓	✓	✓	
8 - 50 - 10R	—	9 5/8	✓	✓	✓	
8 - 50 - 11	—	5/8	✓	✓	✓	
8 - 50 - 12	—	3/4	✓	✓	✓	

Figure 4.3



TABLE A-2. (CONTINUED)

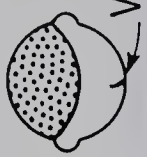
Beam Mark	Distance of Bar Fracture From ζ of the Beam (Towards)		Origin of fracture in bar		Fracture Remarks
	Hinged End (inch)	Roller End (inch)	Bottom	Intersection of Lug and Rib	
Series 5					
8 - 60 - 7	1/2	—	✓		✓ Visible crack at bottom
8 - 60 - 8	3/8	—	✓		✓
8 - 60 - 9	—	1/8	✓		✓
8 - 60 - 10R	—	3/4	✓		✓
8 - 60 - 11	1/8	—	✓		✓
8 - 60 - 12	3/16	—	✓		✓

TABLE A-2. (CONTINUED)

Beam Mark	Distance of Bar Fracture From \mathfrak{C} of the Beam (Towards) Hinged End	Origin of fracture in bar			Fracture Remarks
		Bottom	Intersection of Lug and Rib	Base of Lug	
Series 6	Roller End (inch)				
8-75-7	1 3/8	—	✓	✓	
8-75-8	—	3		✓	Crack initiated midway between long.rib and bar bottom.
8-75-9R	—	3/4	✓	✓	
8-75-10	3/4	—	✓	✓	
8-75-11	2 1/8	—	✓	✓	
8-75-12	—	1	✓	✓	

TABLE A-2. (CONTINUED)

Beam Mark	Distance of Bar Fracture From ζ of the Beam (Towards)			Origin of fracture in bar			Fracture Remarks
	Hinged End (inch)	Bottom (inch)	Intersection of Lug and Rib	Base of Lug			
Series 7							
5 - 50 - 1	1/4	—	✓	✓			
							BRITTLE
5 - 50 - 2	—	1 1/2	✓	✓			VISIBLE CRACKS
5 - 50 - 3R	—	—	✓	✓			
							FRACTURE
5 - 50 - 4	1/4	—	✓	✓			
5 - 50 - 5	1/4	—	✓	✓			
5 - 50 - 6	4 1/2	—	✓	✓			
							Crack initiator was 4 1/2 inch. Towards hinged end.

TABLE A-2. (CONTINUED)

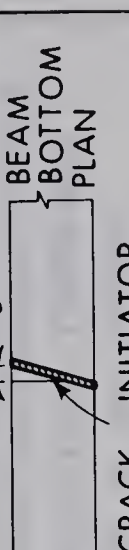
Beam Mark	Distance of Bar Fracture From $\frac{1}{4}$ of the Beam (Towards)			Origin of fracture in bar		Fracture Remarks
	Hinged End (inch)	Roller end (inch)	Bottom	Intersection of Lug and Rib	Base of Lug	
Series 8						
5 - 60 - 1	—	1 1/2	✓		✓	
5 - 60 - 2R	1/2	—	✓		✓	 STRAIGHT EDGE
5 - 60 - 3R	1/2	—	✓		✓	
5 - 60 - 4	1	—	✓		✓	 BEAM BOTTOM PLAN CRACK INITIATOR
5 - 60 - 5	—	1/4	✓		✓	 90° Crack - midway between two lugs
5 - 60 - 6R	3/4	—	✓		✓	

TABLE A-2 . (CONTINUED)

Beam Mark	Distance of Bar Fracture From ξ of the Beam (Towards)			Origin of fracture in bar		Fracture Remarks
	Hinged End	Roller End	Bottom	Intersection of Lug and Rib	Base of Lug	
Series 9	(inch)	(inch)				
5 - 75 - 1R	1 1/2	—	✓		✓	
5 - 75 - 2R	1/2	—	✓		✓	
5 - 75 - 3	6	—		✓		 Crack- midway between two lugs at first major crack.
5 - 75 - 4	2	—		✓	✓	Fracture occurred over the first shear stirrup. (Visible bond failure at the junction)
5 - 75 - 5R	—	3	✓		✓	Failure over first shear stirrup.
5 - 75 - 6R	1	—		✓	✓	

TABLE A-2. (CONTINUED)

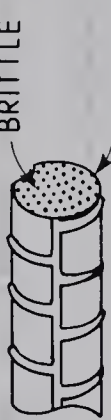
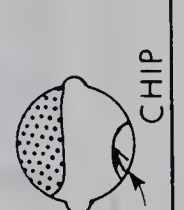
Beam Mark	Distance of Bar Fracture From $\frac{1}{4}$ of the Beam (Towards)	Origin of fracture in bar			Fracture Remarks
		Hinged End (inch)	Roller End (inch)	Bottom	
Series 10				Intersection of Lug and Rib	Base of Lug
10 - 50 - 1	1/4	—	—	✓	
10 - 50 - 2	1/2	—	—	✓	Middle of two lugs 
10 - 50 - 3R	—	—	4 1/2	✓	Fracture over first stirrup. 
10 - 50 - 4R	—	—	—	✓	
10 - 50 - 5	1/2	—	—	✓	
10 - 50 - 6R	1	—	—	✓	

Figure 4.2(a)

TABLE A-2. (CONTINUED)

Beam Mark	Distance of Bar Fracture From \mathcal{Q} of the Beam (Towards)			Origin of fracture in bar			Fracture Remarks
	Hinged End (inch)	Roller End (inch)	Bottom	Intersection of Lug and Rib	Base of Lug		
Series 11							
10 - 60 - 1	2 1/2	—	✓		✓		Beam was slightly warped in casting.
10 - 60 - 2	2	—		✓	✓		
10 - 60 - 3	2	—		✓	✓		
10 - 60 - 4	—	1		✓	✓		
10 - 60 - SR	1/2	—		✓			
10 - 60 - 6	2	—		✓			Figure 4.2(b)

TABLE A-2. (CONTINUED)

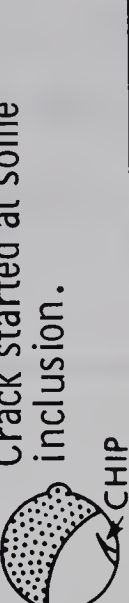
Beam Mark	Distance of Bar Fracture From Ζ of the Beam (Towards)			Origin of fracture in bar			Fracture Remarks
	Hinged End (inch)	Roller End (inch)	Bottom	Intersection of Lug and Rib	Base of Lug		
Series 12							
10 - 75 - 1	1	—	✓	✓	✓		 PLAIN SURFACE Crack started at some inclusion.
10 - 75 - 2	—	—	✓				 CHIP Crack initiated midway between bottom and longitudinal rib.
10 - 75 - 3R	1	—			✓		
10 - 75 - 4	—		2	✓			Crack initiated over shear stirrup.
10 - 75 - 5	1 1/2	—			✓		Figure - 4.2(c)
10 - 75 - 6	1/2	—			✓		

TABLE A-3
RESULTS OF FATIGUE TESTS ON REINFORCED CONCRETE BEAMS

** Beam Number	Maximum Stress psi	Minimum Stress psi	Range of Stress psi	Number of Cycles
SERIES 1				
8-50-1	43,650	5,270	38,380	457,700
8-50-2	38,480	5,160	33,310	730,400
8-50-3	35,900	5,210	30,690	2,005,600
8-50-4	36,050	5,230	30,820	1,837,000
8-50-5	36,080	5,180	30,900	10,234,000*
8-50-6	36,700	5,160	31,540	1,074,200
8-50-11	36,210	5,210	31,000	577,400
SERIES 2				
8-60-1	38,850	6,920	32,000	1,078,300
8-60-2	38,040	6,900	31,140	1,595,600
8-60-3	37,000	6,880	30,120	1,745,600
8-60-4	36,550	6,880	29,670	690,600
8-60-5	36,420	6,860	29,560	9,607,000*
8-60-6	38,900	6,850	32,050	1,270,000
8-60-11	37,600	6,760	30,840	978,000
8-60-12	38,400	6,760	31,640	499,300
8-60-10R	41,920	6,950	34,970	684,300

*Did not fail.

**The letter R in the beam number refers to a retest of a beam which did not fail when tested previously.

TABLE A-3 (Continued)

** Beam Number	Maximum Stress psi	Minimum Stress psi	Range of Stress psi	Number of Cycles
SERIES 3				
8-75-1	39,250	8,500	30,750	782,300
8-75-2	37,900	8,310	29,590	10,400,900
8-75-3	38,650	8,280	30,370	2,725,900
8-75-4	38,900	8,260	30,640	9,000,000*
8-75-5	40,500	8,440	32,060	5,000,000*
8-75-6	42,200	8,240	33,960	1,172,500
SERIES 4				
8-50-7	47,250	20,930	26,320	1,134,600
8-50-8	50,050	21,100	28,950	777,000
8-50-9	46,800	21,270	25,530	5,000,000*
8-50-10	45,850	21,400	24,450	5,000,000*
8-50-12	46,780	21,080	25,700	5,000,000*
8-50-9R	52,900	21,270	31,630	282,200
8-50-10R	58,200	21,400	26,800	207,300
8-50-12R	50,980	21,080	29,900	525,600
SERIES 5				
8-60-7	55,100	27,800	27,300	2,856,400
8-60-8	58,000	28,000	30,000	541,300
8-60-9	54,750	28,220	26,530	1,463,900
8-60-10	53,750	28,400	25,350	5,000,000*
8-60-13	54,980	28,600	26,380	4,703,700
8-60-14	53,240	27,840	25,400	5,000,000*
8-60-14R	60,040	27,840	32,200	322,400

TABLE A-3 (Continued)

** Beam Number	Maximum Stress psi	Minimum Stress psi	Range of Stress psi	Number of Cycles
SERIES 6				
8-75-7	61,300	33,800	27,500	3,341,300
8-75-9	64,240	34,000	30,240	1,240,500
8-75-9	61,000	34,300	26,700	5,000,000*
5-75-10	60,150	34,550	25,600	1,133,700
8-75-11	60,300	34,650	25,650	234,900
8-75-12	59,100	34,700	24,400	4,903,000
8-75-9R	69,850	34,300	35,550	381,400
SERIES 7				
5-50-1	43,480	6,080	37,400	331,600
5-50-2	40,150	5,900	34,250	882,100
5-50-3	36,820	5,720	31,100	5,000,000*
5-50-3R	49,840	5,540	44,300	124,400
5-50-4	38,010	5,360	32,650	852,800
5-50-5	37,080	5,180	31,900	1,056,000
5-50-6	36,100	5,000	31,100	979,200
SERIES 8				
5-60-1	39,275	6,575	32,700	908,300
5-60-2	35,175	6,575	28,600	5,000,000*
5-60-2R	41,875	6,575	37,300	2,058,800
5-60-3	38,075	6,575	31,500	5,000,000*
5-60-3R	46,775	6,575	40,200	311,500
5-60-4	40,975	6,575	34,400	598,700

TABLE A-3 (Continued)

** Beam Number	Maximum Stress psi	Minimum Stress psi	Range of Stress psi	Number of Cycles
5-60-5	38,675	6,575	32,100	1,335,500
5-60-6	38,175	6,575	31,600	5,000,000*
5-60-6R	42,175	6,575	35,600	569,500
SERIES 9				
5-75-1	42,140	8,940	33,200	5,000,000*
5-75-1R	53,340	8,940	44,400	521,400
5-75-2	43,740	8,940	34,800	5,000,000*
5-75-2R	50,140	8,940	41,200	882,100
5-75-3	46,740	8,940	37,800	2,788,000
5-75-4	46,140	8,940	37,200	2,263,400
5-75-5	45,040	8,940	36,100	5,000,000*
5-75-5R	51,540	8,940	42,600	342,100
5-75-6	46,740	8,940	37,800	5,000,000*
5-75-6R	48,540	8,940	39,600	1,260,300
SERIES 10				
10-50-1	38,000	4,970	33,030	630,000
10-50-2	34,940	4,970	29,970	1,803,600
10-50-3	33,340	4,970	28,370	5,000,000*
10-50-3R	40,340	4,970	35,370	460,900
10-50-4	34,970	4,970	30,000	5,000,000*
10-50-4R	40,970	4,970	36,000	781,800
10-50-5	36,970	4,970	32,000	1,296,300
10-50-6	35,270	4,970	30,300	5,000,000*
10-50-6R	39,970	4,970	35,000	919,700

TABLE A-3 (Continued)

** Beam Number	Maximum Stress psi	Minimum Stress psi	Range of Stress psi	Number of Cycles
SERIES 11				
10-60-1	36,800	6,420	30,380	1,361,700
10-60-2	35,400	6,420	28,980	4,750,000
10-60-3	35,400	6,420	28,980	750,700
10-60-4	35,420	6,420	29,000	2,669,900
10-60-5	34,420	6,420	28,000	5,000,000*
10-60-5R	41,420	6,420	35,000	504,200
10-60-6	35,170	6,420	28,750	3,225,900
SERIES 12				
10-75-1	39,680	8,300	31,380	742,100
10-75-2	38,080	8,300	29,780	538,100
10-75-3	37,800	8,300	29,000	5,000,000*
10-75-3R	41,800	8,300	33,500	565,800
10-75-4	38,300	8,300	30,000	558,900
10-75-5	38,300	8,300	30,000	2,029,400
10-75-6	38,800	8,300	29,500	1,327,300

TABLE A-4
RESULTS OF ROTATING BEAM FATIGUE TESTS
Un-notched Specimens Machined from No. 8 Bars

Mark	Nominal Range of Stress* psi	No. of Cycles
SERIES A		
U-50-1	54,800	11,632,700**
U-50-1R	67,800	16,421,200**
U-50-1RR	84,800	19,642,400**
U-50-1RRR	106,000	116,300
U-50-2	84,800	11,672,200**
U-50-2R	95,400	1,813,500
U-50-3	89,000	17,598,400**
U-50-3R	93,200	20,165,400**
U-50-3RR	97,400	20,821,300**
U-50-3RRR	113,000	41,900
U-50-4	95,400	943,300
U-50-5	93,200	1,262,000
U-50-6	92,500	1,046,200
U-50-7	100,000	2,004,700
U-50-8	92,500	1,562,700
U-50-9	91,000	20,000,000**
U-50-9R	99,000	11,476,300**
U-50-9RR	102,500	659,200
U-50-10	99,000	1,604,600

*Computed for minimum diameter ignoring stress concentrations.

**Specimen did not fail.

***Counter jammed at 999,900.

TABLE A-4 (Continued)

Mark	Nominal Range of Stress* psi	No. of Cycles
SERIES B		
U-60-1	115,000	359,700
U-60-2	110,000	20,000,000**
U-60-2R	120,000	16,254,300**
U-60-2RR	130,000	220,900
U-60-3	120,000	377,600
U-60-4	116,000	542,600
U-60-5	112,500	20,460,000**
U-60-5R	125,000	413,100
U-60-6	113,750	607,700
U-60-7	112,500	(999,900)***
U-60-8	112,500	601,500
U-60-9	111,000	20,000,000**
U-60-10	114,000	20,000,000**
U-60-10R	126,000	326,300
SERIES C		
U-75-1	110,600	17,360,800**
U-75-1R	130,000	18,372,400**
U-75-1RR	150,000	119,400
U-75-2	135,000	17,475,400**
U-75-3	142,500	666,800
U-75-4	140,000	2,571,400
U-75-5	137,500	2,313,000
U-75-6	130,000	19,565,100**

TABLE A-4 (Continued)

Mark	Nominal Range of Stress* psi	No. of Cycles
U-75-6R	145,000	1,257,300
U-75-7	137,500	2,500,400
U-75-8	136,000	16,362,400**
U-75-8R	147,500	366,100
U-75-9	137,000	17,175,400**
U-75-9R	146,000	262,200
U-75-10	139,000	2,380,200
SERIES D		
F-50-1	62,000	572,700
F-50-2	58,000	946,800
F-50-3	54,000	15,000,000**
F-50-3R	60,000	1,764,500
F-50-4	56,000	15,000,000**
F-50-4R	64,000	1,357,600
F-50-5	58,000	3,923,000
F-50-6	57,000	1,132,300
F-50-7	57,000	10,000,000**
F-50-7R	70,000	942,000
F-50-8	58,000	3,213,300
F-50-9	65,000	1,425,300
SERIES E		
F-60-1	60,000	15,000,000**
F-60-1R	70,000	15,000,000**

TABLE A-4 (Continued)

Mark	Nominal Range of Stress* psi	No. of Cycles
F-60-1RR	80,000	490,000
F-60-2	75,000	640,000
F-60-3	70,000	1,108,500
F-60-4	65,000	10,000,000**
F-60-4R	74,000	20,000,000**
F-60-4RR	80,000	1,932,900
F-60-5	72,000	10,000,000**
F-60-5R	78,000	10,000,000**
F-60-5RR	84,000	10,000,000**
F-60-5RRR	90,000	1,122,300
F-60-6	80,000	1,150,900
F-60-7	74,000	2,648,800
F-60-8	72,000	10,000,000**
F-60-8R	86,000	246,400
F-60-9	73,000	754,100
F-60-10	77,500	10,000,000**
F-60-10R	85,000	10,000,000**
F-60-10RR	94,000	242,500
F-60-11	82,500	450,600
F-60-12	77,500	913,600
SERIES F		
F-75-1	90,000	10,000,000**
F-75-1R	99,800	806,400

TABLE A-4 (Continued)

Mark	Nominal Range of Stress* psi	No. of Cycles
F-75-2	95,000	1,206,400
F-75-3	91,200	10,000,000**
F-75-3R	110,000	9,473,700
F-75-4	95,000	10,000,000**
F-75-4R	112,000	1,663,300
F-75-5	104,500	433,100
F-75-6	100,000	10,000,000**
F-75-6R	110,000	10,000,000**
F-75-6RR	117,000	10,000,000**
F-75-6RRR	125,000	542,300
F-75-7	117,000	542,300
F-75-8	110,000	740,000
F-75-9	104,500	612,600
F-75-10	100,000	274,200
F-75-11	97,500	595,800
F-75-12	96,000	906,300

APPENDIX B
DESIGN CHARTS FOR THE EFFECT OF DEAD LOAD
TO LIVE LOAD RATIO ON FATIGUE STRENGTH

APPENDIX B

DESIGN CHARTS FOR THE EFFECT OF
DEAD LOAD TO LIVE LOAD RATIO ON
FATIGUE STRENGTH

The fatigue test data on hot rolled reinforcing bars presented in section 5.1 suggest that the stress ranges at varying minimum stress levels may be approximated by Eq. (B.1), which has been derived from the modified Goodman Law.

$$\sigma_r = \frac{\sigma_{f1}}{1 + \beta \frac{\sigma_{f1}}{f_u}} \quad (B.1)$$

where σ_r = stress range

β = ratio of the dead load stresses to the live load stresses

σ_{f1} = stress range corresponding to a cycle having a minimum stress of zero.

f_u = ultimate tensile strength of the metal.

In Eq. (B.1) the stress range (σ_r) has been expressed in terms of β , rather than the minimum stress in the cycle, since in this way it is not necessary to check the maximum stress of the cycle. Equation (B.1) has been plotted in non-dimensional form in FIGURE (B.4) for values of β ranging from 0 to 1.0. This figure facilitates finding the stress range corresponding to any value of β for a stress cycle with zero minimum stress given stress range at minimum stress of zero. The values of minimum stress

and maximum stress may be calculated from Eqs. (B.2) and (B.3).

$$\sigma_{\min} = \beta \cdot \sigma_r \quad (B.2)$$

$$\sigma_{\max} = (1 + \beta) \cdot \sigma_r \quad (B.3)$$

The test findings suggest that the allowable fatigue stresses in hot rolled deformed reinforcing bars should not be based on constant limiting stress range, as recommended by previous investigators (11,20, 26), because this design criterion may not be justified for a variety of reinforced concrete structures under fatigue loads. In these structures the ratio of dead load stresses to live load stresses vary considerably, which may influence the fatigue strength of reinforcing bars.

For design purposes the allowable fatigue stresses for hot rolled reinforcing bars may be specified at zero dead load or any suitable ratio of dead load stresses to live load stresses. This permissible stress may further be modified by using Eq. (B.1) or FIGURE (B.4) for actual ratio of dead load stresses to live load stresses in ordinary reinforced concrete structures.

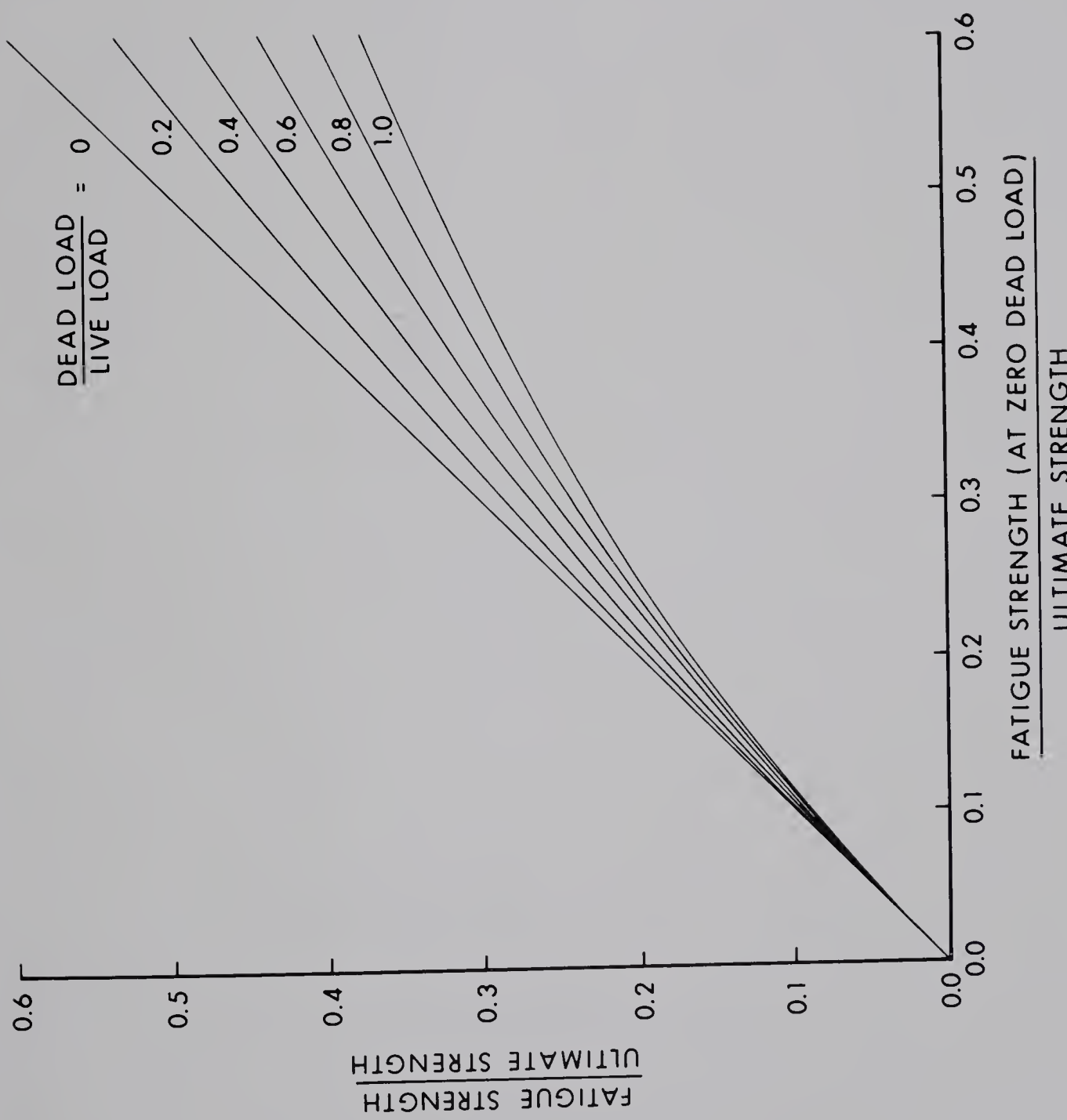


FIGURE B.1 EFFECT OF RATIO OF DEAD LOAD TO LIVE LOAD ON
FATIGUE STRENGTH.

FIGURE B.1

B29909